University of Torino

Doctoral School in Life and Health Sciences
PhD Program in Complex System for Life Sciences

Gender and estrogens as key factors in the response to immunotherapy in non-small cell lung cancer

Candidate:
Sofia La Vecchia

Relators:
Prof. Luca Primo
Prof.ssa Chiara Riganti

INDEX

Introduction

1.1 Epidemiology, diagnosis, subtypes and treatment

Lung cancer (LC) is the main cause of cancer death worldwide with two million newly diagnosed cases and it represents 13% of all cancers diagnosed in 2021 [1]. It is most frequently diagnosed among people aged 65–74 and the median age at death is 72 years old [2]. Age-adjusted rates for new LC cases have been falling on average 2.2% each year over 2009–2018. Age-adjusted death rates have been falling on average 3.8% each year over 2010–2019. It is the second and third most frequently occurring cancer in men (15%), and women (12%), respectively, with 42,500 new estimated cases in Italy. Non-Small Cell Lung Cancer (NSCLC) accounts for 80%–90% of lung cancers. Smoking is the main risk factor for LC, being responsible for 85% -90% of the cases observed [3]. Other risk factors are asbestos and radon exposure with consistent evidence of carcinogenicity, based on epidemiological studies conducted on humans, such as exposure to fine particles and air pollution. Genetic susceptibility and polymorphism play a marginal role while environmental factors remains predominant in the etiology of LC [4][5].

For secondary prevention of lung cancer, periodic LC screening may be useful. Early detection might be a valuable approach to diagnose the disease at an earlier, asymptomatic and potentially curable stage. However, LC diagnosis is usually carried out at advanced stages with the majority of patients presenting with metastatic disease. Most early-stage LCs are asymptomatic, often detected by imaging procedures performed for other reasons [6].

Screening evaluated in relatively small trials failed to show benefit if periodical chest X-ray and/or sputum cytology were used; screening by these techniques is not recommended. The much larger National Lung Cancer Screening Trial (NLST) comparing annual low-dose computed tomography (LDCT) to standard chest X-ray in high-risk subjects (≥ 30 pack-years or ≤ 15 years since smoking cessation), aged between 55 and 74 years old, showed a 20% reduction in LC-related deaths and an

overall all-cause mortality reduction of 6.7% [7] [8].

The study findings favored the introduction of recommendations for the implementation of annual screening with LDCT scan for US and National Comprehensive Cancer Network (NCCN) [9]. Likewise, the NELSON study in Europe confirmed benefit of recurring screening with LDCT compared to observation alone in a population of subjects similar to that of NLST study, with a reduction in mortality of 26% in males and 39% in females across a 10-year follow-up period [10]. A further confirmation of the benefit of screening in high-risk patients for LC comes from the MILD study, which recently demonstrated how LDCT of the chest, with annual or biennial frequency, for a total period of 10 years, is associated with a reduction in LC-related mortality at 10 years of 39% compared to observation alone. However, considering the high rate of over-diagnosis of indolent cancers (20-25% of surgery performed in LDCT screening trial have been performed for benign lesions) and the fear of radiation exposure, screening with LCDT has not been endorsed in Europe yet, while an annual screening with chest LDCT in high-risk individuals (30 pack-year smoking history) from age 55 to 80 years old is currently recommended in the United States. More than 95% of LCs can be traced back to three main histological subtypes: squamous cell carcinoma (CS; 30%), adenocarcinoma (ADC; 40%), and large cell carcinoma (CGC; 3–9%) [11] [12].

In the last few years, an accurate histological definition of NSCLC has become critical for the development of new therapies related to the isotype [9] [13], improving significantly both survival outcomes and quality of life of patients with advanced NSCLC. Immunohistochemistry (IHC), including p40, cytokeratin5/6 (CK5/6) and p63 for CS and TTF1, CK7 and napsin A for ADC, is generally required to increase the specificity of diagnosis in the small sample setting and reduce the number of diagnoses of NSCLC-NOS (not otherwise specified) [9] [13]. CGC is a tumor lacking morphologic or IHC-based evidence of clear lineage, with negative or uninformative staining for both CS and ADC. For differential diagnosis between ADC and CS, the use of only the "antibody pair" TTF-1 and p40 is currently the best approach, also to preserve neoplastic samples for molecular

investigations, to evaluate all predictive biomarkers necessary for the first line of therapy. For patients with advanced NSCLC, it is needed to assess PD-L1 (Programmed Death Ligand 1) status and possible ALK (Anaplastic Lymphoma Kinase) translocation through validated antibodies for use formalin-fixed and paraffin-embedded (FFPE) samples, as well as to perform a screening in IHC for ROS1 alterations. The last pathologic classification highlighted the concept that personalized medicine for patients with advanced LC is determined by histology and genetics, and that tissue/cell management of small biopsy/cytology samples is critical for pathologic and molecular diagnosis in order to prevent the loss of tissue in less important analysis [12] [14].

The identification of oncogenic drivers on the basis of specific genomic alterations and the development of targeted therapies led to a radical shift from pathological to molecular classification of NSCLC, establishing a new paradigm of "personalized therapy". Mutations in some genes have been shown to be extremely effective predictors of response to targeted therapies. The NSCLC genome can be extremely heterogeneous: the genetic abnormalities present can affect multiple genes and include point mutations, small deletions or insertions and fusion genes. The most frequently encountered changes in lung ADC affect the *EGFR, KRAS, ALK, ROS1, RET, BRAF* and *HER2* genes. In particular, the most frequently mutated protooncogenes are *EGFR* and *KRAS*, whose mutations are generally mutually exclusive [15].

Currently, decision of first-line therapy with advanced NSCLC is based on the evaluation of following parameters:

- Histology (squamous versus non-squamous)
- Molecular profile (sensitizing mutations of EGFR, BRAF and rearrangements of ALK or ROS1)
- PD-L1 expression level
- Clinical characteristics (age, performance status (PS), comorbidities) and preferences of patients.

EGFR activating mutations have been identified in about 40–60% of Asian, 15– 20% of Caucasian, and 30% of Latin American NSCLC patients [16].

Activating mutations significantly increased autophosphorylation of intracellular tyrosine residues

with the subsequent constitutive activation of downstream RAS/RAF/ERK/MAPK and PI3K/AKT pathways, favoring tumor cell proliferation, angiogenesis, and metastasis. Lung ADC with mutated EGFR has significant clinical sensitivity to tyrosine kinase inhibitors (TKI) of first- (gefitinib and erlotinib), second- (afatinib, dacomitinib) and third-generation (osimertinib) drugs selectively targeting and inhibiting EGFR [17]. Thus, EGFR mutational testing is actually recommended in all patients with newly diagnosed advanced ADC. It has been observed that tumors with mutations in the exon 19 of EGFR have better overall survival than those with exon 21 mutations when treated with TKIs [18]. Also the EGFR mutation analysis on circulating tumor DNA (ctDNA) demonstrated an adequate diagnostic accuracy [19] as compared to tumor tissue analysis and is currently recommended as an alternative approach in a subgroup of patients with newly diagnosed metastatic disease who cannot undergo biopsy or received uninformative results from tissue molecular analysis. In contrast to EGFR where strong data exists, the assessment of other genomic alterations using ctDNA in treatment-naive patients is more limited. However, as endorsed by most international scientific societies, the detection of an actionable alteration in ctDNA, if using a validated assay, would eventually represent sufficient evidence to initiate a targeted treatment, albeit not without reimbursement variations among all the different countries [20]. Besides EGFR mutations, the G12C mutation in exon 2 of KRAS is a common event in lung ADC; this somatic mutation is the most frequently found in Caucasian population smokers, with an incidence rate of 25% to 35%. Recently, of particular clinical interest is the c.1799T> A point mutation in exon 15 of the *BRAF* gene (responsible for $BRAF^{V600E}$mutation) and activating mutations in the region of the *HER2* gene, which encodes the tyrosine-kinase domain of the related protein. Activating mutations in the *BRAF* gene, which are generally mutually exclusive from *EGFR* mutations or *ALK* rearrangements, act as an alternative oncogenic driver in NSCLC. The most common of these mutations, $BRAF^{V600E}$, is observed in 1– 2% of lung ADC. Although the prognostic implications of $BRAF^{V600E}$ mutation are unclear, several studies have associated $BRAF^{V600E}$ with poor outcomes and randomized clinical studies demonstrated that patients with V600E mutation in *BRAF* gene receive a benefit from

treatment with combination BRAF and MEK tyrosine kinase inhibition, dabrafenib and trametinib [2].

Another potent oncogenic driver in NSCLC is the rearrangement of ALK with EML-4 or with other fusion partners on the short arm of the chromosome 2, resulting in a constitutive activation of the intracellular tyrosine kinase domain of ALK receptor and downstream RAS/MAPK, PI3K/AKT, and JAK/STAT3 signaling pathways [21]. Chromosomal rearrangements of ALK have been detected in about 3-7% of NSCLC and define a new molecular subtype of NSCLC that is exquisitely sensitive to treatment with ALK tyrosine kinase inhibitors of first- (crizotinib), second- (alectinib, ceritinib), and third generation (lorlatinib, brigatinib) [22][23]. More recently, chromosomal rearrangements of *ROS1* proto-oncogene have been identified in about 1 - 2% of NSCLC and were associated with a great response rate to ALK inhibitors [24]. Other molecular alterations recently found in NSCLC include rearrangements of the *RET* and *NTRK* 1-3 genes, and mutations of exon 14 in *MET*. Although these targeted therapies have profoundly improved NSCLC patients' outcome, they inevitably experience tumor progression and recurrence. Resistance onset is frequently due to the acquisition of new molecular alterations such as additional mutations or amplifications [25].

1.2 Clinical staging and molecular classification

For all NSCLC patients with stage IIIB-IIIC and stage IV, it is recommended to include in the diagnostic workflow the immunohistochemical evaluation of PD-L1 expression levels together with the molecular characterization of EGFR mutations, ALK, ROS-1 translocations, and BRAF genetic aberration. In all patients with unresectable stage IIIA/IIIB (N3) or IIIC, similarly to stage IV NSCLC, multimodal treatment is indicated and evaluated in a multidisciplinary context.

Pathological stage is the most relevant prognostic factor for recurrence and death in NSCLC patients. The 5-year survival rate after surgery for stage I is 60-80%, 40-60% in stage II, while in stage III it is 20-40%. Recurrence peaks of disease occur around ninth month after surgery and two subsequent peaks at the end of the second and fourth years. Although a relapse risk is estimated to be between

6% and 10% per person/year within 4 years after surgery and 2% after 4 years, some data suggest that the risk of relapse after the fifth year persists and is estimated between 3.5% and 15%. The pattern of relapse differs depending on the time, with local relapses in the first two years and with a distant relapse rate that increases after third year from end of primary treatment [26] [27].

The early detection of relapse following primary surgery for NSCLC and the characterization of emerging subclones seeding metastatic sites might offer new therapeutic approaches to limit tumor recurrence. In patients with nonmetastatic lung cancers, a subset can be cured after primary surgical resection, radiotherapy, and/or combined treatment approaches, including chemotherapy [28]. Unfortunately, outcomes are especially poor after clinical disease progression [29].

1.3 Immunotherapy: definition and role in NSCLC

Immunotherapy is emerging more and more with a growing worldwide enthusiasm in cancer field. Understanding the steps in immune recognition and eradication of cancer cells is vital to reach optimal therapies with an optimistic view for the future perspectives in LC immunotherapy. The treatment landscape of NSCLC is rapidly evolving. Immune-checkpoint inhibitors (ICIs), specifically those targeting PD-1 or PD-L1, have demonstrated durable efficacy in a subset of patients with NSCLC, in the first-line therapy. Approved immunotherapeutic strategies for treatment patients include monotherapy, immunotherapy, or chemotherapy–immunotherapy combinations. Several emerging biomarkers and novel therapeutic strategies are currently under investigation, and these might further refine the current treatments [30].

In recent years the introduction into the clinical practice of these novel drugs has revolutionized the prognosis in many cancers, such as metastatic melanoma but also NSCLC.

Immunotherapy's rationale is based on reactivating the patient's own innate T-cells to actively recognize the tumor's antigens and thus perform tumor cell killing. Indeed, many solid malignancies have the ability to 'switch off' T cells (ie, cytotoxic T $CD8^+$ lymphocytes) expressing, on their surface, negative regulators such as the cytotoxic T lymphocyte associated protein 4 (CTLA-4) and

programmed death (PD-1). These molecules would physiologically serve as checkpoints to control immune reactions and limit an excessive $CD8^+$ T cell response. Of note, tumors can exploit this mechanism to their advantage, thus evading immune response. Immune checkpoint inhibitors (ICIs) are monoclonal antibodies that inhibit this checkpoint-receptor interaction and prevent the switching off of T cell response [31].

Among predictive biomarkers tested in patients with advanced NSCLC, there is the evaluation of PD-L1 expression, for selection of first-line immunotherapy treatment with pembrolizumab. In clinical practice, only one clinically validated method is approved and involves the application of the Tumor Proportion Score (TPS). This is based on percentage assessment of PD-L1 positivity on membrane of neoplastic cells. In the last two decades, the advent of new effective drugs including targeted therapies and immunotherapies revolutionized the treatment strategies and the natural history of advanced diseases, significantly improving both patients' survival and quality of life [32]. In patients with advanced NSCLC without molecular driver alterations, the current treatment decision-making is mainly based on histology, clinical conditions, comorbidities, and on level of PD-L1 expression. About 30% of patients with advanced NSCLC have tumors with TPS for PD-L1 >50% and the advent of immunotherapy has recently led to a paradigm shift of their first-line treatment [32]. Phase III KEYNOTE-024 randomized trial show that anti-PD1 checkpoint inhibitor pembrolizumab significantly improved progression free survival (PFS) and overall survival (OS), as compared to platinum chemotherapy, becoming the new standard of care in this subset of patients [33]. Despite some initial concerns of toxicity profiles, the association of ICIs (pembrolizumab or atezolizumab) with platinum-based chemotherapy had improved OS and PFS in NSCLC patients, when compared to chemotherapy alone, making these regimens the current standard of care in the first-line treatment of non-oncogene-addicted NSCLC patients, irrespective of PD-L1 expression [34].

1.4 Gender in oncology as prognostic factor of response to immunotherapy

Sex is an important factor in the development of many types of cancers, including those who are not 'sex-specific', such as prostate and breast cancer [31].

Furthermore, sex disparities in clinical outcomes are well described in literature [35] and it is often observed that males have higher mortality rates compared to females. Even though this is partly attributed to sex differences in cancer incidence rate, the differential outcomes could also reflect different gene-environment interactions and dimorphisms in immune system response, which could in turn affect the efficacy of novel treatments in solid malignancies [36]. An example of this difference in therapy response has come from the use of ICIs in advanced-stage patients with NSCLC.

Despite their proven efficacy in NSCLC patients, important discrepancies in clinical response to their usage between male and female patients have arisen. Indeed, how sex associates with ICI efficacy is not completely elucidated [36].

1.5.1 Preclinical studies: hormonal receptors and their influence on response to therapy

Lung development during embryogenesis is a complex and articulated process [37]. Nonetheless, it has been well established that the estrogen-mediated signaling pathway are some of the main factors directing this process, withthe estrogen receptor (ER) β playing a pivotal role in postnatal lung development and homeostasis [38].

Indeed, once the most active estrogen, 17-β-estradiol, binds to its cytoplasmic receptor, the latter is phosphorylated and can activate both the EGFR downstream effectors, namely RAS, RAF, MEK, ERK, and the PI3K pathway, leading to increased cell survival, growth and increased metabolism. Furthermore, the active complex receptor-ligand can migrate to the nucleus and act as a transcription factor by binding to Estrogen Responsive Elements (EREs) in specific gene promoters, thereby

leading to the activation of several genomic pathways, in turn promoting proliferation, and angiogenesis [37]. Besides their physiological role, estrogens have been shown to contribute to the development and progression of LC. Both estrogen receptors, ERα and ERβ, were shown to be expressed at higher levels in LC tissues compared to normal lung tissue (ref). As far as estrogen synthesis is concerned, it can also happen autocrinally in LC, via the intratumor aromatase enzyme that catalyzes the conversion of androgens to estrone and estradiol [39].

One estrogen-dependent mechanism of tumorigenesis is the activation of the Mek/Erk signaling via ERβ [40]. This pathway has been linked to increased migration and has been demonstrated to be an interesting vulnerability that can be exploited by direct targets. Indeed, the 17-β-estradiol and EGF-induced ERK phosphorylation were downregulated in the presence of tamoxifen and/or gefitinib, thus suggesting a direct involvement of ER signaling in survival pathways crucial for the cell. Moreover, this finding also suggests a functional cross-talk between the ER and EGFR pathways in LC, thus paving the way for further clinical studies. Targeted therapy with TKIs and immunotherapy with ICIs have recently represented novel therapeutic tools to treat advanced-stage NSCLC. However, as of today, their efficacy is not universal for all eligible patients and the lack of response predictor is still a problem [40].

In addition, it is well established that estrogens play a role also in the adaptive immune response, as both ER isoforms are upregulated in T and B lymphocytes. With this regard, it has been suggested [41] that the PD-1/PD-L1 pathway is modulated by sex hormones and this could be implicated in the regulation of antitumor immunity in endometrial and breast cancer cells. Erα also affects the composition of the immune infiltrate in animal models [42].

Within such picture, several hormonal markers have been linked *in vitro* to clinical outcome in NSCLC, such as:

- circulating estrogens, which correlate with worse survival in women and men, as well as with poorly differentiated tumors and advanced stages in post-menopausal women [37],

- aromatase, whose overexpression correlates with worse survival in postmenopausal women and tumor progression [43] [44],
- ERβ, which is linked with worse prognosis in female and good prognosis in men [45],
- Co-expression of ERβ and aromatase that can predict poor survival in women and men [45],
- Co-expression of ERβ and EGFR that is linked with high survival if treatment with ER inhibitors and TKI is performed [46] [47][48].

All in all, the development of anti-estrogen therapy for hormone-positive breast cancers has been the direct cause of a 28-fold decrease in breast cancer mortality in the United States alone since the late 1980s. This success may indeed serve as a model for the advancement of antiestrogenic therapy for NSCLC [39].

Furthermore, estrogen treatment of ovariectomized syngeneic mice transplanted with ER-negative breast cancer, melanoma or lung cancer tumors significantly enhanced tumor growth via interactions with ERα present in cancer-associated fibroblasts (ref). This suggests that estrogens play an important role in promoting a protumoral microenvironment by several mechanisms, many of which could represent a novel therapeutic target especially for metastatic NSCLC [42].

Besides ER, the progesterone receptor (PR), another gender-dependent factor, has been shown to be a prognostic factor and a potential therapeutic target in NSCLC. Indeed, despite the lack of unanimous consensus about the immuno-localization of PR, consistent results indicate that progesterone modulates cell cycle regulators such as p21, p27, cyclin A, cyclin E and it also reduces the growth of PR-positive NSCLC cell lines [49]. To further corroborate this observation, low total PR has been identified as an independent negative predictor of time to progression and tumors expressing high ERβ-1/low PR have an aggressive behavior [45]. Additionally, smoking has been shown to disrupt several hormonal pathways in lung cells such as decreasing PR protein expression, promoting malignant transformation [50].

1.5.2 Clinical trials testing antiestrogenic therapy in NSCLC

The increasing amount of evidence around the role of estrogens in promoting and sustaining NSCLC led to the design of several clinical trials exploring the use of antiestrogenic therapy in advanced-stage disease.

For instance, the Woman trial 2x2 arms parallel open-label randomized phase II trial compared the use of gefitinib alone versus gefitinib + fulvestrant in the EGFR mutated group and erlotinib alone versus erlotinib + fulvestrant in the EGFR wild-type group. Unfortunately, despite an increase in PFS, especially in the EGFR mutated group, the combination therapy with fulvestrant failed to delay the recurrence and increase survival [51].

Another open-label, single arm phase II trial [NCT00592007] tried to explore the potentially advantageous effects of combination therapy with fulvestrant and erlotinib in patients with stage IIIb/IV NSCLC. Unfortunately this study was terminated due to slow subject accrual, so no data are available. Despite that, no serious adverse events were reported and this study may serve as a guide for future trials exploring the combination between antiestrogenic agents and anti-EGFR drugs.

Indeed, another randomized open-label, phase II trial ventured in this field by investigating the potential benefits of giving erlotinib together with fulvestrant in patients with stage IIIB or stage IV NCSLC. A total of 108 patients were recruited. ORR was 16.4% for combination arm versus 12.1% for erlotinib alone arm, but no statistical significance was achieved. Overall, the median PFS was 3.5 months for erlotinib plus fulvestrant and 1.9 months for erlotinib alone, and the median OS was 9.5 months for erlotinib plus fulvestrant versus 5.8 months for erlotinib alone, but these results were not statistically significant. Furthermore, regardless of treatment arm, ORR, PFS, and OS were greatly superior in EGFR mutant patients when compared to EGFR wild-type (WT) patients. On the other

hand, in EGFR WT patients, but not in EGFR mutant patients, fulvestrant plus erlotinib increased PFS.

Interestingly, dual therapy benefit in EGFR WT patients may partly be explained by HR positivity.

Regarding AEs (Adverse Events), no statistical difference in between the treatment arms. The most common grade 3–4 AEs included diarrhea, rash, anorexia, and/or fatigue [52].

Besides targeting the ER, another promising therapeutic target that emerged in preclinical studies was the aromatase enzyme. Following this rationale, a phase II randomized trial [NCT02666105] tested whether dual anti-estrogen therapy (anastrozole and fulvestrant) could slow the time to progression in postmenopausal women with advanced NSCLC who have previously received first-line platinum-based chemotherapy with or without Bevacizumab. Unfortunately, despite the good premises, this trial stopped because of the poor enrollment, so no data are available.

Another recently completed phase I clinical trial [NCT01664754] explored the possibility to use a combination therapy with carboplatin, pemetrexed and exemestane in post-menopausal women with metastatic non-squamous NSCLC. The collected data demonstrate that the combination is safe and well-tolerated and thus this supports future clinical trials to establish efficacy with this combination regimen.

1.6 General and specific aims

Gender is an important stratification and prognostic factor in oncology in the response to treatments, particularly to the immunotherapy. The anti-PD-1/PD-L1 ICIs (Pembrolizumab, Nivolumab, Atezolizumab) have improved the prognosis of non-small cell lung cancer (NSCLC) patients in 20-35% cases, but with a lower efficacy in females [53]. The different steroid hormones - estrogens, progesterone or androgens - present in both genders have often contrasting effects on the activity of the host immune system, partly explaining the differences observed. It is not known if metabolic features of cancer cells of male and female patients may impact on the immune system response and

immunotherapy efficacy.

The aim of this work is to clarify if there are gender-dependent and/or hormonal-dependent molecular circuitries explaining the differential gender response to ICIs often observed in clinical studies. To achieve this goal, we set up an analytical pipeline based on patient-derived samples, cell lines and humanized male and female mice bearing gender-matched NSCLC xenografts, aimed at discovering how the 17-β-estradiol and ERα transcription could regulate PD-L1 levels in both genders.

Since PD-L1 is an integral membrane protein, in the second part of the Thesis I investigated whether the effects of letrozole, an estrogen synthesis inhibitor leading to an impairment of intracellular sterols (e.g. cholesterol, cholesterol esters), may also alter the lipidome composition of cell membranes and whetherpart of its effect were due to changes in physio-chemical properties. We thus performed an untargeted lipidomic analysis to investigate if parts of the immune-sensitizing effects observed with the aromatase inhibitor letrozole, were due to changes in lipid profiling. We found that letrozole decreased the saturated fatty acids (SFAs)/mono- or poly-unsaturated fatty acids (MUFAs-PUFAs) ratio, and the cholesterol/cholesterol esters ratio. These changes led to an increase of membrane fluidity that affected in turn the binding between anti-PD-1/PD-L1. As proof of concept, we evaluated if other membrane fluidifiers as ω-3PUFAs recapitulate the same effects than letrozole.

Finally, we set up a prototypical spheroid-based gender-tailored platform, that we aim to use as effective, cheaper and less time-consuming tool to investigate the metabolic circuitries causing the gender-related differential response to ICIs and to repurpose metabolic modifiers as novel immune-adjuvant agents in NSCLC. Since rewiring of cellular metabolism is crucial for sustaining the increased growth and proliferation of tumor cells, I have first initiated the metabolic profile in 3D live cells and tested the potential anti-tumor effects of SFA and MFAs.

2. Materials and methods

Chemicals and materials. Fetal bovine serum (FBS) and culture medium were from Invitrogen Life Technologies (Carlsbad, CA). Plasticware for cell cultures was from Falcon (Becton Dickinson, Franklin Lakes, NJ). The protein content in cell extracts was assessed with the BCA kit from Sigma-Merck-Millipore (St. Louis, MO). Electrophoresis reagents were obtained from Bio-Rad Laboratories (Hercules, CA). If not otherwise specified, the reagents were purchased by Sigma-Merck-Millipore.

Patients' selection, tissue management and ethical regulation. Eighty-six patients with diagnosis of advanced (stage IV) NSCLC and treated with 2nd or 3rd line immune checkpoint inhibitors (anti-PD-1) were included in the study. Clinic-pathological data were collected from seven different Italian centers and retrospectively reviewed. For each patient a tumoral tissue specimen was stored, either from early stage diagnosis – if patient initially underwent to surgery - or at metastatic presentation.

Tissue evaluation. FFPE blocks were first triaged by a thoracic pathologist and a threshold of at least 50% of neoplastic cells was set, through analysis of hematoxylin-eosin (H/E) slides under light microscopy, in order to proceed with further analysis. Then, based on the specimen's cellularity, different slides (4-µm-thick) were cut and placed in eppendorf tubes for RNA extraction. At least 4 slides were harvested for immunohistochemistry analyses.

Total RNA extraction and NanoString IO360 assay. Gene expression analysis was performed on 86 FFPE tissue samples. Total RNA was isolated from 2 to 6 FFPE tissue sections (5-µm-thick), collected in a sterile Eppendorf tube (the number of sections was increased in case of scant material). RNA isolation was performed using the FFPET RNA Isolation Kit (Roche Diagnostics GmbH,

Mannheim, Germany), according to the manufacturer's protocols. Total RNA concentration was assessed using a NanoDrop spectrophotometer (Thermo Fisher Scientific, Inc., Wilmington, DE, USA). 300 ng of total RNA from each sample were hybridized to the nCounter® PanCancer IO360™ Panel, according to the manufacturer's instructions (LBL-10504 Sept 2017 NanoString PanCancer IO360 Gene Expression Panel Best Practices Guide for FFPE Samples; JULY 2016 MAN-10023-11_nCounter_XT_Assay_User_Manual - NanoString Technologies, Seattle, WA, USA). This panel detects the expression of 750 immune-related genes and 20 housekeeping genes. One lane of each cartridge was reserved to run the PanCancer IO 360™ Panel Standard, containing a pool of synthetic DNA oligonucleotides corresponding to the target sequence of each of the 770 unique probe targets in the panel. Hybridized RNAs were processed on the NanoString nCounter preparation station using the high-sensitivity protocol. The cartridges were then scanned on the nCounter Digital Analyzer (NanoString Technologies, USA) using maximum scan resolution.

NanoString IO 360 data analyses. The analyses were set up according to the protocol provided by the manufacturer. Expression data were normalized and analyzed with the nSolver Analysis Software (version 4.0.62), as suggested by the manufacturer's protocol (LBL-10504 Sept 2017 NanoString PanCancer IO360 Gene Expression Panel Best Practices Guide for FFPE Samples - NanoString Technologies). The means of the supplied positive controls and the geometric mean of the housekeeping genes were used to normalize the measured expression values. Additionally, the Advanced Analysis module (version 2.0.115) was used to perform differential expression analyses between two selected conditions. Briefly, for each gene a single linear regression was fit using all selected covariates to predict expression. A volcano plot was generated to display each gene's -log10 (p-value) and log2 fold change with the selected covariate. Highly statistically significant genes fell at the top of the plot above the horizontal lines, and highly differentially expressed genes fell to either side. Horizontal lines indicated various p-value thresholds. In addition, data were uploaded to ROSALIND software v3.19.0.7 (OnRamp BioInformatics Inc., San Diego, CA) for pathway analyses and cell type profiling analyses..

Cell lines. Human NSCLC cell lines were purchased from ATCC (Manassas, VA, USA) and maintained in the respective culture media, RPMI 1640 1X from Invitrogen (Carlsbad, CA) with 10% v/v FBS, 1% v/v penicillin-streptomycin and 1% v/v glutamine. All cell lines were authenticated by microsatellite analysis, using the PowerPlex kit (Promega Corporation, Madison, WI, USA; last authentication: November 2019). *Mycoplasma spp*. contamination was checked every 2 weeks by RT-PCR; contaminated cells were discharged. The cell features as provided by ATCC are reported in Table 1.

Table 1. Cell lines characteristics

Cell line	Gender	Age	Smoke	Site	Histotype	EGFR
NCI-H1385	F	49	Y	M	Adeno	WT
NCI-H1435	F	35	N	P	Adeno	WT
NCI-H1734	F	56	N	P	Adeno	WT
NCI-H1793	F	52	N	P	Adeno	WT
NCI-H2347	F	54	N	P	Adeno	WT
NCI-H2073	F	47	Y	P	Adeno	WT
NCI-H2228	F	n.d.	N	P	Adeno	Mut (het T790M; het L858R)
NCI-H1975	F	n.d.	N	P	Adeno	WT
NCI-H2066	F	70	n.d.	P	Mixed	WT
NCI-H2286	F	57	Y	P	Mixed	WT
A549	M	58	n.d.	P	Adeno	WT
Calu-3	M	25	n.d.	P	Adeno	WT
NCI-H2087	M	69	Y	M	Adeno	WT
NCI-H23	M	51	n.d.	P	Adeno	WT

NCI-H2126	M	65	n.d.	M	Adeno	WT
NCI-H1299	M	43	n.d.	M	Adeno	WT
NCI-H1437	M	60	Y	M	Adeno	WT
NCI-H1563	M	n.d.	N	P	Adeno	WT
NCI-H661	M	43	n.d.	M	Adeno	WT
NCI-H522	M	58	Y	P	Adeno	WT
NCI-H1651	M	71	N	P	Adeno	WT
NCI-H2085	M	45	n.d.	n.d.	Adeno	WT
NCI-H2342	M	55	N	P	Adeno	WT
NCI-H1703	M	54	Y	P	Squamous	WT
NCI-H441	M	n.d.	n.d.	M	Adeno	WT
NCI-H1650	M	27	Y	P	Adeno	Mut (het p.E746_A750 del)
NCI-H596	M	73	n.d.	P	Mixed	Mut (unknown)
NCI-H460	M	n.d.	n.d.	M	Adeno	Mut (unknown)
NCI-H2170	M	n.d.	N	P	Squamous	Mut (unknown)

F: female; M: male; Y: yes; N: no; P: primary tumor; M: metastasis; Adeno: adenocarcinoma; n.d.: not determined

Flow cytometry. 1×10^4 cells were washed once in PBS and fixed with 4% v/v paraformaldehyde for 5 min, incubated with anti-CD274/PD-L1, fluorescein isothiocyanate (FITC)-conjugated antibody (MIH1; Becton Dickinson, dilution 1/10) and washed 3 times with PBS-FBS 1%. Cells incubated with an isotype control antibody, followed by a FITC-conjugated secondary antibody, were included as control of specificity. The results were analyzed with a Guava® easyCyte flow cytometer (Millipore, Billerica, MA), equipped with the InCyte software (Millipore).

RT-PCR. Total RNA was extracted and reverse-transcribed using iScript^{TM} cDNA Synthesis Kit (Bio-Rad Laboratories). The RT-PCR was performed with the IQ SYBR Green Supermix (Bio-Rad Laboratories). The relative quantitation was performed by comparing each PCR product with the housekeeping gene *S14*, using the Bio-Rad Software Gene Expression Quantitation (Bio-Rad Laboratories). The primer sequences are listed in Table 2.

Table 2. Primers used in the study

Gene	Forward primer	Reverse primer
ERα	CAGGATCTCTAGCCAGGCAC	ATGATCAACTGGGCGAAGAG
ERβ	ACCAAAGCATCGGTCACG	CATGATCCTGCTCAATTCCA
PR	CGATGCAGTCATTTCTTCCA	GTCCTTACCTGTGGGAGCTG
AR	AGTCAATGGGCAAAACATGG	TTGTGTCAAAAGCGAAATGG
CXCL12	TCAGCCTGAGCTACAGATGC	CTTTAGCTTCGGGTCAATGC
IGFBP4	CGCAACGGCAACTTCCACC	CAGGCCTCACTCTCGAAAGC
ABCA3	GGCCATCATCATCACCTCCCACAGCA	AGCGCCTCCTGTTGCCCTTCACTCTG
FSHR	CTCACCAAGCTTCGAGTCATCCAA	GCTCATCTA-GTTGGGTTCCATT
LHR	CCGGAAGGCGTCGTTGTGCAT	GCGTCGACCTCCGGGCCAT
PD-L1	CACGGTTCCCAAGGACCTAT	GGCCCTCTGTCTGTAGCTAC
CD274/PDL-1 promoter ERE1	AAAGGGAGCACACAGGCACG	CAAGATGACAGACGATGGTGT
CD274/PDL-1 promoter ERE2	ACAGCTTTATTCCTAGGACACCA	CCAAGGCAGCAAATCCAGTT
Non-specific primers (ChIP)	GTGGTGCCTGAGGAAGAGAG	GCAACAAGTAGGCACAGCA
S14	GGTGCAAGGAGCTGGGTAT	TCCAGGGGTCTTGGTCCTATTT

ERα: estrogen receptor α; ERβ: estrogen receptor β; PR: progesterone receptor; AR: androgen receptor; CXCL12: C-X-C Motif Chemokine Ligand 12; IGFBP4: insulin-like growth factor binding protein 4; ABCA3: ATP binding cassette transporter A3; FSHR: follicle stimulating hormone receptor; LHR; luteinizing hormone receptor; PD-L1: programmed cell death 1-ligand 1; ERE: estrogen response element.

17-β-estradiol, progesterone, testosterone measurement. 17-β-estradiol, progesterone, testosterone were measured spectrophotometrically in the supernatants of 1×10^6 cells, using the Human Estradiol E2 ELISA Kit, the Human Progesterone ELISA Kit , the Testosterone ELISA Kit (all from Abcam, Cambridge, UK) as per manufacturer's instructions. Results were expressed in pg/ml (17-β-estradiol) or ng/ml (progesterone, testosterone).

Immunoblot. Cells were lysed in MLB buffer (125 mM Tris-HCl, 750 mM NaCl, 1% v/v NP40, 10% v/v glycerol, 50 mM $MgCl_2$, 5 mM EDTA, 25 mM NaF, 1 mM $NaVO_4$, 10 mg/ml leupeptin, 10 mg/ml pepstatin, 10 mg/m1 aprotinin, 1 mM phenylmethylsulphonyl fluoride, pH 7.5), sonicated and centrifuged at 13,000 g for 10 min at 4°C. Nuclear extracts were prepared using the Nuclear Extract kit (Active Motif, La Hulpe, Belgium). 30 µg of proteins of whole cell lysate and 10 µg of nuclear proteins were subjected to immunoblotting, using the following antibodies: anti-ERα (ab75635, Abcam, dilution 1/400), anti-phospho(Ser118)ERα (E91, Abcam, dilution 1/1000), anti-PR (αPR6, Abcam, dilution 1/500), anti-AR (ER179(2), Abcam, dilution 1/2500), anti-aromatase (ab35604, Abcam, dilution 1/800), anti-EGFR (EP38Y, Abcam, dilution 1/5000), anti-phospho(Thr308)Akt (6F5, Millipore, dilution 1/1000), anti-Akt (SKB1, Millipore, dilution 1/500), anti-phospho(Thr202/Tyr204)-ERK1/2 (#9101, Cell Signalling Technology, dilution 1/1000, Danvers, MA), anti-ERK1/2 (137F5, Cell Signalling Technology, dilution 1/1000). Anti-β-tubulin (sc-5274, Santa Cruz Biotechnology Inc., Santa Cruz, CA, dilution 1/1000) and anti-TFIID/TATA box-binding protein (TBP) (58C9, Santa Cruz Biotechnology Inc., dilution 1/250) antibodies were used as control of equal protein loading. The proteins were detected by enhanced chemiluminescence (Bio-Rad Laboratories).

Promoter analysis and chromatin immunoprecipitation (ChIP). The ERE sites on *CD274/PD-L1* promoter were identified using the Transfac® Database ([2]). ChIP samples were prepared as described previously [54], using ChiP grade anti-ERα (E115, Abcam, dilution 1/600) or anti-ERβ (14C8, Genetex, Irvine, CA, dilution 1/500) antibodies. Primers for ERE1 and ERE2 site in *CD274/PD-L1* promoter, and primers mapping on a non-specific 10000 bp upstream sequence used as negative internal controls, are reported in the table above. The immunoprecipitated products were amplified by RT-PCR. The signal of non-specific primers was subtracted from the signal of EREs sequence.

Akt, ERK1/2 and EGFR activity. Akt and ERK1/2 activities were measured fluorometrically in cell lysates using the TruLight Akt1/PKBα Kinase Assay kit (Merck, Kenilworth, NJ) and the TruLight ERK1/2 Assay kit (Merck), respectively. Results were expressed as relative fluorescence units (RFU)/mg cellular proteins. The kinase activity of EGFR was measured with the chemiluminescence-based EGFR Kinase Assay kit (Promega Corporation). Results were expressed as relative luminescence units (RLU)/mg cellular proteins.

Phospho(Ser118)ERα quantitative measurement. The amount of phospho(Ser118)ERα in cell lysates was measured with the RayBio® Human Phospho-Estrogen receptor (Ser118) ELISA Kit (RayBiotech, Norcross, GA). Results were expressed as optical density (OD) units/mg cellular proteins.

EGFR knock-out and over-expression. 5×10^5 cells were transduced with 1 μg CRISPR pCas vectors (EGFR Human Gene Knockout Kit, #KN414877, Origene, Rockville, MD, USA) targeting EGFR, following the manufacturer's instructions. Stable KO cells were selected in medium containing 1 μg/ml puromycin for 4 weeks. 5×10^5 knocked-out cells were then transduced with 1 μg EGFR (NM_005228) Human Mutant ORF Clone (L858R) (RC400290, Origene) and selected medium containing 1 mg/ml neomycin for 3 weeks to generate stable clones. The presence of L858R EGFR was verified by RT-PCR using the primers provided by the manufacturer.

***In vivo* experiments.** 1×10^6 female-derived NCI-H1385 and NCI-H1975 cells, mixed with 100 µl matrigel, were injected subcutaneously (s.c.) in female NOD SCID gamma mice engrafted with human hematopoietic $CD34^+$ cells (Hu-$CD34^+$; The Jackson Laboratories, Bar Harbor, MA). 1×10^6 male-derived A549 and NCI-H1650 cells, mixed with 100 µl matrigel, were injected s.c. in male Hu-$CD34^+$ mice. Animals were housed (5 per cage) under 12 h light/dark cycle, with food and drinking provided *ad libitum*. Tumor growth was measured daily by caliper, according to the equation $(LxW^2)/2$, where L=tumor length and W=tumor width. When tumor reached the volume of 100 mm^3, mice were randomized. In a first experimental set, animals were divided in the following groups: 1) Vehicle group, treated intraperitoneally (i.p.) with 100 µl saline solution (days 1, 7, 14, 21, 28, 35 after randomization); 2) Pembrolizumab group, treated with 10 mg/kg i.p. of 100 µl saline solution of the drug (day 1), followed by 5 mg/kg i.p. (days 7, 14, 21, 28, 35); 3) letrozole group, treated with 1 mg/kg *per os* of 100 µl saline solution of the drug daily (days 1-35); 4) Pembrolizumab + letrozole group, treated with 10 mg/kg i.p. of 100 µl saline solution of Pembrolizumab (day 1), followed by 5 mg/kg i.p. (days 7, 14, 21, 28, 35) and 1 mg/kg *per os* of 100 µl saline solution of letrozole daily (days 1-35). Mice were euthanized on day 40 with zolazepam (0.2 ml/kg) and xylazine (16 mg/kg). In a second experimental set, animals were left untreated after day 35, to monitor PFS and OS. In a third set, animals were treated 5 weeks with Pembrolizumab + letrozole as in group 4), then divided into 3 cohorts: the first cohort of animals was left untreated until week 15; the second cohort was treated with 1 mg/kg *per os* of 100 µl saline solution of letrozole daily until week 15; the third cohort was treated with 1 mg/kg *per os* of 100 µl saline solution of letrozole daily from week 6 to week 10, then treated with Pembrolizumab + letrozole as in group 4), from week 11 to week 15. Mice were euthanized at week 15. Animal care and experimental procedures were approved by the Bio-Ethical Committee of the Italian Ministry of Health (#627/2018-PR, 10/08/2018).

Tumor cells and tumor infiltrating lymphocyte (TILs) analysis. Tumors were resected, digested with 1 mg/ml collagenase and 0.2 mg/ml hyaluronidase (1 h at 37 °C) and filtered using a 70 µm-cell strainer to obtain a single cell suspension. Tumor cells were isolated with the Tumor Cell Isolation

Kit (Miltenyi Biotec, Teterow, Germany) and stained with an anti-CD274/PD-L1 antibody (Becton Dickinson). Non-tumor cells were enriched in TILs with the Pan T Cell Isolation kit (Miltenyi Biotec) and stained with the following antibodies (Miltenyi Biotec, dilution 1/10 if not otherwise specified): anti-CD8 (BW135/80) for $CD8^+$ T-lymphocytes; anti-CD56 (AF127H3) for natural killer (NK) cells; anti-TCR Vγ9 (Becton Dickinson, dilution 1/50) for Vγ9Vδ2 T-lymphocytes. Each population was co-stained with anti-Ki67 (REA183) and anti-INF-γ (REA600) antibodies. Cells were quantified using a Guava® easyCyte flow cytometer and InCyte software. Results were expressed as percentage of $CD8^+Ki67^+IFN\gamma^+$cells over $CD8^+$cells, $CD56^+Ki67^+IFN\gamma^+$cells over $CD56^+$cells, $V\gamma9^+Ki67^+IFN\gamma^+$over $V\gamma9^+$cells.

Lipidome analysis. Samples were prepared using the automated MicroLab STAR® system (Hamilton, Reno, Nevada). Samples were homogenized in deionized water. A portion of each homogenate was reserved for Bradford quantification of proteins for normalization purposes. The rest of each homogenate was subjected to a modified Bligh-Dyer extraction using methanol/water/dichloromethane in the presence of internal standards. The extracts were concentrated under nitrogen and reconstituted in 0.25mL of 10mM ammonium acetate dichloromethane:methanol (50:50). The extracts were transferred to inserts and placed in vials for infusion-MS analysis, performed on a LC with nano PEEK tubing and the Sciex SelexIon-5500 QTRAP (Shimadzu, Kyoto, Japan). The samples were analysed via both positive and negative mode electrospray. The 5500 QTRAP scan was performed in MRM mode with the total of more than 1,100 MRMs. Individual lipid species were quantified by taking the peak area ratios of target compounds and their assigned internal standards, then multiplying by the concentration of internal standard added to the sample. Lipid species concentrations were background-subtracted using the concentrations detected in process blanks (water extracts) and run day normalized (when applicable). The resulting background-subtracted, run-day normalized lipid species concentrations were then used to calculate the lipid class and fatty acid total concentrations, as well as the mol% composition values for lipid species, lipid classes, and fatty acids. Raw data was extracted, peak-identified and quality-checked

processed using Metabolon's hardware and software. Compounds were identified by comparison to library entries of purified standards or recurrent unknown entities, based on authenticated standards that contain the retention time/index (RI), mass to charge ratio (*m/z)*, and chromatographic data including mass spectrometry/mass spectrometry (MS/MS) spectral data on all molecules present in the library. Furthermore, biochemical identifications were based on three criteria: retention index within a narrow RI window of the proposed identification, accurate mass match to the library +/- 10 ppm, the MS/MS forward and reverse scores between the experimental data and authentic standards. The MS/MS scores are based on a comparison of the ions present in the experimental spectrum to the ions present in the library spectrum. While there may be similarities between these molecules based on one of these factors, the use of all three data points can be utilized to distinguish and differentiate biochemical compounds. Raw data are available at https://portal.metabolon.com/.

Membrane fluidity. Membrane fluidity was measured fluorometrically using the Membrane Fluidity Kit (#ab189819, Abcam), as per manufacturer's instructions, using a Synergy HTX 96 well reader. Results were expressed as relative fluorescence unit, considering the fluorescence units of untreated cells as 1.

In vitro PD-1/PD-L1 binding assay. 35 x 10^3 HEK-293 cells were seeded into 96-well plates and transiently transfected with PD-L1 and T cell receptor, using the components of the PD-1:PD-L1/PD-L2 Cell-Based Inhibitor Screening Assay Kit following the manufacturer's instructions (BPS Bioscience, San Diego, CA). HEK-293 cells were co-incubated at 1:1 ratio overnight with growth-arrested PD-1/NFAT reporter-Jurkat cells, constitutively transfected with luciferase (BPS Bioscience). NFAT-luciferase activation is inhibited when PD-1 is bound by PD-L1, but it increases when the binding decreases. The chemiluminescence was measured with a Synergy HTX 96 well reader. Results, taken as an index of PD-1/PD-L1 binding, were expressed as relative luminescence units, considering the luminescence units of untreated cells as 1.

Spheroid generation. NSCLC cell line 1.5 × 10^4 cells/well were seeded in ultra-low attachment 96 well plates (Corning, NY, United States), 100 µl medium.. After 48 h spheroids started to form cells

were controlled daily by regular light microscopy. Spheroid growth was monitored using live-cell phase contrast microscope (Axio Observer, Zeiss) and spheroid area was measured by Fiji software.

Real time metabolic profiling. Real-time measurements of oxygen consumption rate (OCR) and extracellular acidification rate (ECAR) were made using a Seahorse XFe96 Extracellular Flux Analyzer (Agilent Technologies, Santa Clara, CA). OCR was measured by using the Seahorse XFe96 Mito Stress Test Kit under basal conditions (i.e. in unbuffered DMEM medium pH 7.4 supplemented with 10 mM glucose and 2 mM glutamine) and in response to 1 μM oligomycin, 1.5 μM of carbonylcyanide-4- (trifluoromethoxy)-phenylhydrazone (FCCP) and 1 μM of Antimycin and Rotenone. ECAR was measured using the Glycolysis Stress Test kit, in basal conditions (i.e. in unbuffered DMEM medium pH 7.4 supplemented with 2 mM glutamine) and in response to 10 mM glucose, 1 μM oligomycin and 50 mM of 2-Deoxy-D-glucose (2- DG). All reagents were from Agilent. Data were then normalized according by the protein content per well, as assessed by Bradford-based protein dosage. Data are the mean ± SEM from 3 separate experiments, with 3 replicates/sample.

Confocal microscopy. Spheroids were cultured on glass cover slips in 24-well plates before incubation with primary antibodies. Before staining, coverslips were rinsed, fixed (4% PFA, 10 minutes, room temperature), permeabilized (0.1% saponin in PBS, 20 minutes, room temperature) and saturated with pre-immune goat serum (1 hour, 4 °C). Cells were then stained with the indicated primary and secondary antibodies and counter-stained with AlexaFluor 568-conjugated phalloidin (1:100) and 4',6-Diamidino-2-phenylindole (DAPI, 1:30,000, both from Thermo Fisher Scientific). Fluorescence was acquired using a TCS SP8 laser scanning confocal microscope, equipped with LAS AF software (both from Leica Microsystems, Milan, Italy). Pixel intensity was calculated using the ImageJ software.

Statistical analysis. All data are provided as means ± SD. The results were analyzed by a one-way analysis of variance (ANOVA), using Statistical Package for Social Science (SPSS) software (IBM SPSS Statistics v.19). $p<0.05$ was considered as significant. The sample size for animal studies was

calculated with the G*Power software (www.gpower.hhu.de), setting $\alpha<0.05$ and $1-\beta=0.80$. OS was defined as the time passed from the starting of treatment to the date of death. PFS was defined as the time passed from the starting of treatment to the time of tumor re-growth ($\geq$10% of increase in tumor volume, confirmed in three consecutive measures). The Kaplan-Meier method was used to calculate OS and PFS. Log rank test was used to compare the outcome of each group.

3. Results

3.1 Patients' clinicopathological features

A total of 86 NSCLC patients met the inclusion criteria and were considered for further analyses. Baseline demographic and clinicopathological characteristics are summarized in Table 3.

	All patients N = 86	
	N.	%
Age		
30-49	6	7
50-69	14	16
70-89	66	77
Sex		
Female	36	42
Male	50	58
Smoking		
Never	11	13
Ex/Current	75	87
TNM stage*		
IB-IIIC	37	43
IV	49	57
Tissue timing		
Baseline	71	83
Re-biopsy	15	17
Histology		
Adeno	67	78
Non-adeno	19	22
PS ECOG		
0	22	26
1	49	57
2	15	17
Treatment line		
2nd line	51	59
3rd line	35	41
ICIs		
Nivolumab	65	76
Pembrolizumab	21	24
Best response		
CR+PR+SD	46	53
PD	40	47
OS at 6 months		
> 6 mo	56	65
< 6 mo	30	35
OS at 18 months		
> 18 mo	29	34
< 18 mo	57	66

Table 3. Clinical and pathological features of the patients (*at diagnosis).

Overall patients' median age was 64 years, the majority of them were male (58%), ex- or current smokers at the time of diagnosis (87%). Forty-nine patients (57%) were diagnosed at advanced (stage IV) stage, with 83% of bioptic specimens harvested baseline at first tumor characterization before starting any medical treatments. At the histological evaluation, the majority of patients' tumors had ADC phenotype, with a minority (22%) having other isotypes. ICIs were administered preferentially at second line treatment (51 patients vs 35 at third line) and in most of the case (76%) patients received nivolumab. At the time of treatment beginning, only a slight fraction of patients reported a poor performance status (PS) (17% with PS2) while 83% of them presented good clinical conditions. Response to treatment was radiologically defined based on iRECIST criteria; patients were homogeneously distributed among responders – including Complete Response, Partial Response and Stable Disease – and non-responders (with Progressive Disease). Patients' median follow-up was of 25.5 months (range 4-119) and OS was evaluated at 6 months, where the majority of patients were still alive, and at 18 months, with a 66% of patients dead.

3.2 Gene expression analyses using NanoString IO360

The gene expression profile of our cohort was characterized through transcriptome analysis based on the NanoString nCounter platform. A high-level exploratory view of the data is reported in **Figure 1.** Interestingly, the NSCLC samples included in our cohort were separated into subgroups indicating immune transcriptional diversity within samples.

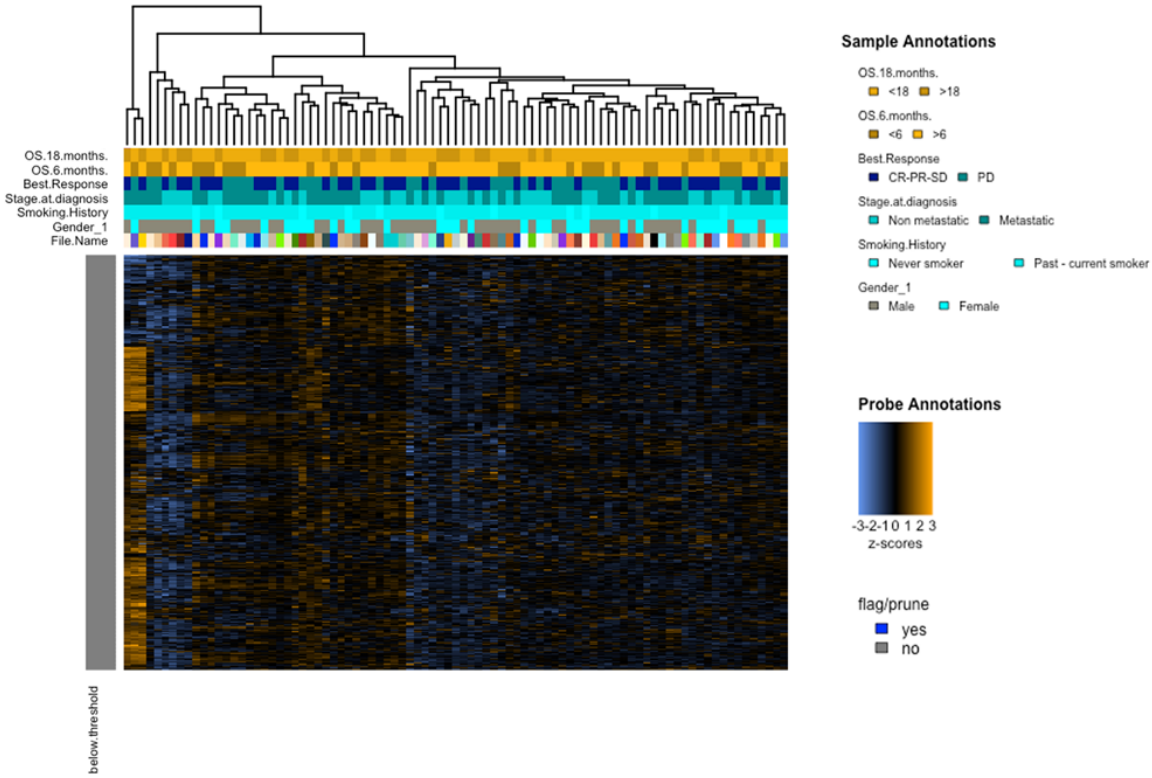

Figure 1. Heatmap of the normalized data, scaled to give all genes equal variance of the NanoString IO360 analysis, was generated via unsupervised clustering through the nSolver Advanced Analysis module.

A differential gene expression analysis was performed between male and female subjects, as shown in **Figure 2A**: few genes were statistically different between the two groups. *ESR1* and *IFI6* were up-regulated (*p-value*s = 0.013 and 0.0352, respectively) while *IL12RB2* resulted down-regulated (*p-value* = 0.0343) in females, compared to the baseline of males. *IL12RB2* was up-regulated (*p-value* = 0.00306), together with *CD209* and *MET* (*p-values* = 0.0082 and 0.0187, respectively) in metastatic cases compared to baseline non-metastatic subjects. *ESR1*, on the contrary, was down-regulated in the same group (*p-value* = 0.0187) (**Figure 2B**). Stratifying cases according to response to treatment, *C5* gene resulted up-regulated (*p-value* = 0.0321) in non-responder subjects, while *IL12RB2*, *ESR1*

and *CCL8* (*p-values* = 0.000308, 0.00162 and 0.0398, respectively) genes showed significantly higher expression levels in responder patients (**Figure 2C**). Patients were also stratified according to overall survival: OS was evaluated at 6 months and at 18 months. In patients with OS>6 months, there was a down-regulation of *MET* (*p-value* = 0.025) and a higher expression level of *TDO2* gene (*p-value* = 0.0375). *ESR1* gene, up-regulated in patients with 0S>6 months without reaching a statistically significant difference compared to cases with OS<6 months (*p-value* = 0.001), showed a significantly higher expression levels in patients with 0S>18 months (*p-value*= 0.00813), together with *IL12RB2* gene (*p-value* = 2.48e-08) (**Figure 2D**).

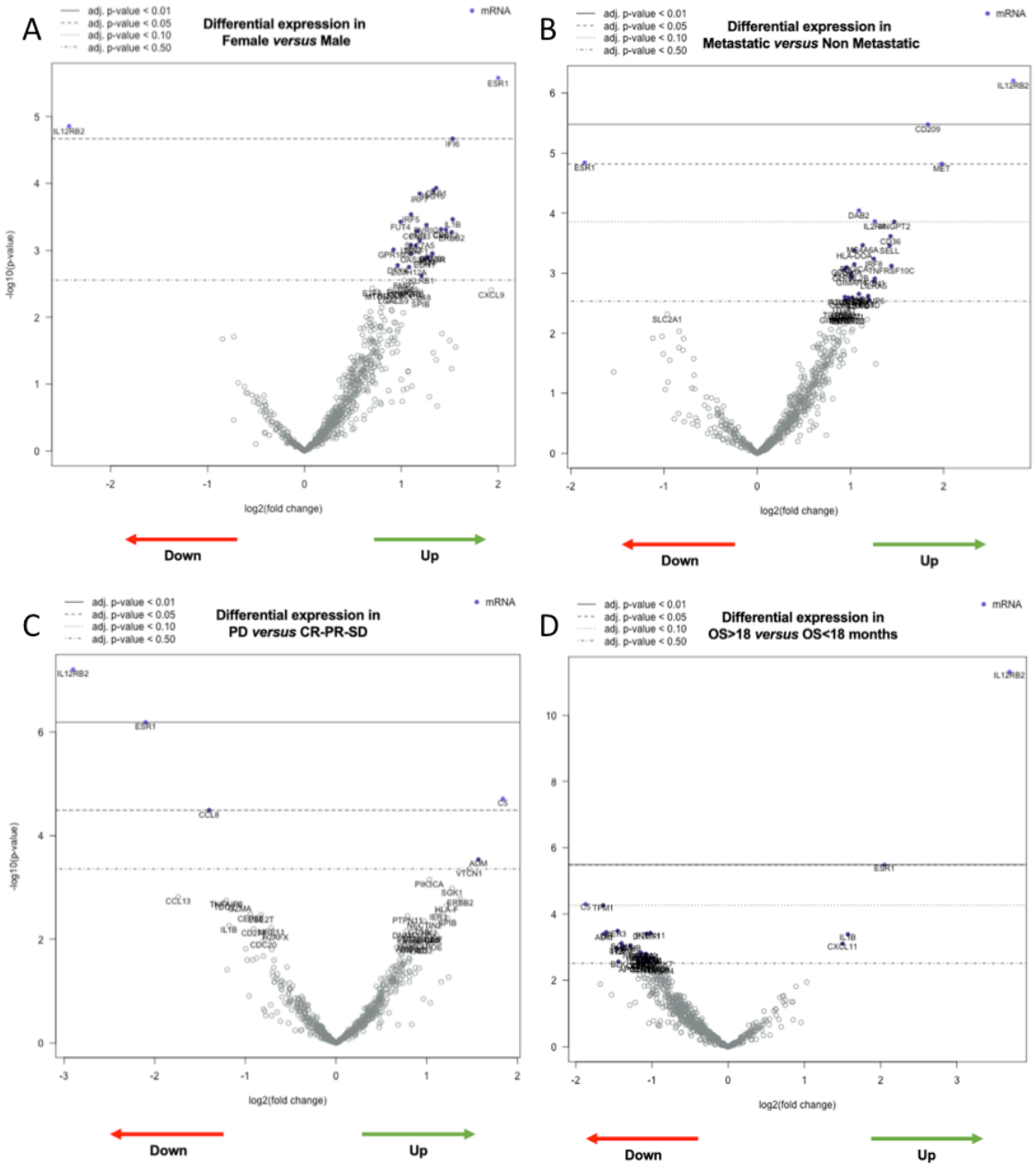

Figure 2. Volcano plots of the differentially expressed genes, obtained from the NanoString IO360 analysis, in female versus male (**A**), metastatic versus non-metastatic patients (**B**), responders (CR, PR, SD: complete response, partial response, stable disease) versus non-responders (PD: progressive disease) (**C**), survival at 18 months (**D**).

3.3 NanoString IO360 identifies differential pathways score and immune cell type profiles

The Pathway Score analysis was interrogated to summarize the data from pathway's genes into a single score, in order to understand if our cohort was affected by pathway changes in relation to treatment response and OS.

Figure 3 shows the pathway scores mapped against response: several signatures resulted down-regulated in non-responder group. In particular, samples from patients who experienced clinical benefit showed higher scores for the following pathways: angiogenesis (*p-value* = 0.0098), antigen presentation (*p-value* = 0.0298), cytokine and chemokine signaling (*p-value* = 0.0102), cytotoxicity (*p-value* = 0.0269), immune cell adhesion and migration (*p-value* = 0.0261), interferon signaling (*p-value* = 0.0321), lymphoid compartment (*p-value* = 0.0250), matrix remodeling (*p-value* = 0.0241), myeloid compartment (*p-value* = 0.0366) and PI3K-Akt (*p-value* = 0.0369) (**Figure 3A**). The pathway scores were mapped also against OS: patients with OS>18 months presented a higher score for lymphoid compartment (*p-value* = 0.0117), cytokine and chemokine signaling (*p-value* = 0.0268), costimulatory signaling (*p-value* = 0.0323), cytotoxicity (*p-value* = 0.0412) and myeloid compartment (*p-value* = 0.0513) (**Figure 3B**).

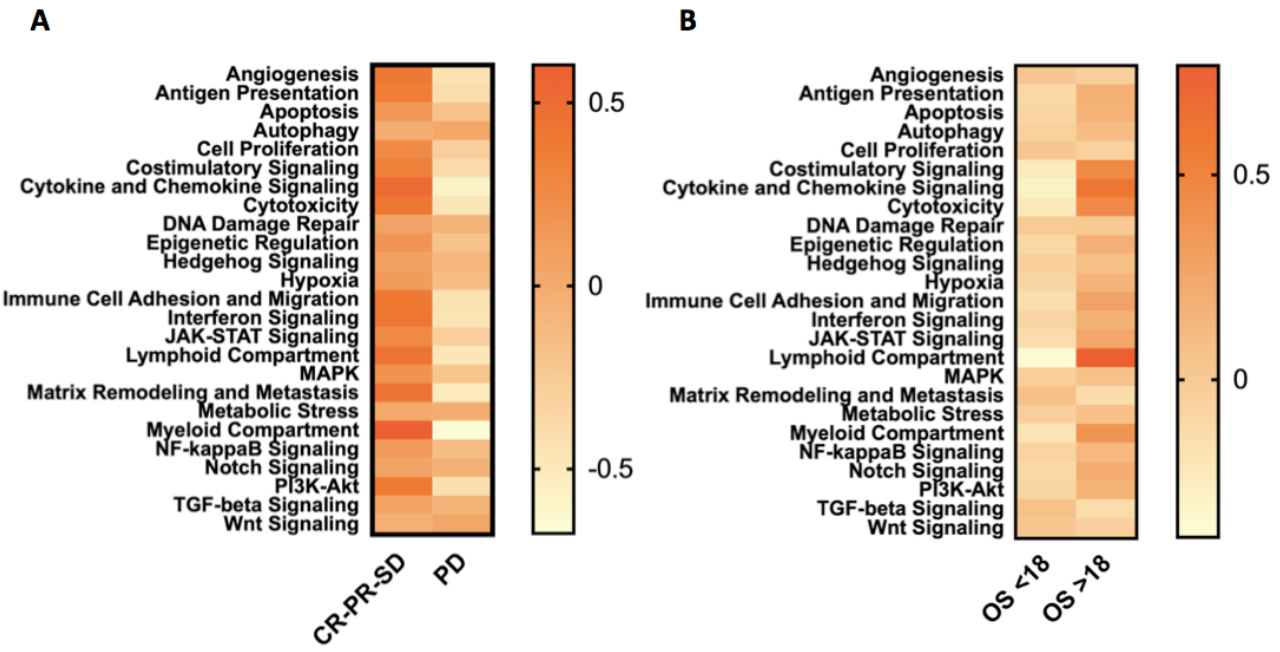

Figure 3. Pathway Score analysis applied to NanoString IO360 data, to identify the most differentially expressed pathways between responders (CR, PR, SD: complete response, partial response, stable disease) versus non-responders (PD: progressive disease) (**A**), and in patients with a different overall survival (OS) rate 18 months (**B**).

Gene expression profiling also correlated with the fluctuation of different immune cell types in the microenvironment of NSCLC cases. Through the nSolver Advanced Analysis module and ROSALIND software, the expression level of genes previously shown to be characteristic of various cell population, were used to measure these populations' abundance. The cell type scores were statistically different between responders and non-responders *(p-value* = 0.0103). A higher expression level related to the following cell populations was identified in responder patients: macrophages (*p-value* = 0.0405), dendritic cells (*p-value* = 0.005), T-cells (*p-value* = 0.0425), CD8 T-cells (*p-value* = 0.0472) and cytotoxic cells (*p-value* = 0.0122). (**Figure 4A**).

Statistically significant differences were also identified between patients with OS< 18 months and OS>18 months (*p-value* < 0.0001). In patients with OS>18 months higher levels of the following cell type scores were detected: dendritic cells (*p-value* = 0.0172), T-cells (*p-value* = 0.0246), CD8 T-cells

(*p-value* = 0.0175), Th1 cells (*p-value* = 0.0353), Treg (*p-value* = 0.0336) and cytotoxic cells (*p-value* = 0.0337) (**Figure 4B**).

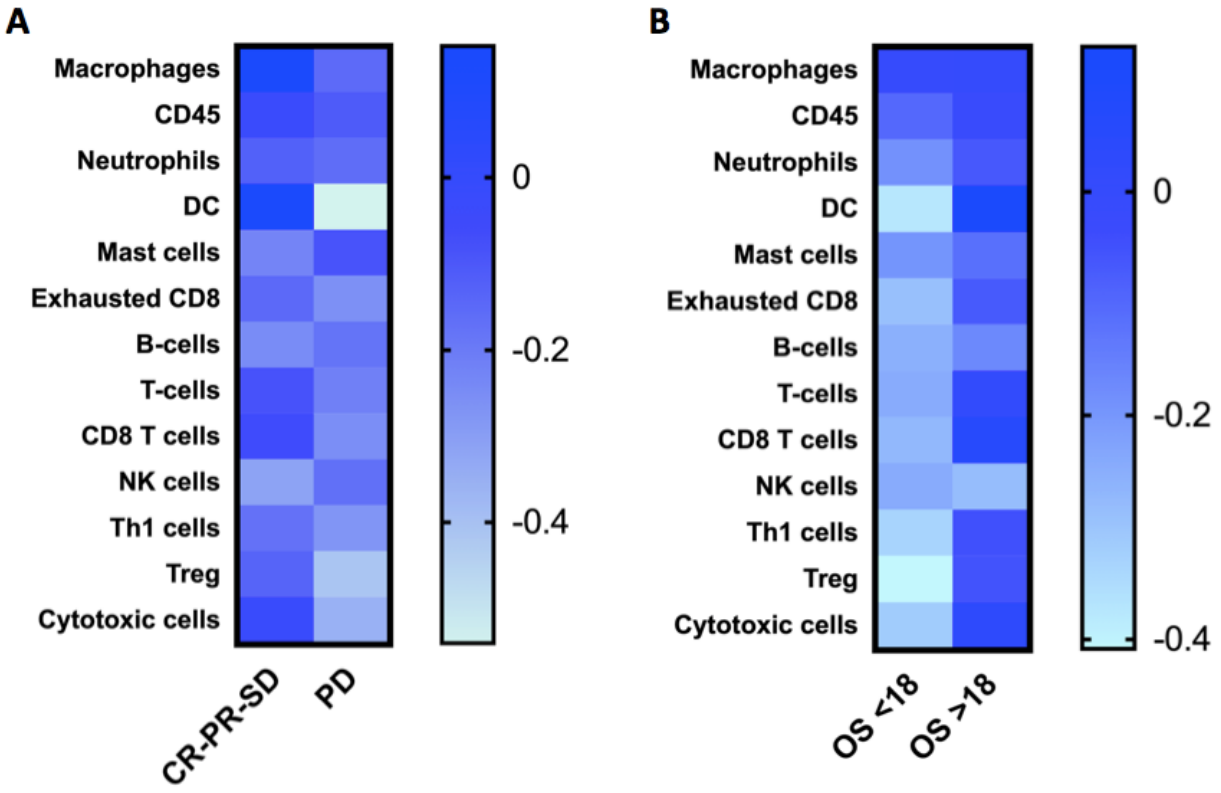

Figure 4. ImmuneScore analysis applied to NanoString IO360 data, performed with nSolver Advanced Analysis module and ROSALIND software, to identify the different immune populations present in responders (CR, PR, SD: complete response, partial response, stable disease) versus non-responders (PD: progressive disease) (**A**), and in patients with a different overall survival (OS) rate 18 months (**B**).

Overall, these data indicate that the most differential expressed genes between genders are *ESR1*, *IFI6* and *IL12RB2*, and that *ESR1* and *IL12RB2* were also associated with a differential response to ICIs. The differentially expressed genes were associated with the up- or down-regulation of different pathways related to immune system activity (cytokine and chemokine signaling, immune cell adhesion and migration, interferon signaling, lymphoid compartment, myeloid compartment) and with different abundance of immune cells infiltrating the tumors. The present thesis is focused on the

role of *ESR1*, encoding for ERα, as the factor most associated with gender and hormonal status of the patients.

3.4 ERα up-regulates PD-L1 in non-small cell lung cancer cells

To have a functional tool to investigate how gender, *ESR1* expression, and response to anti PD-1/PD-L1 are related, we screened a panel of 30 commercially available NSCLC cell lines, derived from male and female patients of different age, primary tumors or metastatic localization, smoking habits (**Table 1**). As shown in **Figure 5A**, there was a positive correlation between the levels of *ERα* mRNA, encoded by *ESR1* gene, and the levels of PDL-1 in the pool of cell lines. The correlation was robust in female-derived cell lines, weak in male-derived cells. A similar correlation, stronger in female-derived cells, was detected between the production of 17-β-estradiol and the amount of PD-L1 (**Figure 5B**). Both *ERα* (**Figure 6A**) and 17-β-estradiol (**Figure 6B**) levels resulted higher in female-derived cell lines than in male-derived cell lines, in cell lines derived from primary tumors than in cell lines derived from metastases. By contrast, PD-L1 levels did not vary in these subgroups (**Figure 6C**). None of these parameters differed in cell lines derived from smokers and non-smoker patients. This screening indicates that the commercial cell lines well recapitulated the findings observed in patients, in terms of *ERα* expression correlated to gender and metastatic status.

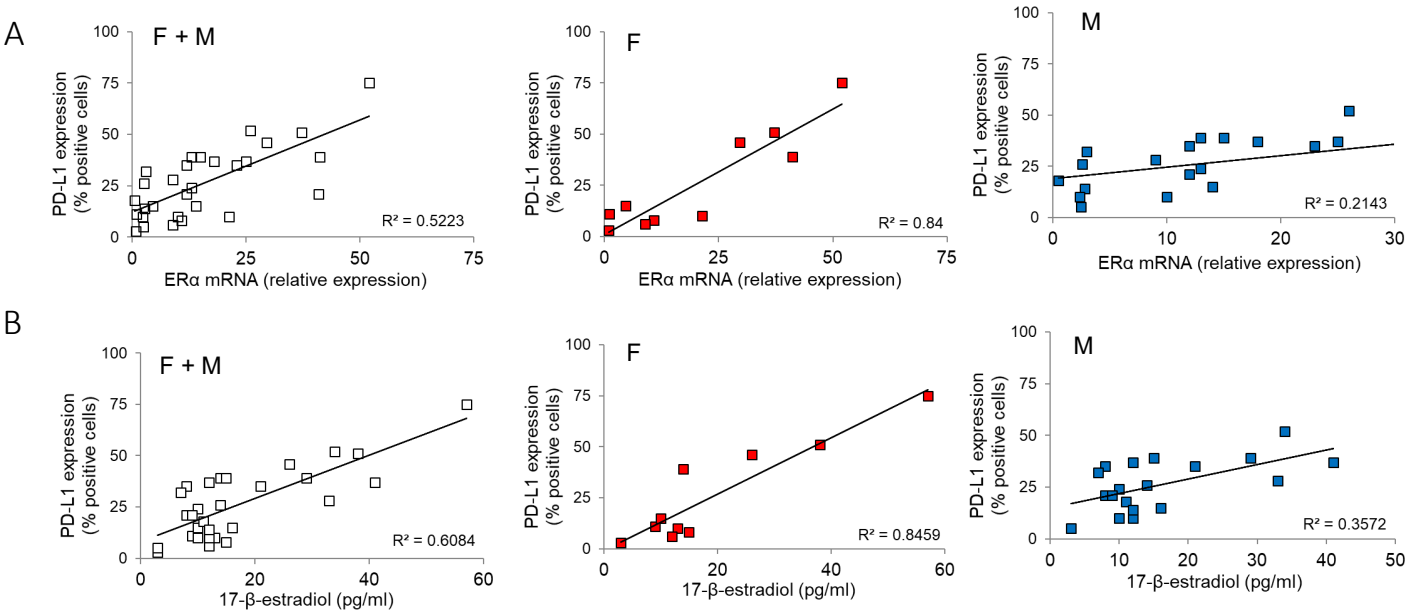
A
F + M
PD-L1 expression (% positive cells)
ERα mRNA (relative expression)
R² = 0.5223
F
R² = 0.84
M
R² = 0.2143
B
F + M
17-β-estradiol (pg/ml)
R² = 0.6084
F
R² = 0.8459
M
R² = 0.3572

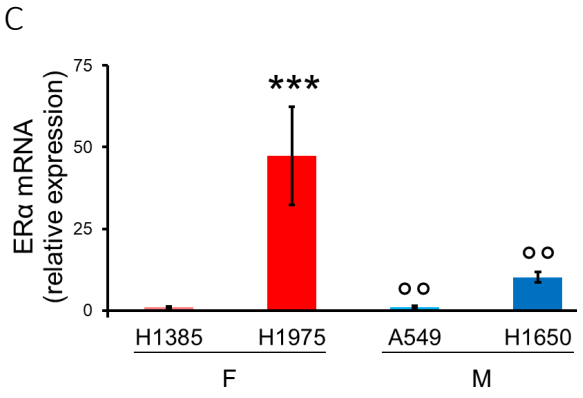
C
ERα mRNA (relative expression)
***
oo
oo
H1385
H1975
A549
H1650
F
M

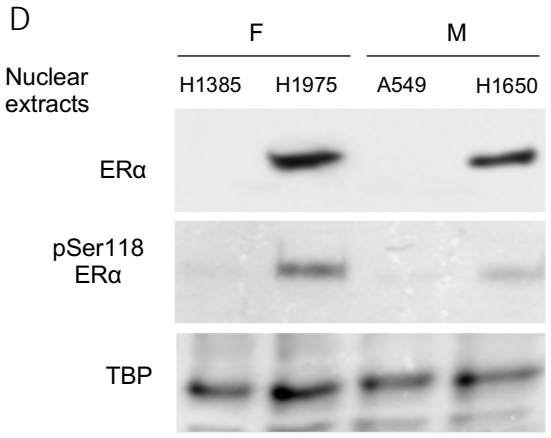
D
F
M
Nuclear extracts
H1385
H1975
A549
H1650
ERα
pSer118 ERα
TBP

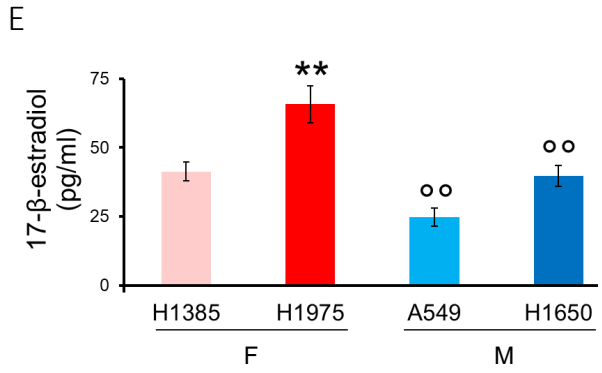
E
17-β-estradiol (pg/ml)
**
oo
oo
H1385
H1975
A549
H1650
F
M

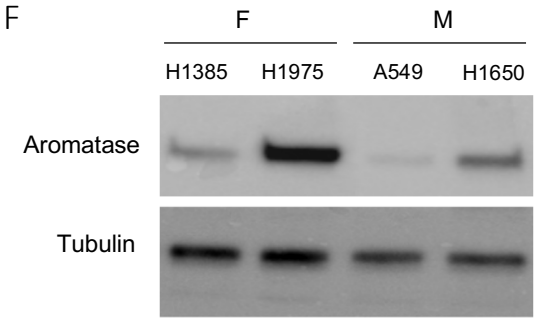
F
F
M
H1385
H1975
A549
H1650
Aromatase
Tubulin

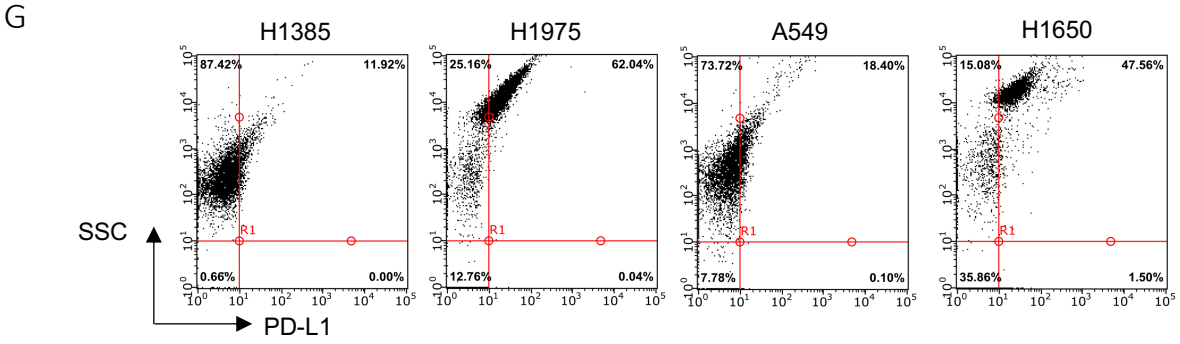
G
H1385
H1975
A549
H1650
87.42%
11.92%
0.66%
0.00%
25.16%
62.04%
12.76%
0.04%
73.72%
18.40%
7.78%
0.10%
15.08%
47.56%
35.86%
1.50%
R1
SSC
PD-L1

Figure 5. ERα, 17-β-estradiol and PD-L1 levels in human non-small cell lung cancer cell lines

A. Expression of ERα mRNA, measured by RT-qPCR in triplicate, plotted versus expression of surface PD-L1, measured by flow cytometry in triplicate, in 30 human NSCLC cell lines derived from female (F) or male (M) patients. **B.** Levels of 17-β-estradiol, measured by ELISA in triplicate, plotted versus expression of surface PD-L1, measured by flow cytometry in triplicate, in 30 human NSCLC cell lines derived from female (F) or male (M) patients. **C.** ERα mRNA, measured by RT-qPCR in triplicate, in female (F)-derived NCI-H1385 and NCI-H1975 cells, and in male (M)-derived A549 and NCI-H1650 cells. The relative expression of ERα in NCI-H1385 cells was considered 1. Data are means ± SD (n=4). ***p<0.001: $^{ERα\ high}$ NCI-H1975 cells versus $^{ERα\ low}$ NCI-H1385; °°p<0.01: male-derived cells versus mean of female-derived cells. **D.** Immunoblot of the indicated proteins in nuclear extracts. TBP is included as control of equal protein loading. The image is representative of 1 out of 3 experiments. **E.** Levels of 17-β-estradiol, measured by ELISA in triplicate. Data are means ± SD (n=3). **p<0.01: $^{ERα\ high}$ NCI-H1975 cells versus $^{ERα\ low}$ NCI-H1385; °°p<0.01: male-derived cells versus mean of female-derived cells. **F.** Immunoblot of aromatase in whole cell extracts. Tubulin is included as control of equal protein loading. The image is representative of 1 out of 3 experiments. **G.** Expression of surface PD-L1, measured by flow cytometry in triplicate. The dot plots are representative of 1 out of 4 experiments. Percentages indicate the positive cells in each quadrant. SSC: side-scatter.

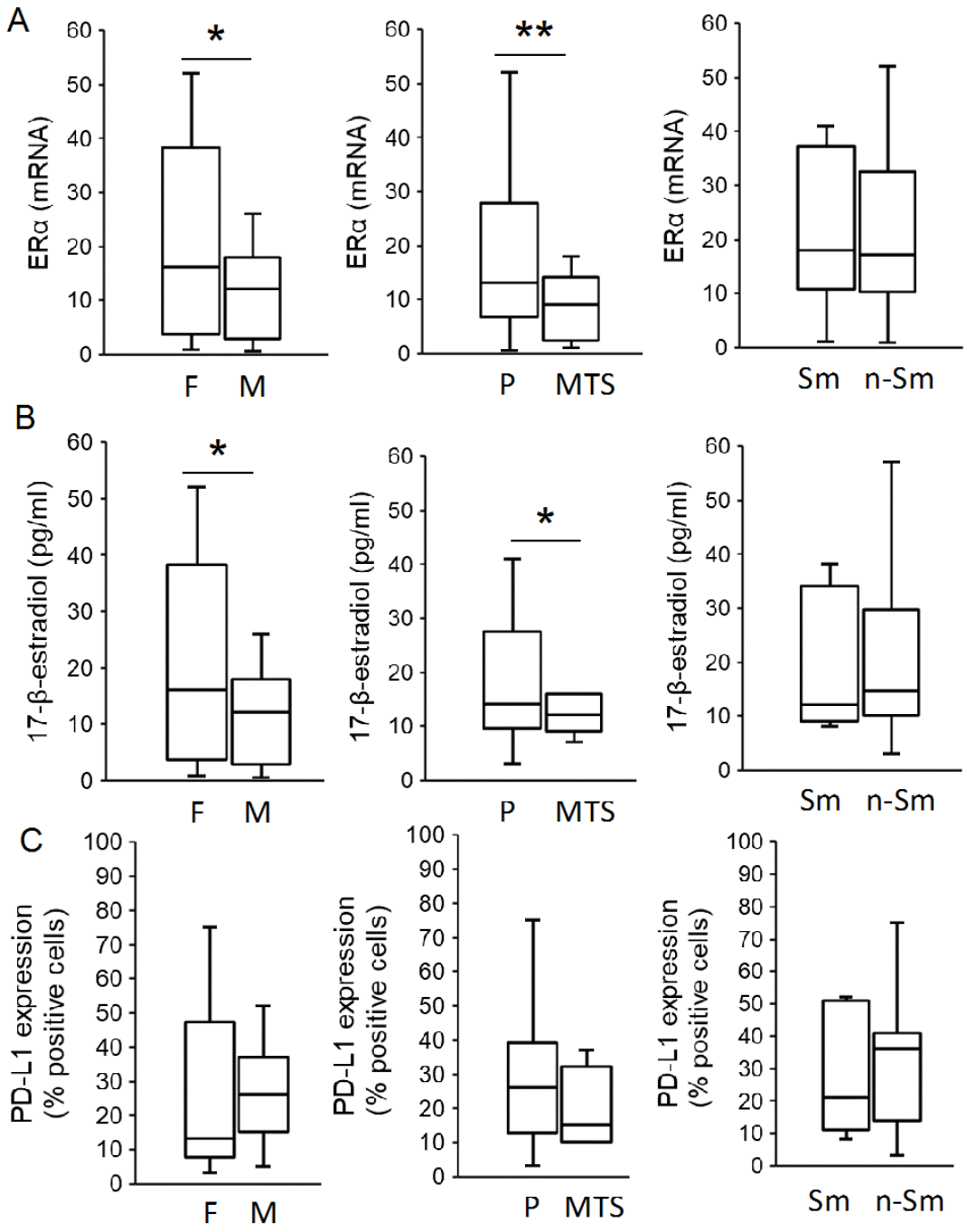

Figure 6. Disaggregated data of ERα, 17-β-estradiol and PD-L1 levels in non-small cell lung cancer cells. A-C. Expression of ERα mRNA, measured by RT-PCR in triplicate (panel **A**), levels of 17-β-estradiol, measured by ELISA in triplicate (panel **B**), expression of surface PD-L1 (panel **C**), measured by flow cytometry in triplicate in 30 human NSCLC cell lines, divided in female (F)- or

male (M)-derived cell lines, primary tumor (P) or metastatic (MTS) localization-derived cell lines, smoker (Sm) or non-smoker (non-Sm) patients. *p<0.05, **p<0.01: F versus M, P versus MTS.

We next focused on the female- and male-derived cell lines with the lowest (NCI-H1385) and highest (NCI-H1975) levels of *ERα*, namely NCI-H1385, NCI-H1975, A59 and NCI-H1650 cells (**Figure 5C**). In all lines, *ERβ* mRNA varied similarly to ERα, although at lesser extent (**Figure 7A**). The correlation between ERβ and PD-L1 levels was low (**Figure 7B**), suggesting that a causal relation between ERβ and PD-L1 was unlikely. We thus focused the attention on ERα: indeed, ERα protein, in particular the active form phospho(Ser118)ERα [Weitsman, 2006], was present in nuclear extracts and followed the expression pattern of mRNA in both female and male-derived cell lines analyzed (**Figure 5D**). Besides being translocated and phosphorylated, ERα was transcriptionally active, since the mRNA levels of three target genes – *CXCL12*, *IGFBP4*, *ABCA3* – varied in accord to the amount of nuclear ERα/phospho(Ser118)ERα protein (**Figure 7C**).

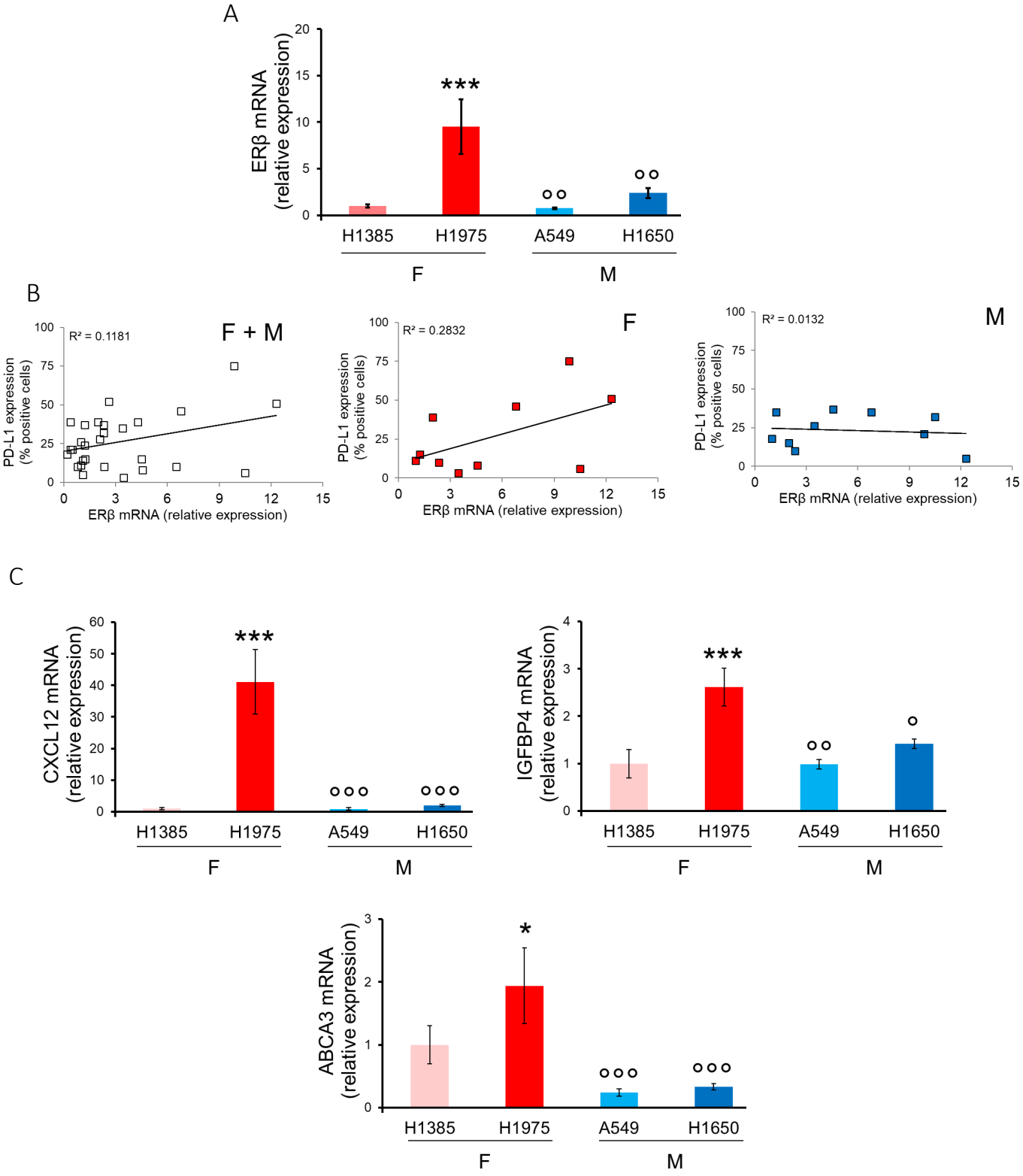

Figure 7. Levels of ERβ and ERα target genes in non-small cell lung cancer cells. A. ERβ mRNA, measured by RT-PCR in triplicate, in female (F)-derived NCI-H1385 and NCI-H1975 cells, and in male (M)-derived A549 and NCI-H1650 cells. The relative expression of ERβ in NCI-H1385 cells

was considered 1. Data are means ± SD (n=3). ***p<0.001: *ERβ high* NCI-H1975 cells versus *ERβ low* NCI-H1385; °°p<0.01: male-derived cells versus mean of female-derived cells. **B.** Expression of ERβ mRNA, measured by RT-PCR in triplicate, plotted versus expression of surface PD-L1, measured by flow cytometry in triplicate, in 30 human NSCLC cell lines derived from female (F) or male (M) patients, in female and in male cells. **C.** Expression of ERα-target genes *CXCL12*, *IGFBP4* and *ABCA3*, measured by RT-PCR in triplicate. The relative expression of each gene in NCI-H1385 cells was considered 1. Data are means ± SD (n=3). *p<0.05, ***p<0.001: *ERα high* NCI-H1975 cells versus *ERα low* NCI-H1385; °p<0.05, °°p<0.01, °°°p<0.001: male-derived cells versus mean of female-derived cells.

Female-derived cell lines had a higher production of 17-β-estradiol than male-derived cell lines (**Figure 5E**). The production is likely of autocrine origin, as suggested by the lack of differences in *FSHR* and *LHR* (**Figure 8A-B**) and by the detection of aromatase. This enzyme was higher in female-derived cells than in male-derived cells, and, within the same gender, higher in 17-β-estradiol highly-producing cells (**Figure 5F**).

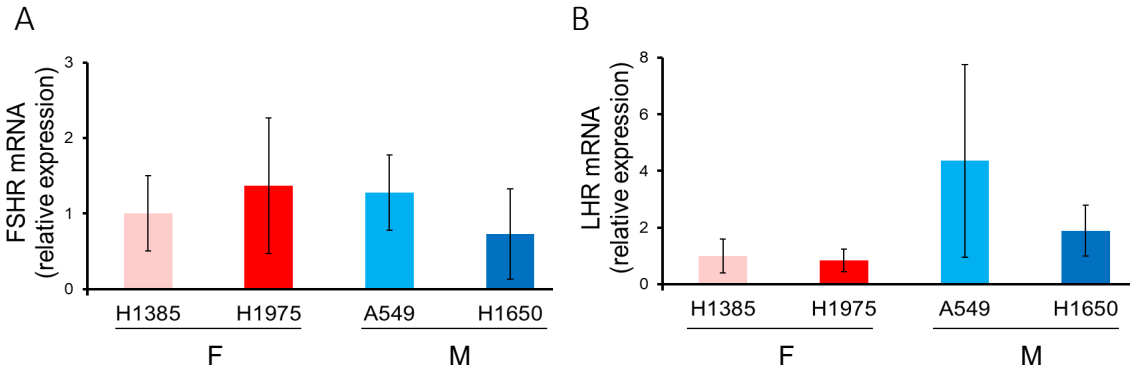

Figure 8. Levels of FSHR and LHR in non-small cell lung cancer cells

FSHR (panel **A**) and *LHR* (panel **B**) mRNA, measured by RT-PCR in triplicate, in female (F)-derived NCI-H1385 and NCI-H1975 cells, and in male (M)-derived A549 and NCI-H1650 cells. The relative expression of each gene in NCI-H1385 cells was considered 1. Data are means ± SD (n=3).

17-β-estradiol/ER was the only steroid hormone-competent axis in the NSCLC cell lines analyzed: indeed, progesterone was homogeneously produced in all the cell lines (**Figure 9A**), testosterone was higher in male-derived cell lines (**Figure 9B**), but the production rate of these hormones was unrelated to the expression levels of the respective receptors as mRNA (**Figure 9C-D**) and protein (**Figure 9E**).

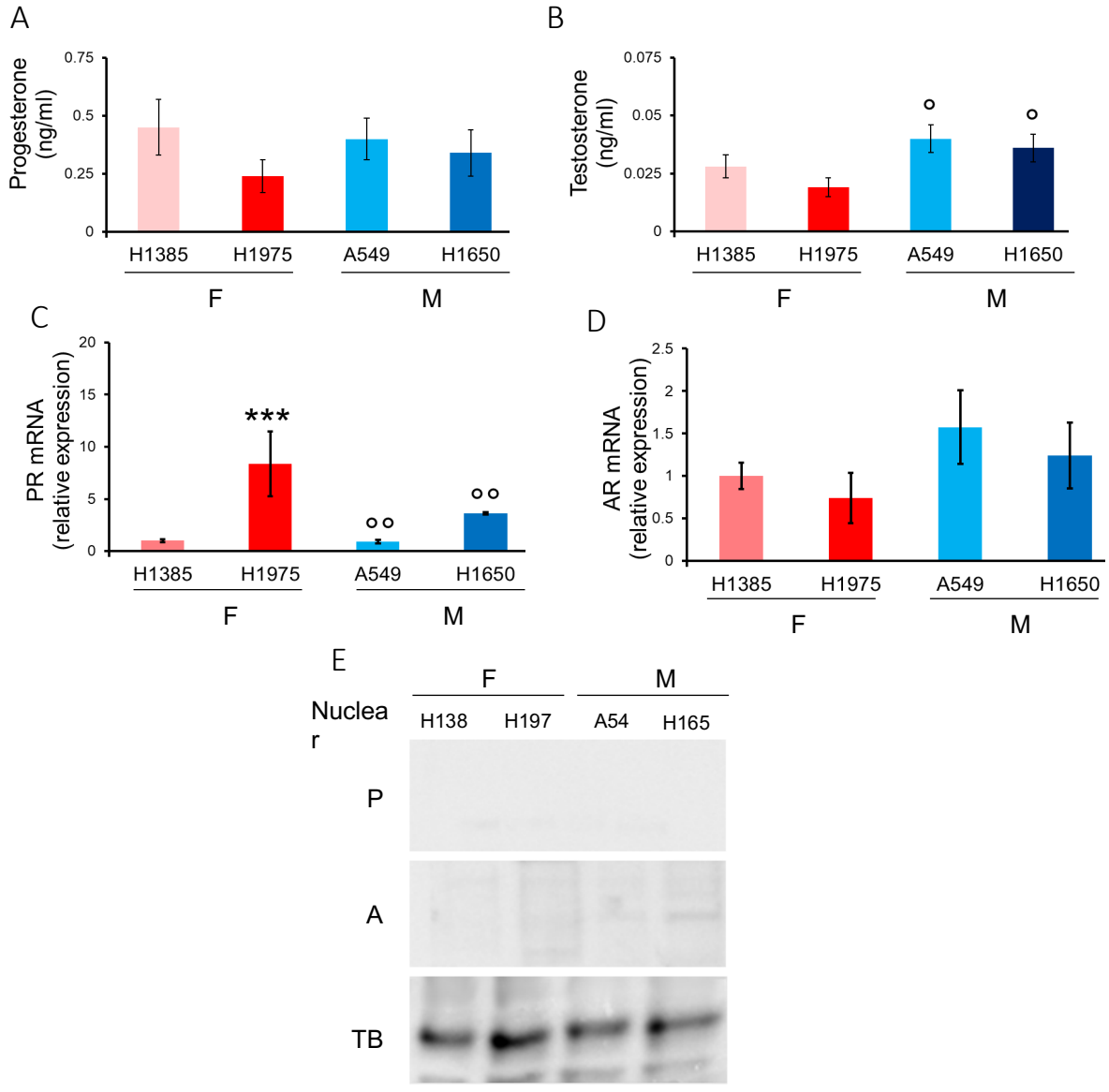

Figure 9. Levels of progesterone, testosterone and respective receptors in non-small cell lung cancer cells. A-B. Levels of progesterone (panel **A**) and testosterone (panel **B**), measured by ELISA in triplicate, in female (F)-derived NCI-H1385 and NCI-H1975 cells, and in male (M)-derived A549 and NCI-H1650 cells. Data are means ± SD (n=3). °p<0.05: male-derived cells versus mean of

female-derived cells. **C-D**. *PR* (panel **C**) and *AR* (panel **D**) mRNA, measured by RT-PCR in triplicate. The relative expression of each gene in NCI-H1385 cells was considered 1. Data are means ± SD (n=3). ***p<0.001: NCI-H1975 cells versus NCI-H1385; °°p<0.01: male-derived cells versus mean of female-derived cells. **E.** Immunoblot of the indicated proteins in nuclear extracts. TBP is included as control of equal protein loading. The image is representative of 1 out of 3 experiments.

In accord with the data obtained on the whole pool cell lines (**Figure 5A-B**), PD-L1 levels on cell surface showed the same expression pattern of 17-β-estradiol/ERα amount, following this rank order: female *17-β-estradiol/ERα high* NCI-H1975 > male *17-β-estradiol/ERα high* NCI-H1650 > female *17-β-estradiol/ERα low* NCI-H1385 ≥ male *17-β-estradiol/ERα low* A549 cells (**Figure 5G**).

To investigate the circuitries linking ERα and PD-L1, we analyzed which of them control the expression of the other. Since the anti-PDL1 inhibitor Atezolizumab, used at blocking concentrations [55], did not change the nuclear levels of ERα and its phosphorylation (**Figure 10**), we excluded that the activity of PD-L1 modulates the expression and activity of ERα.

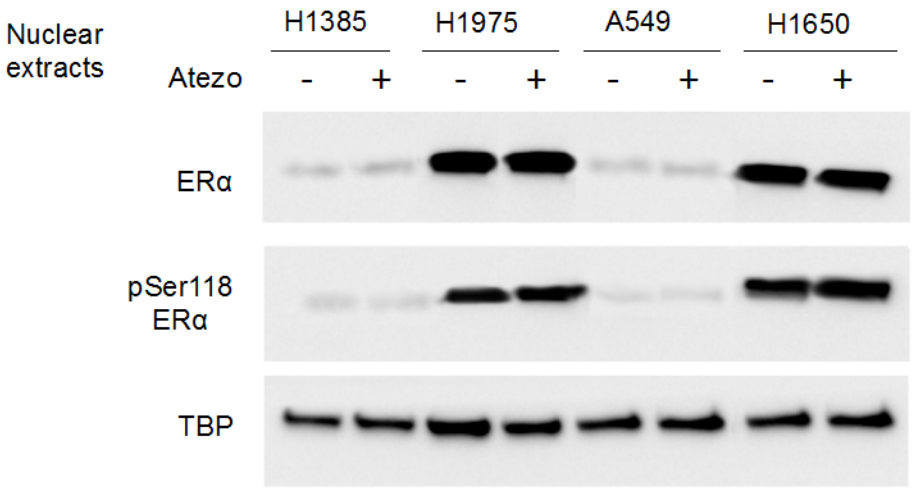

Figure 10. PD-L1 inhibition does not affect amount and phosphorylation of ER α. Female (F)-derived *ERα low* NCI-H1385 and *ERα high* NCI-H1975 cells, and male (M)-derived *ERα low* A549 and *ERα high* NCI-H1650 cells were treated 24 h in the absence (-) or presence (+) of 1 μg/mL Atezolizumab (Atezo), a PD-L1 inhibitor, then lysed and analyzed for the indicated proteins in nuclear extracts.

TBP is included as control of equal protein loading. The image is representative of 1 out of 3 experiments.

To the contrary, the ERα inhibitor fulvestrant and the aromatase inhibitor letrozole, used at concentrations significantly reducing ERα transcriptional activity (**Figure 11A**) or 17-β-estradiol synthesis (**Figure 11B**), decreased the amount of PD-L1 present on the surface (**Figure 12A**) and its mRNA (**Figure 12B**) in female *17-β-estradiol/ERα high* NCI-H1975 cells. The scan of *CD274/PD-L1* promoter highlighted the presence of two EREs (ERE1 and ERE2; **Figure 12C**). Of note, both fulvestrant and letrozole reduced the binding of ERα to ERE1 and – at lesser extent – to ERE2, decreasing the ERα-induced transcription of *CD274/PD-L1* in NCI-H1975 cells (**Figure 12D**). ERβ was significantly less active than ERα (**Figure 13**), confirming that it was not the main isoform controlling PD-L1. Interestingly, the ERα-induced up-regulation of PD-L1 was higher in female-derived than in male-derived cell lines (**Figure 12E-F**), indicating that ERα preferentially up-regulates PD-L1 in female NSCLC cells.

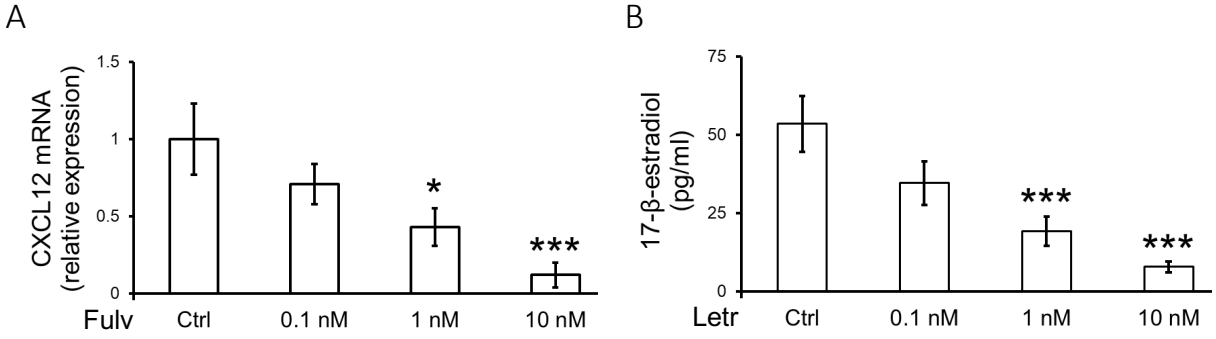

Figure 11. Dose-dependent effects of fulvestrant and letrozole

ERα high NCI-H1975 cells were grown 24 h in fresh medium (Ctrl) or in medium containing 0.1, 1, 10 nM fulvestrant (Fulv, panel **A**), an ERα inhibitor, or 0.1, 1, 10 nM letrozole (Letr, panel **B**), an aromatase inhibitor. As read-out assays, the expression of ERα-target gene *CXCL12* was measured by RT-PCR in triplicate, the amount of 17-β-estradiol was measured by ELISA in duplicate. The

relative expression in Ctrl cells was considered 1. Data are means ± SD (n=3). *p<0.05, ***p<0.001: treated cells versus Ctrl cells.

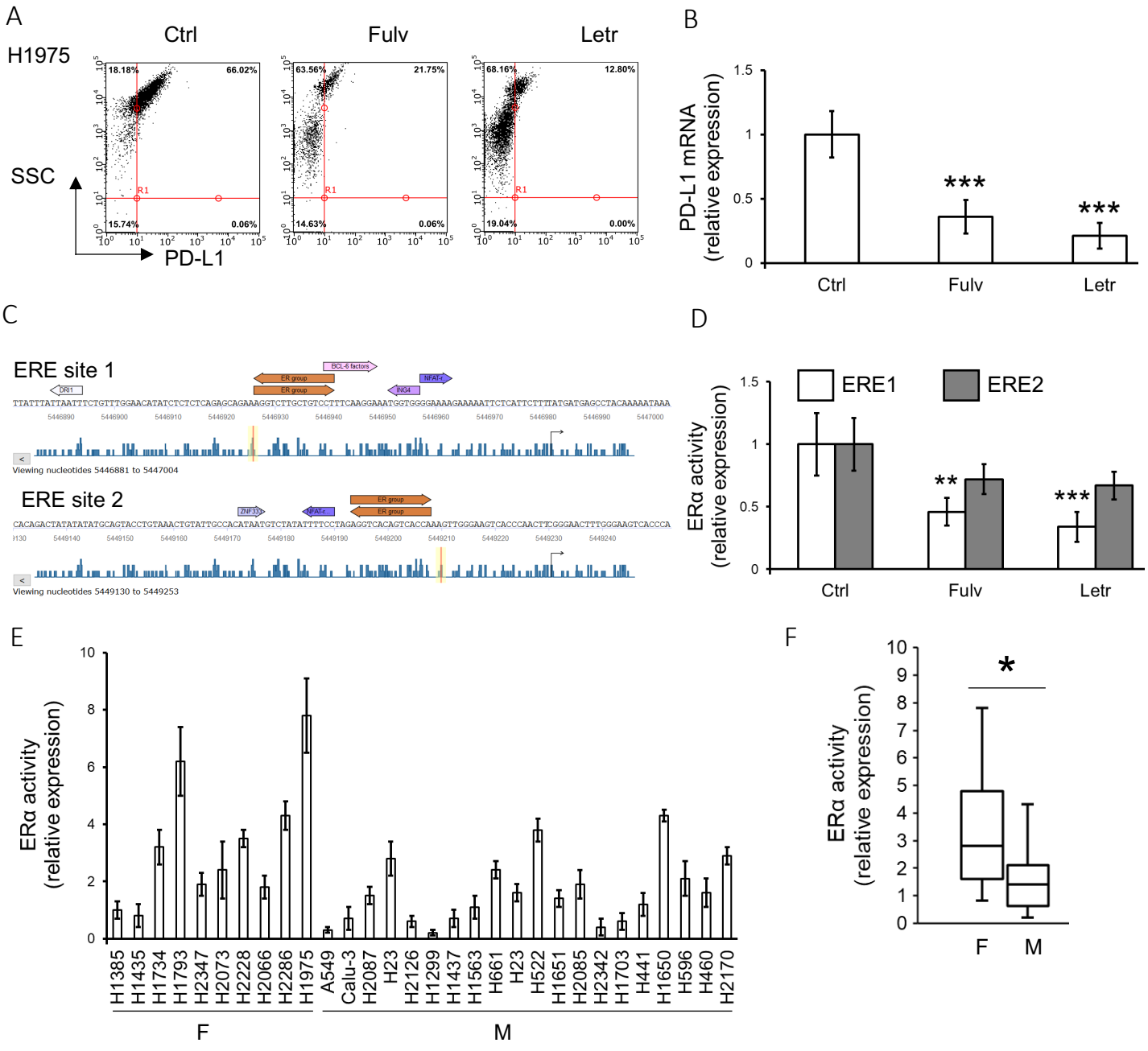

Figure 12. PD-L1 is transcriptionally up-regulated by ERα. *ERα high* NCI-H1975 cells were grown 24 h in fresh medium (Ctrl) or in medium containing 10 nM fulvestrant (Fulv), an ERα inhibitor, or 10 nM letrozole (Letr), an aromatase inhibitor. **A.** Expression of surface PD-L1, measured by flow cytometry in triplicate. The dot plots are representative of 1 out of 3 experiments. Percentages indicate the positive cells in each quadrant. SSC: side-scatter. **B.** *PD-L1* mRNA, measured by RT-PCR in triplicate. The relative expression of *PD-L1* in untreated cells was considered 1. Data are means ± SD (n=3). ***p<0.001: Fulv/Letr-treated cells versus Ctrl cells. **C.** Mapping of ERE1 and ERE2 sites on *CD274/PD-L1* promoter (TRANSFAC® database). **D.** Chromatin immunoprecipitation of ERE1 and ERE2 regions from *CD274/PD-L1* promoter, using an anti-ERα antibody, followed by RT-PCR of the precipitated products. Data are means ± SD (n=3). **p<0.01, ***p<0.001: Fulv/Letr-treated cells versus Ctrl cells. **E.** Chromatin immunoprecipitation of ERE1 from *CD274/PD-L1* promoter, followed by RT-PCR of the precipitated products in 30 human NSCLC cell lines derived from female (F) or male (M) patients. Data are means ± SD (n=3). The activity in NCI-H1385 cells has been considered 1. **F.** Data of panel **E**, pooled for female (F) and male (M) patients. *p<0.05: F versus M.

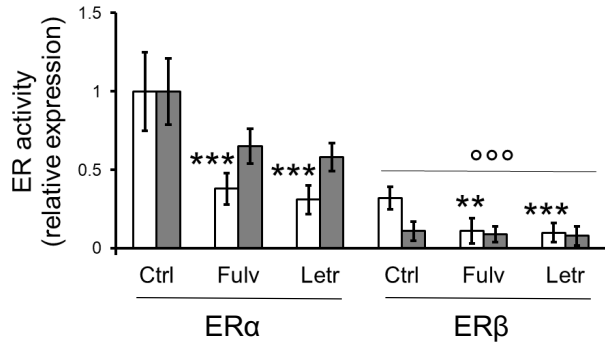

Figure 13. Activity of ERβ on *CD274/PD-L1* promoter. Chromatin immunoprecipitation of ERE1 and ERE2 regions from *CD274/PD-L1* promoter, using an anti-ERα or an anti-ERβ antibody, followed by RT-PCR of the precipitated products, in *ERα high* NCI-H1975 cells, grown 24 h in fresh medium (Ctrl) or in medium containing 10 nM fulvestrant (Fulv), an ERα inhibitor, or 10 nM

letrozole (Letr), an aromatase inhibitor. Data are means ± SD (n=3). **p<0.01, ***p<0.001: treated cells versus Ctrl cells; °°°p<0.001: anti-ERβ versus anti-ERα.

3.5 EGFR signaling contributes to modulate PD-L1 by regulating ERα phosphorylation

Two factors are required for an efficient transcriptional activity of ERα: the binding of 17-β-estradiol and the phosphorylation on Ser118 [56]. Since 17-β-estradiol increases the activity of EGFR and downstream effectors ERK1/2 and Akt [57], two kinases involved in the activation of ERα [58][59], we evaluated the effects of inhibiting doses of MK-2206 (an Akt inhibitor), U-0126 (a ERK1/2 inhibitor) and AZD9291/Osimertinib, a clinically-approved EGFR inhibitor (**Figure 14A-C**), on ERα amount and phosphorylation.

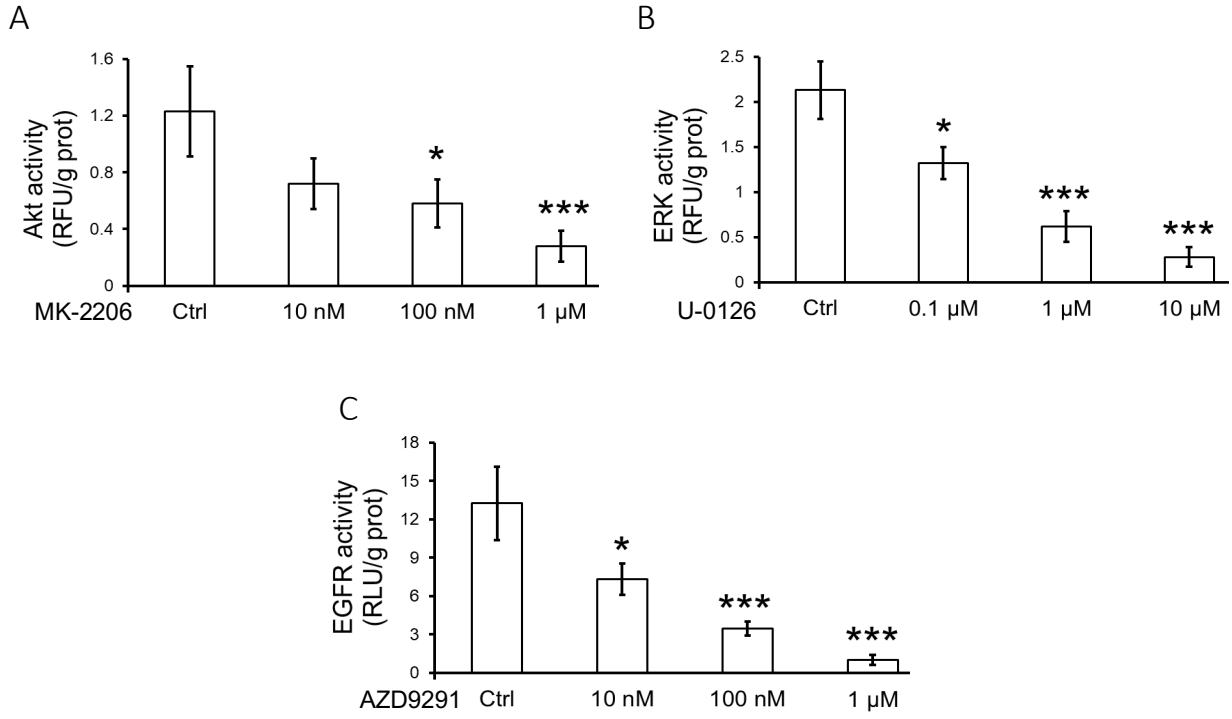

Figure 14. Dose-dependent inhibition of Akt, ERK1/2 and EGFR. *ERα high* NCI-H1975 cells were grown 24 h in fresh medium (Ctrl) or in medium containing 10 nM, 100 nM, 1 μM of the Akt inhibitor MK-2206 (Akti, panel **A**), 0.1 μM, 1 μM, 10 μM of the ERK1/2 inhibitor U-0126 (ERKi, panel **B**), 10 nM, 100 nM, 1 μM of the EGFR inhibitor AZD9291/Osimertinib (EGFRi, panel **C**). As read-out assays, Akt and ERK1/2 activity were measured by ELISA in duplicate, EGFR kinase activity was measured by a chemiluminescence-based assay in duplicate. Data are means ± SD (n=3). *p<0.05, ***p<0.001: treated cells versus Ctrl cells.

None of the inhibitors altered the amount of nuclear ERα, but they all reduced the phosphorylation on Ser118 in NCI-H1975 and NCI-H1650 cells, where it was constitutively higher (**Figure 15A**). These two cell lines shared a higher EGFR signaling than the other cell lines analyzed, as demonstrated by the basally higher phosphorylation of Akt and ERK1/2, effectively reduced by AZD9291 (**Figure 15B**). Indeed, a direct correlation between EGFR activity and ERα phosphorylation on Ser118 emerged from the analysis of the whole pool of NSCLC cell lines (**Figure 15C**). Again, such correlation was stronger in female-derived cells (**Figure 15D**).

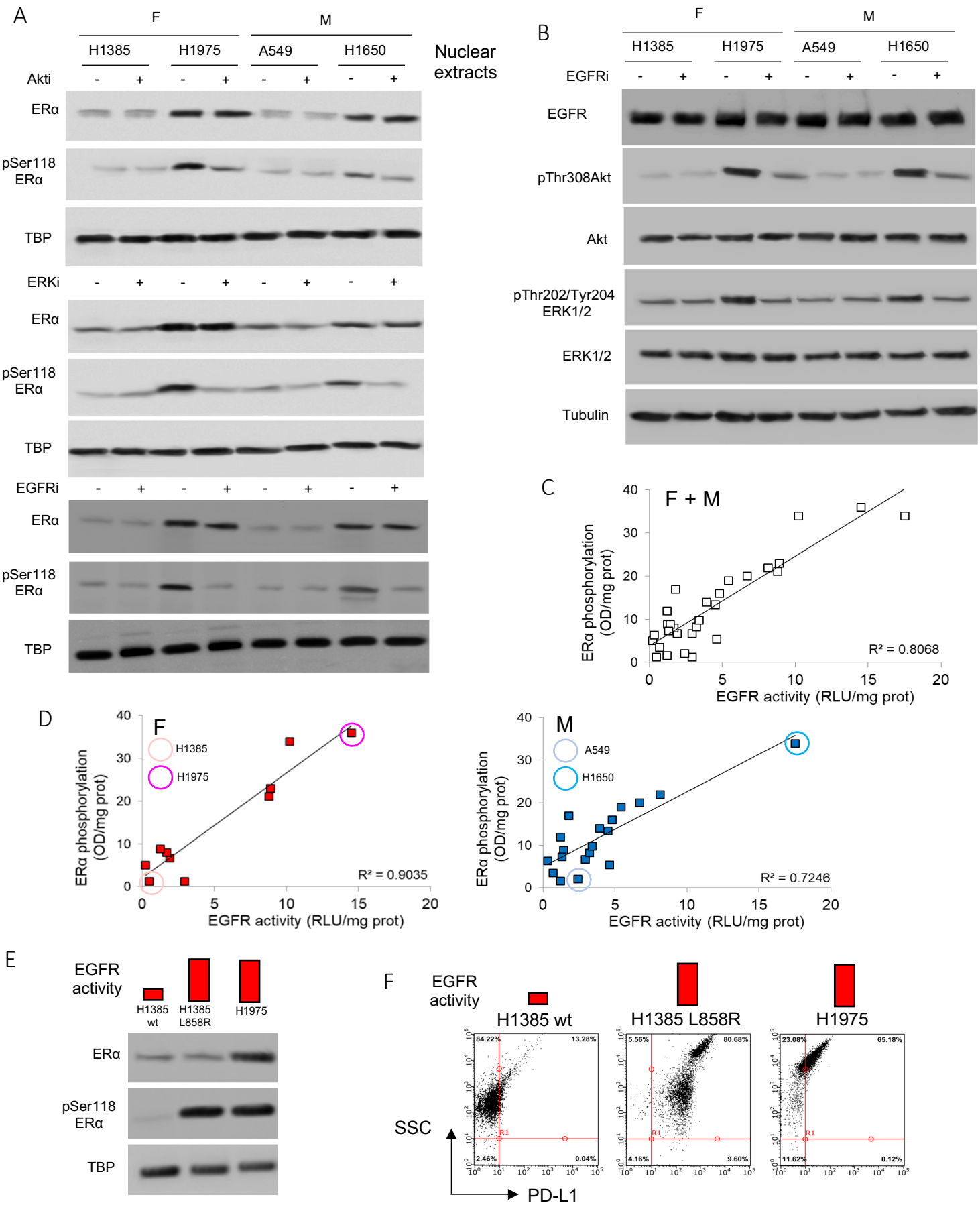
A
F
M
H1385
H1975
A549
H1650
Nuclear extracts
Akti
ERα
pSer118 ERα
TBP
ERKi
EGFRi
B
EGFR
pThr308Akt
Akt
pThr202/Tyr204 ERK1/2
ERK1/2
Tubulin
C
F + M
ERα phosphorylation (OD/mg prot)
EGFR activity (RLU/mg prot)
R² = 0.8068
D
F
H1385
H1975
R² = 0.9035
M
A549
H1650
R² = 0.7246
E
EGFR activity
H1385 wt
H1385 L858R
H1975
F
SSC
PD-L1

Figure 15. EGFR signaling controls ERα phosphorylation and PD-L1 expression. A. Female (F)-derived $^{ERα\ low}$ NCI-H1385 and $^{ERα\ high}$ NCI-H1975 cells, male (M)-derived $^{ERα\ low}$ A549 and $^{ERα\ high}$ NCI-H1650 cells were treated 24 h in the absence (-) or presence (+) of 1 μM MK-2206, an Akt inhibitor (Akti), 10 μM U-0126, a ERK-1/2 inhibitor (ERKi), 1 μM AZD9291/Osimertinib, an EGFR inhibitor (EGFRi), then lysed and analyzed for the indicated proteins in nuclear extracts. TBP is included as control of equal protein loading. The image is representative of 1 out of 3 experiments. **B.** Cells were treated 24 h in the absence (-) or presence (+) of 1 μM AZD9291/Osimertinib (EGFRi). The indicated proteins were measured in the whole cell lysates. Tubulin is included as control of equal protein loading The image is representative of 1 out of 3 experiments. **C.** EGFR kinase activity, measured with a chemiluminescence-based assay in duplicate, plotted versus the amount of phospho(Ser118)ERα, measured by an ELISA assay in duplicate, in 30 human NSCLC cell lines. **D.** Data of panel **C**, disaggregated for female (F) and male (M) patients. **E.** $^{EGFR\ activity\ low}$ wild-type NCI-H1385 cells were knocked-out for endogenous EGFR and transfected with the L858R EGFR expression vector (H1385 L858R clone). NCI-H1975 cells were included as control of female-derived $^{EGFR\ activity\ high}$ cells. Cells were lysed and analyzed for the indicated proteins in nuclear extracts. TBP is included as control of equal protein loading. The image is representative of 1 out of 3 experiments. **F.** Expression of surface PD-L1, measured by flow cytometry in triplicate, in $^{EGFR\ activity\ low}$ wild-type NCI-H1385 cells, $^{EGFR\ activity\ high}$ L858R NCI-H1385 cells, $^{EGFR\ activity\ high}$ NCI-H1975 cells. The dot plots are representative of 1 out of 3 experiments. Percentages indicate the positive cells in each quadrant. SSC: side-scatter.

To prove that ERα phosphorylation was dependent on EGFR activity in NSCLC cells, we artificially increased EGFR activation in NCI-H1385 cells (**Figure 16A**), i.e. the female-derived cell line with the lowest EGFR activity and ERα phosphorylation. Wild-type NCI-H1385 cells were knocked-out for endogenous EGFR (**Figure 16B**), transfected with the constitutively-activated L858R-EGFR (**16C-D**) and compared with NCI-H1975 cells, i.e. the female cell line with the highest EGFR activity

and ERα phosphorylation (**Figure 16D**). The newly generated *EGFR switch on activity* NCI-H1385 cells had increased amounts of phospho(S118)ERα (**Figure 16E**), coupled with increased levels of PD-L1 on their surface (**Figure 16F**). They significantly differ from wild-type NCI-H1385 cells, but they were comparable with NCI-H1975 cells, bearing the same EGFR activating mutation [60]. These findings suggest that EGFR/ERα activity controls the levels of PD-L1 in NSCLC cells, in particular in cells of female patients.

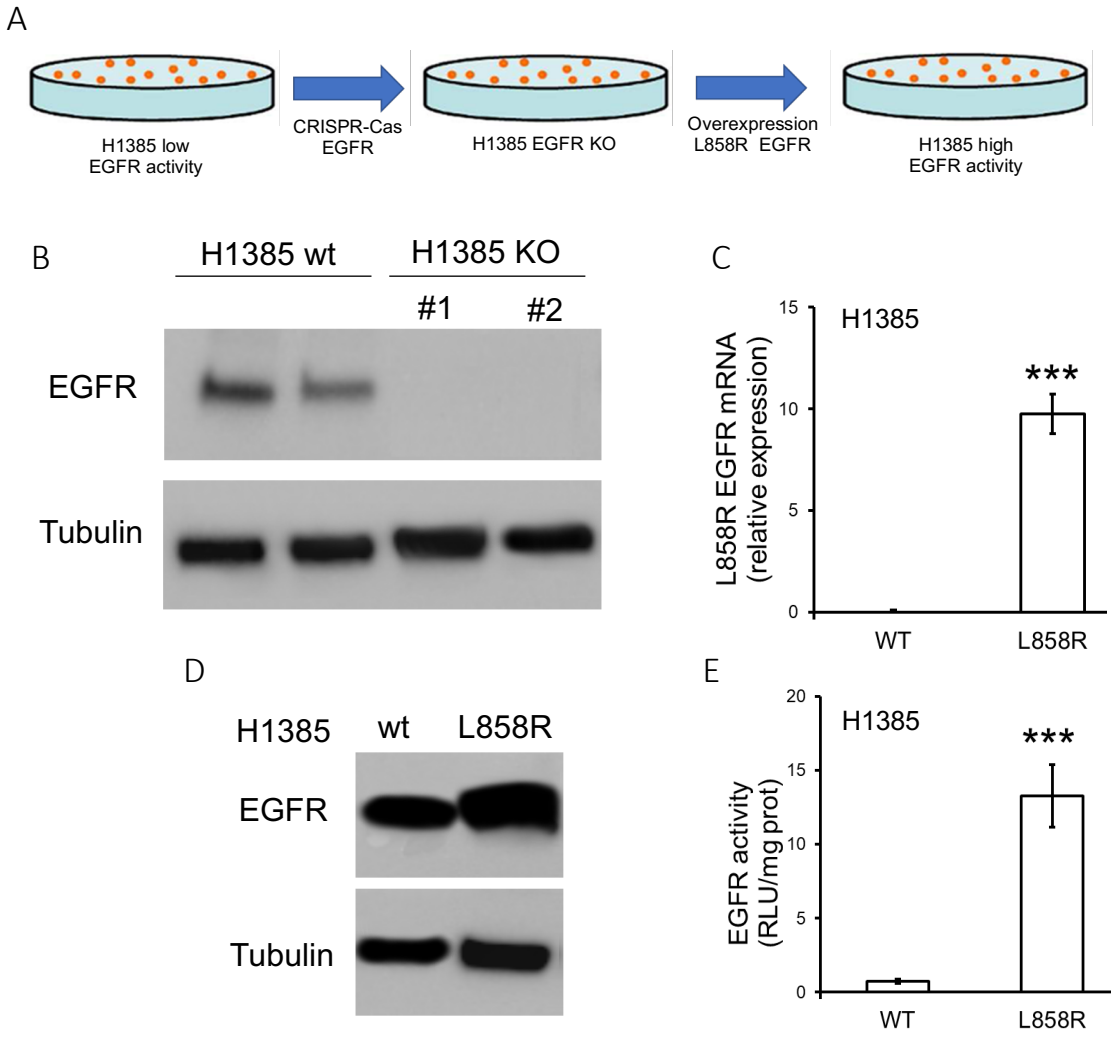

Figure 16. Switch-off/on of EGFR activity in NCI-H1385 cells. A. Experimental scheme: *EGFR activity low* wild-type NCI-H1385 cells were knocked-out for endogenous EGFR by a CRISPR/Cas vector, then stably transfected with an expression vector encoding L858R EGFR. **B.** Immunoblot of

EGFR in wild-type (wt) NCI-H1385 cells and in clones subjected to two (#1, #2) EGFR-CRISPR/Cas vectors. Tubulin is included as control of equal protein loading. The image is representative of 1 out of 3 experiments. **C.** *L858R EGFR* mRNA levels in WT NCI-H1385 cells and in cells stably transfected with the L858R EGFR-expression vector, measured by RT-PCR in triplicate. Data are means ± SD (n=3). ***p<0.001: L858R cells versus WT cells. **D.** Immunoblot of EGFR in WT and L858R NCI-H1385 cells. Tubulin is included as control of equal protein loading. The image is representative of 1 out of 3 experiments. **E.** EGFR kinase activity, measured in WT and L858R NCI-H1385 cells by a chemiluminescence-based assay in duplicate. Data are means ± SD (n=3). ***p<0.001: L858R cells versus WT cells.

3.6 Aromatase inhibitor enhances the effects of Pembrolizumab in highly expressing ERα immuno-xenografts by relieving the PD-L1-mediated immune-suppression

Since 17-β-estradiol/ERα levels are critical in determining the expression of PD-L1, we wondered if estrogen-targeting agents could be useful as adjuvant agents in IOT protocols, using Hu-CD34^{+} NSG mice xenografts. This platform, recently exploited to study the efficacy of anti-PD-1/PD-L1 [61], was tailored to study the gender-differences by implanting female-derived NCI-H1385 and NCI-H1975 tumors, and male-derived A549 and NCI-H1650 tumors in mice of the same gender. Notwithstanding the different rate of growth of each line, Pembrolizumab reduced tumor growth (intended as mean reduction of NCI-H1385 and NCI-H1975 tumor volume compared to mean reduction of A549 and NCI-1650 tumor volume) with higher efficacy in female xenografts than in males. Within each gender, $^{ERα\ high}$ tumors responded to Pembrolizumab better than $^{ERα\ low}$ tumors (**Figure 17A**). Letrozole alone did not change tumor growth, leading to exclude that NSCLC is dependent on estrogen for its growth. Interestingly, the co-administration of Pembrolizumab and letrozole markedly reduced tumor growth, with a different efficacy depending on ERα levels and gender. Female $^{ERα\ high}$ NCI-H1975 tumors were the most sensitive to the combination therapy, followed by male $^{ERα\ high}$ NCI-H1650 and

female $^{ERα\ low}$ NCI-H1385 tumors. The less responsive were male $^{ERα\ low}$ A549 tumors (**Figure 17A**). Consistently, Pembrolizumab-treated female mice had a better PFS (**Figure 17B**) and OS (**Figure 17C**) than males. Within each gender, animals bearing $^{ERα\ high}$ tumors had higher PFS and OS, recapitulating the clinical findings observed in NSCLC patients. Again, Pembrolizumab, particularly in combination with letrozole, improved PFS and OS with higher efficacy in female than in male xenografts, as well as in animals bearing $^{ERα\ high}$ tumors (**Figure 17B-C**). Letrozole, alone or combined with Pembrolizumab, reduced the percentage of PD-L1^{+}NSCLC cells in tumors (**Figure 17D**). Both Pembrolizumab and letrozole alone slightly increased the amount of cytotoxic CD8^{+}TILs, proliferating (i.e. Ki67^{+}) and activated (i.e. IFNγ^{+}; **Figure 17E**), as well as the amount of proliferating/activated NK cells (CD56^{+}Ki67^{+}IFNγ^{+}; **Figure 17F**) and Vγ9Vδ2 T-cells (Vγ9^{+}Ki67^{+}IFNγ^{+}; **Figure 17G**). These populations were more significantly increased by the combination of Pembrolizumab and letrozole, with maximal benefits in female $^{ERα\ high}$ NCI-H1975 tumors, followed by male $^{ERα\ high}$ NCI-H1650 and female $^{ERα\ low}$ NCI-H1385 tumors. Again, the lowest increase was detected in male $^{ERα\ low}$ A549 tumors (**Figure 17E-G**).

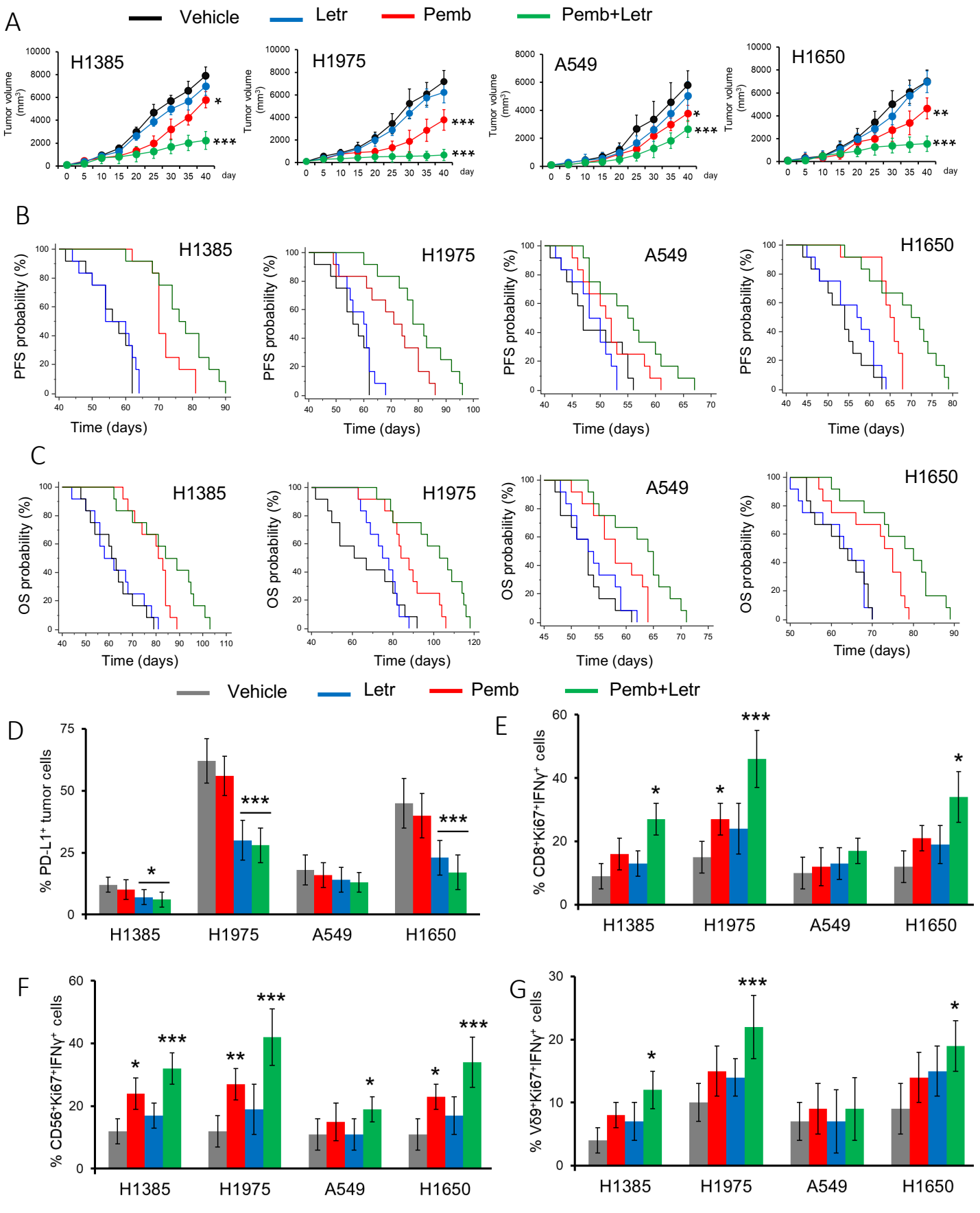
A
Vehicle
Letr
Pemb
Pemb+Letr
H1385
H1975
A549
H1650
Tumor volume (mm³)
day
B
PFS probability (%)
Time (days)
C
OS probability (%)
Time (days)
D
% PD-L1⁺ tumor cells
E
% CD8⁺Ki67⁺IFNγ⁺ cells
F
% CD56⁺Ki67⁺IFNγ⁺ cells
G
% Vδ9⁺Ki67⁺IFNγ⁺ cells

Figure 17. The efficacy of Pembrolizumab and aromatase inhibitor is related to gender and ERα expression in non-small cell lung cancer xenografts

A. 1 × 10^6 female-derived $^{ERα\ low}$ NCI-H1385 cells and $^{ERα\ high}$ NCI-H1975 cells were implanted subcutaneously (s.c.) in 6-week old Hu-CD34$^+$NSG female mice. 1 × 10^6 male-derived $^{ERα\ low}$ A549 cells and $^{ERα\ high}$ NCI-H1650 cells were implanted s.c. in 6-week old Hu-CD34$^+$NSG male mice. When tumor reached the volume of 100 mm^3, mice (n= 10/group) were randomized in the following groups: 1) Vehicle group, treated intraperitoneally (i.p.) with 100 µl saline solution (days 1, 7, 14, 21, 28, 35 after randomization); 2) Pembrolizumab (Pembr) group, treated with 10 mg/kg i.p. of 100 µl saline solution of the drug (day 1), followed by 5 mg/kg i.p. (days 7, 14, 21, 28, 35); 3) Letrozole (Letr) group, treated with 1 mg/kg *per os* of 100 µl saline solution of the drug daily (days 1-35); 4) Pembrolizumab + Letrozole (Pembr + Letr) group, with 10 mg/kg i.p. of 100 µl saline solution of Pembrolizumab (day 1), followed by 5 mg/kg i.p. (days 7, 14, 21, 28, 35) and 1 mg/kg *per os* of 100 µl saline solution of letrozole daily (days 1-35). Tumor growth was monitored daily with a caliper. Mice were euthanized on day 40. Data are mean volumes $\pm$ SD. *p<0.05, **p>0.001, ***p<0.001: treatments group versus vehicle group (day 40). **B-C.** Progression-free survival (PFS) and overall survival (OS) of female Hu-CD34$^+$NSG mice bearing NCI-H11385 and NCI-H1975 tumors, and of male Hu-CD34$^+$ NSG mice bearing A549 and NCI-H1650 tumors, treated as reported at point **A** (n=16 mice/group). p<0.001: Pembr+Letr group versus Vehicle group (PFS and OS, all groups); p<0.001: Pembr group versus Vehicle group (both PFS and OS, all groups except A549); p<0.01: Pembr group versus vehicle group (OS, A549 group). **D.** PD-L1 expression was measured by flow cytometry on dissociated tumor cells after explants (n= 10/group). *p<0.05, ***p<0.001: treatments group versus Vehicle group. **E-G**. On TILs isolated from tumor extracts, the percentage of CD8$^+$KI67$^+$IFNγ$^+$ cells (panel **E**), CD56$^+$Ki67$^+$IFNγ$^+$ cells (panel **F**), Vγ9$^+$Ki67$^+$IFNγ$^+$ cells (panel **F**) was measured by flow cytometry (n=10/group). *p<0.05, **p<0.01, ***p<0.001: treatments group versus Vehicle group.

To investigate if this effect on tumor and its immune-environment was durable, we analyzed different cohorts of animals treated for 5 weeks with Pembrolizumab and letrozole, then left untreated for 10 weeks or treated with letrozole alone for 10 weeks or treated with letrozole for 5 weeks followed by Pembrolizumab and letrozole for additional 5 weeks. The discontinuation of letrozole after the first 5 weeks of co-administration with Pembrolizumab determined a progressive increase of tumor volumes, in particular in male xenografts and $^{ERα\ low}$ tumors (male $^{ERα\ low}$ A549 > male $^{ERα\ high}$ NCI-H1650> female $^{ERα\ low}$ NCI-H1385 > female $^{ERα\ high}$ NCI-H1975) (**Figure 18A**). Notwithstanding the tumor growth, the percentage of PD-L1^{+} cells derived from tumors explanted at week 15 (**Figure 18B**), the amount of activated CD8^{+}T-lymphocytes (**Figure 18C**), NK (**Figure 18D**) and Vγ9Vδ2 T-cells (**Figure 18E**) was similar to the animals treated with 5 weeks of Pembrolizumab and letrozole, in particular in female $^{ERα\ high}$ NCI-H1975 tumors. Letrozole administration for additional 10 weeks strongly reduced the tumor growth (**Figure 18A**) and the amount of PD-L1 in tumor extracts (**Figure 18B**). In this experimental set, the amount of CD8^{+}KI67^{+}IFNγ^{+} (**Figure 18C**), CD56^{+}Ki67^{+}IFNγ^{+} (**Figure 18D**), Vγ9^{+}Ki67^{+}IFNγ^{+} (**Figure 18E**) cells was higher than in animals treated with 5 weeks of Pembrolizumab and letrozole, and then left untreated. The tumor reduction and the increase in activated TILs were maximal in female bearing $^{ERα\ high}$ NCI-H1975 tumors while being minimal in male bearing $^{ERα\ low}$ A549 tumors. Most importantly, an alternative protocol of Pembrolizumab and letrozole for 5 weeks, letrozole alone for 5 weeks, Pembrolizumab and letrozole for 5 weeks achieved the maximal control of tumor growth, inducing an arrest or even a regression during the second cycle of the combination therapy (**Figure 18A**). This protocol was accompanied by the strongest decrease in tumor PD-L1 (**Figure 18B**) and increase in activated T-lymphocytes and NK cells (**Figure 18C-E**). Tumor regression and activation of TILs were higher in female xenografts ($^{ERα\ high}$ NCI-H1975 > $^{ERα\ low}$ NCI-H1385 tumors) than in male xenografts ($^{ERα\ high}$ NCI-H1650 > $^{ERα\ low}$ A549 tumors).

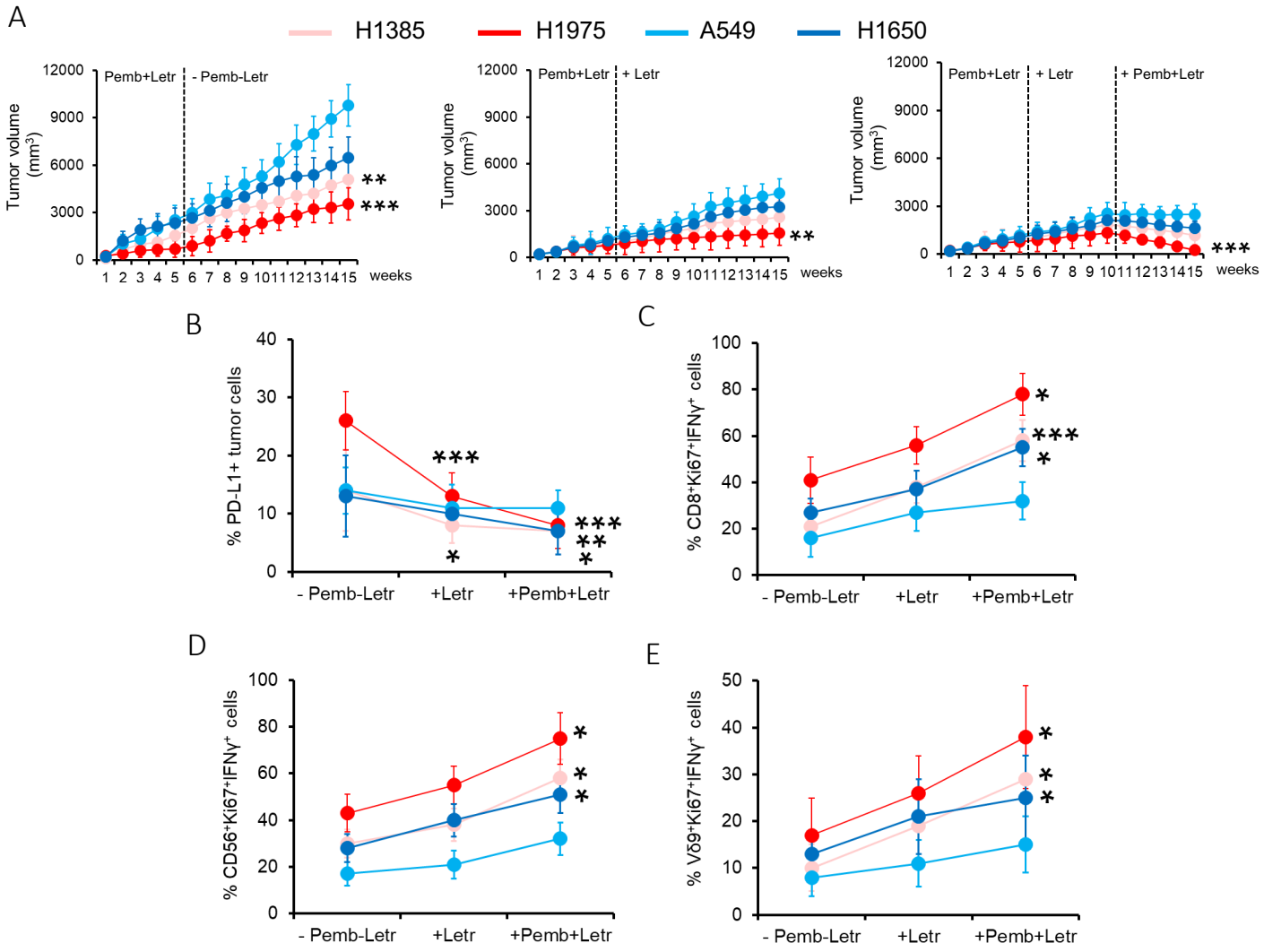

Figure 18. Letrozole sensitizes xenografts to a second cycle of Pembrolizumab by modulating the tumor-associated immune-environment.

Female Hu-CD34^{+}NSG mice bearing $^{ERα\ low}$ NCI-H11385 and $^{ERα\ high}$ NCI-H1975 tumors, and male Hu-CD34^{+} NSG mice bearing $^{ERα\ low}$ A549 and $^{ERα\ high}$ NCI-H1650 tumors were treated 5 weeks with Pembrolizumab + Letrozole with 10 mg/kg i.p. of 100 µl saline solution of Pembrolizumab (day 1), followed by 5 mg/kg i.p. (days 7, 14, 21, 28, 35) and 1 mg/kg *per os* of 100 µl saline solution of letrozole daily (days 1-35), then divided into 3 cohorts (n= 20/group). The first cohort of animals (*left panel*) was left untreated until week 15 (-Pemb-Letr); the second cohort (*middle panel*) was treated with 1 mg/kg *per os* of 100 µl saline solution of letrozole daily until week 15 (+Letr); the third cohort

(*right panel*) was treated with 1 mg/kg *per os* of 100 µl saline solution of letrozole daily from week 6 to week 10, then treated with Pembrolizumab + Letrozole from week 11 to week 15 (+Pemb+Letr). **A.** Tumor growth was monitored daily with a caliper. Data are mean volumes ± SD. *p<0.01, **p<0.001: volume of female $^{ERα\ low}$ NCI-H1385 and $^{ERα\ high}$ NCI-H1975 tumors versus mean volume of male $^{ERα\ low}$ A549 and $^{ERα\ high}$ NCI-H1650 tumors. **B.** PD-L1 expression was measured by flow cytometry on dissociated tumor cells after explants at week 15 (n= 12/group). *p<0.05: +Pemb+Letr treatment versus -Pemb-Letr (NCI-H1650 tumors), +Letr treatment versus -Pemb-Letr (NCI-H1385 tumors); **p<0.01: +Pemb+Letr treatment versus -Pemb-Letr (NCI-H1385 tumors); ***p<0.001: +Letr/+Pemb+Letr treatment versus -Pemb-Letr (NCI-H1975 tumors). **C-E**. On TILs isolated from tumor extracts (week 15), the percentage of $CD8^+KI67^+IFN\gamma^+$ cells (panel **C**), $CD56^+Ki67^+IFN\gamma^+$ cells (panel **D**), $V\gamma9^+Ki67^+IFN\gamma^+$ cells (panel **E**) was measured by flow cytometry (n=12/group). $CD8^+KI67^+IFN\gamma^+$ cells: *p<0.05: +Pemb+Letr treatment versus -Pemb-Letr (NCI-H1975 and NCI-H1650 tumors), ***p<0.001: +Pemb+Letr treatment versus -Pemb-Letr (NCI-H1385 tumors). $CD56^+Ki67^+IFN\gamma^+$ cells: *p<0.05: +Pemb+Letr treatment versus -Pemb-Letr (NCI-H1385, NCI-H1975 and NCI-H1650 tumors). $V\gamma9^+Ki67^+IFN\gamma^+$ cells: +Pemb+Letr treatment versus -Pemb-Letr (NCI-H1385, NCI-H1975 and NCI-H1650 tumors).

3.7 Targeting estrogen synthesis alters cholesterol levels, membrane fatty acid composition and binding between PD-1/PD-L1 in NSCLC cells

Since PD-L1 is an integral membrane protein, whose conformation depends on the lipid environment, I next investigated whether the effects of letrozole, that blocks estrogen synthesis leading to an impairment of intracellular sterols (e.g. cholesterol, cholesterol esters), may also alter the lipidome composition of cell membrane and whether part of its effect was due to changes in physio-chemical properties.

To identify the metabolic impact of letrozole treatment after 24 hours, we analyzed the lipidome of three male (A549, NCI-H441, NCI-H1650) and three female (NCI-H1385, NCI-H2229, NCI-H1975) cell lines, already characterized in the first part of the Thesis, using the facilities and software provided by Metabolon Inc. Both neutral lipids (triglycerides, TG, and cholesterol esters, CE) and phospholipids (PLs) as phosphatidylcholine (PC), phosphatidylethanolamine (PE), sphingomyelin (SM), lysophopholipids (lyso-PLs) and ceramide were analyzed for their composition of SFAs, MFAs andPUFAs (.

Although the effects were cell line-dependent, after treatment with letrozole female cell lines had the highest increase of MFAs + PUFAs in the FAs included neutral lipids (**Figure 19A**) and in PLs of membranes (**Figure 19B**). At the same time, letrozole-treated cells had a decrease in free cholesterol (Chol) and an increase in cholesterol esters (CE) (*Figure 20C*), with no significant differences between genders (not shown).

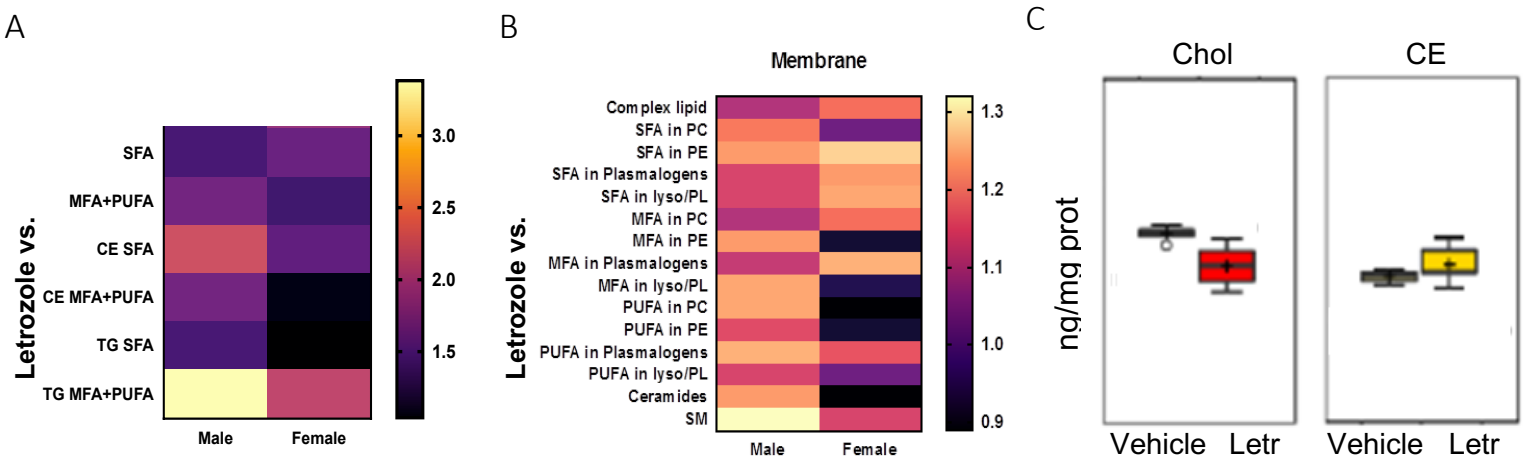

Figure 19. Lipidome analysis. Three male (A549, NCI-H441, NCI-H1650) and three female (NCI-H1385, NCI-H2229, NCI-H1975) cell lines were left untreated (CTRL) or treated with 10 μM letrozole, then subjected to lipid extraction, identification and protein normalization, in sextuplicate. **A-B**. Heatmap representation of the fatty acid (FAs) composition of neutral lipids (**A;** triglyceride:, TG, cholesterol esters: CE) and membrane phospholipids (**B;** phospholipids: PLs;

phosphatidylcholine: PC; phosphatidylethanolamine: PE, sphingomyelin: SM). SFA: saturated fatty acid; MFA: mono-unsaturated fatty acid; PUFAs: poly-unsaturated fatty acid. **C.** Quantification of cholesterol (Chol) and cholesterol ester (CE) in the cell lysates. °p<0.05;]p<: 0.05.

Letrozole increased membrane fluidity in both female (H1385 and H1975) and male (A549 and H1650) cell lines (**Figure 20A**). HEK293 cells overexpressing PD-L1, pretreated with letrozole and co-incubated with the PD-1/NFAT reporter Jurkat cells (**Figure 20B**) displayed a lower PD-1/PD-L1 binding (**Figure 20C**).

A

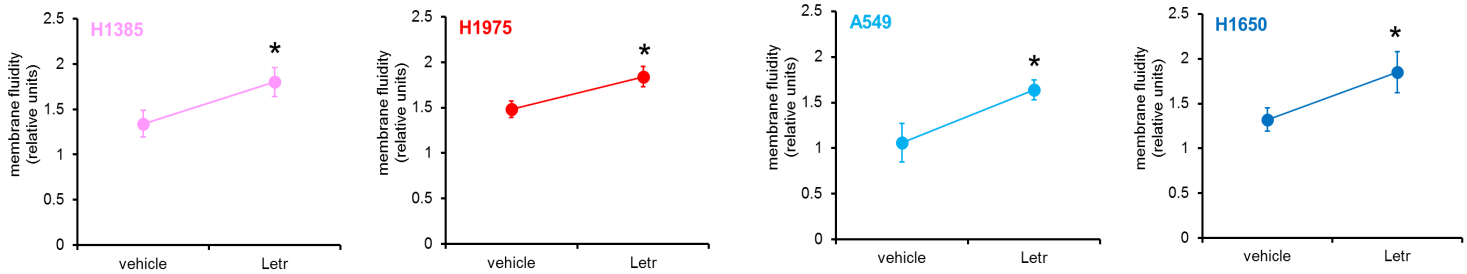

B

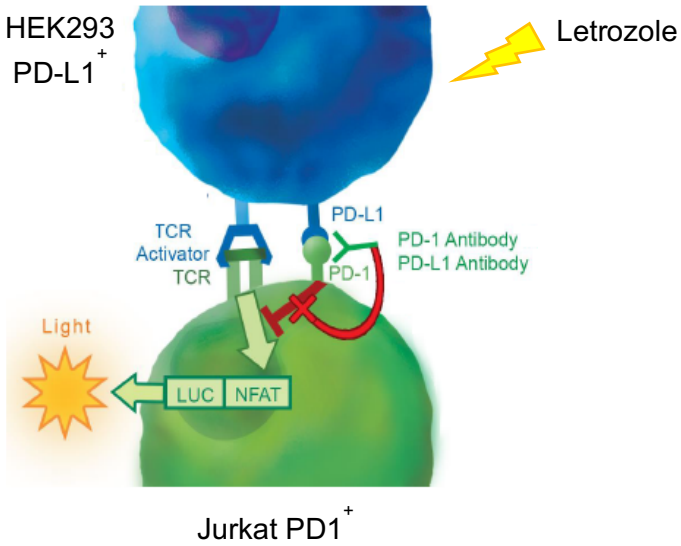

C

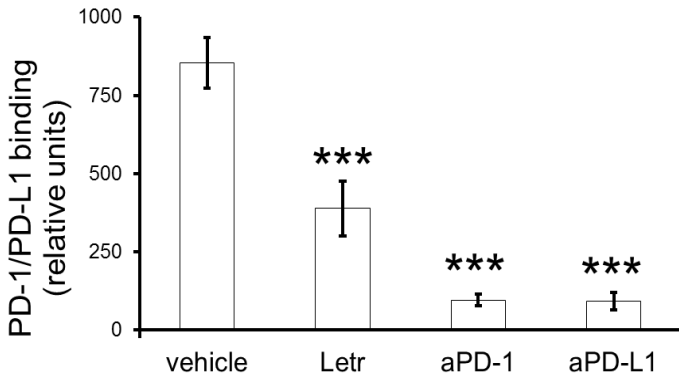

Figure 20. Effects of letrozole on membrane fluidity and PD-L1/PD-1 binding. Female-derived (NCI-H1385, NCI-H1975) and male-derived (A549, NCI-H1650) cells were incubated 24 h in the absence (vehicle) or in the presence of 10 μM letrozole (Letr). **A.** Membrane fluidity was measured fluorometrically, in duplicates. Data are mean ± SD. *p<0.05: Letr vs vehicle. **B**. Schematic representation of the measurement of the binding between HEK293 PD-L1 overexpressing cells and PD-1/NFAT reporter Jurkat cells (adapted from: BPS Biosciences). **C.** Binding between PD-1 and PD-L1, measured by chemiluminescence in duplicates. aPD-1: anti-PD-1 blocking antibody; aPD-L1: anti-PD-L1 blocking antibody, as internal control. ***p<0.001: versus vehicle.

3.8 Poly-unsaturated fatty acids recapitulate the effects of aromatase inhibitors on PD-1/PD-L1 and improve immunotherapy efficacy in NSCLC immuno-xenografts

Since upon the increased MFA+PUFA/SFA ratio and CE/Chol ratio induce by letrozole, we observed an increased membrane fluidity paralleled by a decreased binding PD-1/PD-L1, we hypothesize that a higher membrane fluidity could be an important mechanism reducing the conformation of PD-L1 and the subsequent binding with PD-1. To prove this hypothesis, we treated male and female NSCLC cells with the ω3 PUFA docosahexaenoic acid (DHA) that - together with the ω3 eicosatetraenoic acid (EPA) and ω6 arachidonic acid (AA) (**Figure 21**) - are known to be incorporated in plasma-membrane PLs, where they alter the chemical compositions increasing membrane fluidity [62].

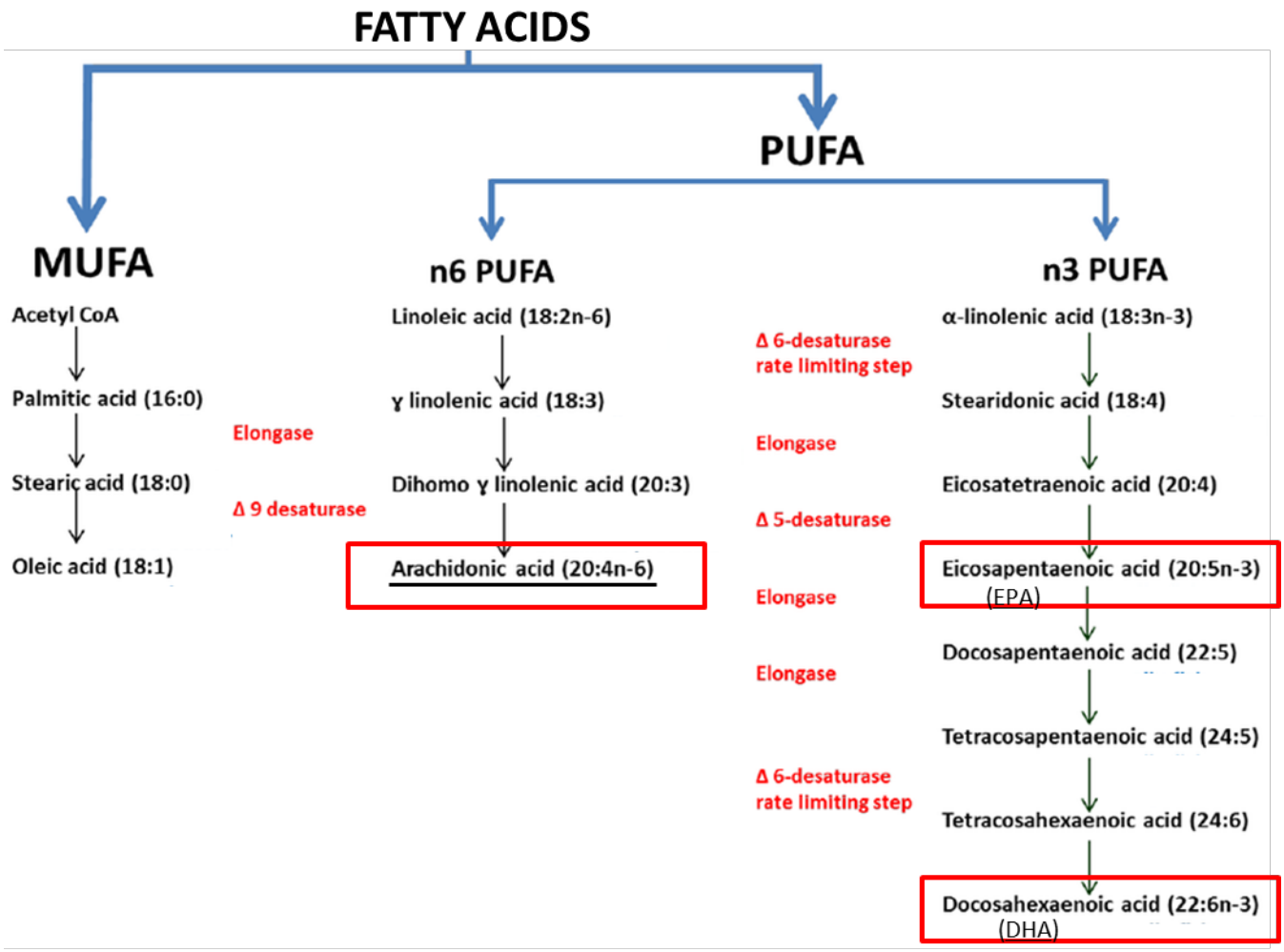

Figure 21. Schematic synthetic pathways of **ω3 and ω6 fatty acids**

Previous studies from our group suggested that DHA was the most effective PUFA incorporated in plasma-membrane by cancer cells, when used at 50-100 μM, without exerting cytotoxic effects [63]. Therefore, we decided to focus on this FA.

DHA recapitulated the phenotype determined by letrozole: indeed, it decreased the amount of SFA incorporated into membrane PLs, had mixed effects on MFA and increased the PUFAs (**Figure 22A**), decreased the amount of Chol and increased CE (**Figure 22B**). Independently from the gender it increased membrane fluidity (**Figure 22C**) and reduced the binding between PD-L1 and PD-1 (**Figure 22D**).

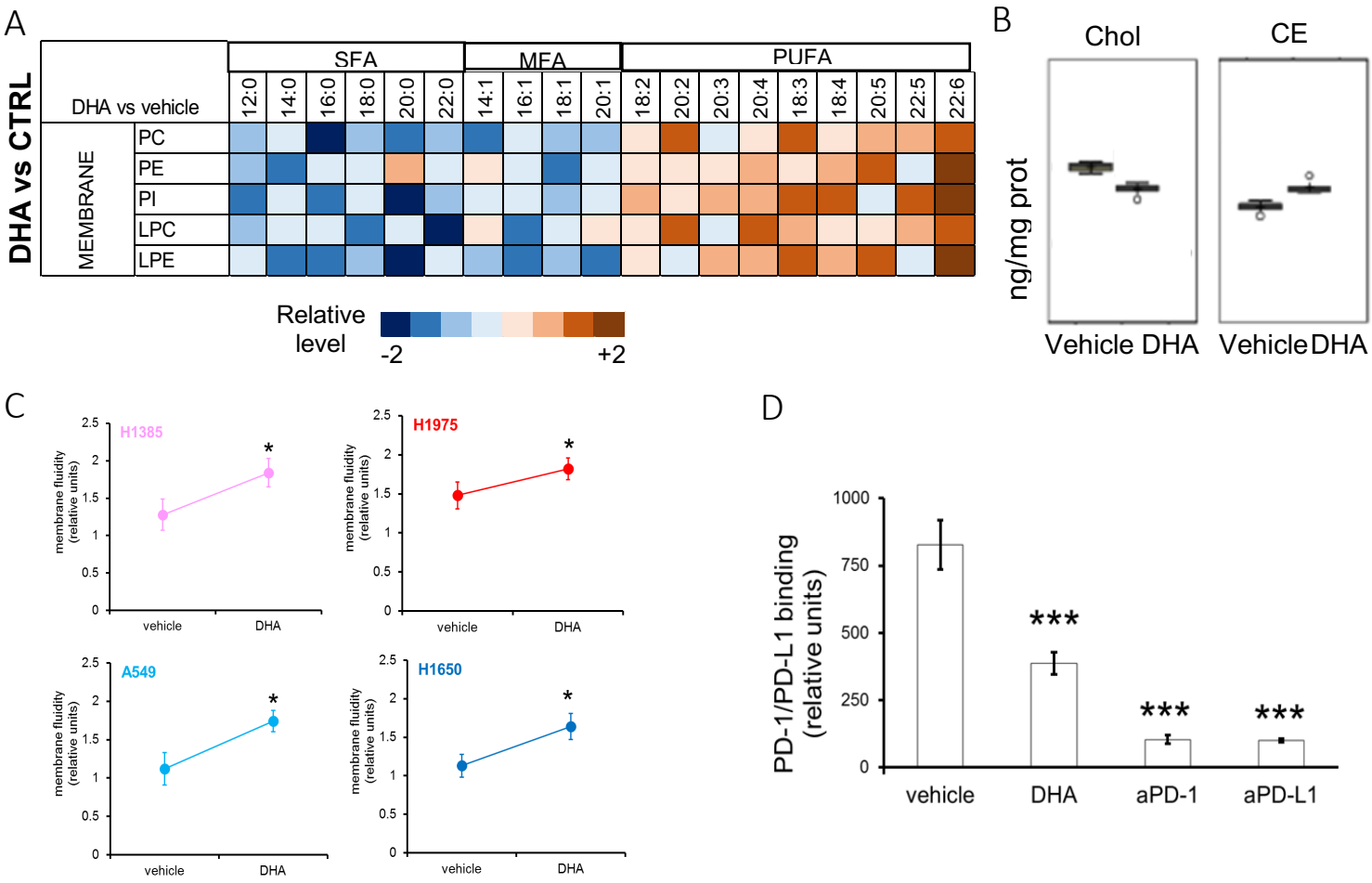

Figure 22. Effects of ω3 fatty acids on lipid membrane composition and fluidity, and PD-1/PD-L1 binding. Three male (A549, NCI-H441, NCI-H1650) and three female (NCI-H1385, NCI-H2229, NCI-H1975) cell lines were left untreated (vehicle) or treated with 100 µM docosahexaenoic acid (DHA), then subjected to lipid extraction, identification and protein normalization, in sextuplicate. **A**. Heatmap representation of the fatty acid (FAs) composition of membrane phospholipids (phosphatidylcholine: PC; phosphatidylethanolamine: PE; phosphatidylinositol: PI; LPC: liso-PC; lPE: lysoPE). SFA: saturated fatty acid; MFA: mono-unsaturated fatty acid; PUFAs: poly-unsaturated fatty acid. **B.** Quantification of cholesterol (Chol) and cholesterol ester (CE) in the cell lysates. °p<0.05: versus vehicle. **C**. Membrane fluidity was measured fluorometrically, in duplicates. Data are mean ± SD. *p<0.05: Letr vs vehicle. **D.** Binding between PD-1 and PD-L1, measured by chemiluminescence in duplicates. aPD-1: anti-PD-1 blocking antibody; aPD-L1: anti-PD-L1 blocking antibody, as internal control. ***p<0.001: versus vehicle.

Finally, we used the Hu-CD34+ platform to test the immune-adjuvant efficacy of letrozole, by implanting female-derived NCI-H1385 and NCI-H1975 tumors, and male-derived A549 and NCI-H1650 tumors, respectively with low and high levels of ERα and PD-L1, in mice of the same gender. As observed in **Figure 23A**, DHA alone did not reduce tumor growth, but it enhanced the effects of pembrolizumab at the same extent in both genders. Consistently, the combination of DHA and Pembrolizumab, significantly increased the amount of cytotoxic $CD8^+$TILs, proliferating (i.e. $Ki67^+$) and activated (i.e. $IFN\gamma^+$; **Figure 23B**), the amount of proliferating/activated NK cells ($CD56^+Ki67^+IFN\gamma^+$; **Figure 23C**) and Vγ9Vδ2 T-cells ($V\gamma9^+Ki67^+IFN\gamma^+$; **Figure 23D**), fully recapitulating the effects of letrozole and even overcoming the differences between genders, ERα and endogenous 17-β-estradiol.

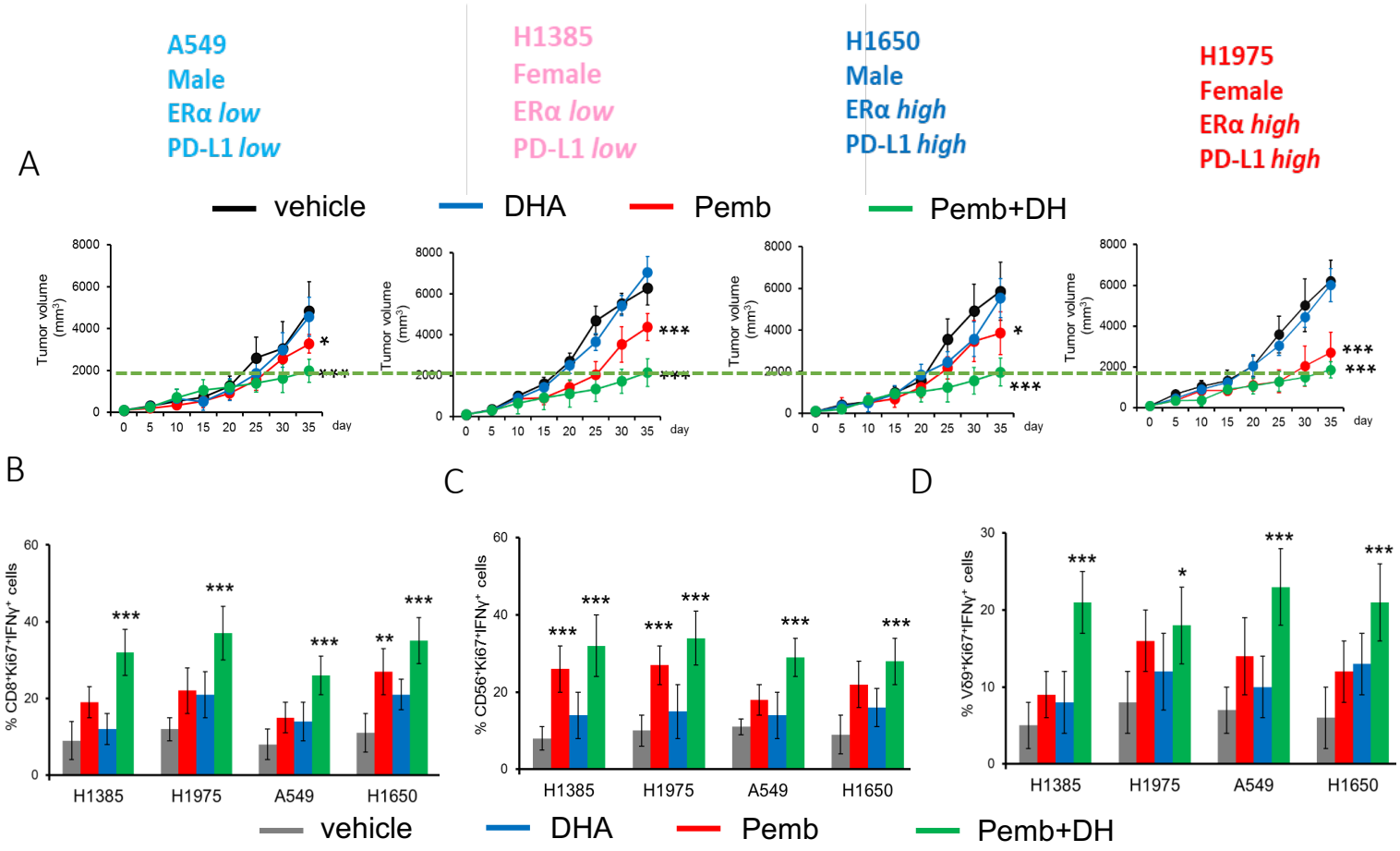

Figure 23. The ω3 fatty acid DHA sensitizes xenografts to Pembrolizumab by modulating the tumor-associated immune-environment.

A. 1 × 10^6 female-derived $^{ERα\ low}$ NCI-H1385 cells and $^{ERα\ high}$ NCI-H1975 cells were implanted subcutaneously (s.c.) in 6-week old Hu-CD34$^+$NSG female mice. 1 × 10^6 male-derived $^{ERα\ low}$ A549 cells and $^{ERα\ high}$ NCI-H1650 cells were implanted s.c. in 6-week old Hu-CD34$^+$NSG male mice. When tumor reached the volume of 100 mm^3, mice (n= 10/group) were randomized in the following groups: 1) Vehicle group, treated intraperitoneally (i.p.) with 100 µl saline solution (days 1, 7, 14, 21, 28, 35 after randomization); 2) Pembrolizumab (Pembr) group, treated with 10 mg/kg i.p. of 100 µl saline solution of the drug (day 1), followed by 5 mg/kg i.p. (days 7, 14, 21, 28, 35); 3) docosahexaenoic acid (DHA) group, treated with 100 µl of DHASCO oil (44.5% v/v DHA) *per os* daily (days 1-35); 4) Pembrolizumab + docosahexaenoic acid (Pembr + DHA) group, with 10 mg/kg i.p. of 100 µl saline solution of Pembrolizumab (day 1), followed by 5 mg/kg i.p. (days 7, 14, 21, 28, 35) and DHASCO oil (44.5% v/v DHA) *per os* daily (days 1-35). Tumor growth was monitored daily with a caliper. Mice were euthanized on day 40. Data are mean volumes ± SD. *p<0.05, ***p<0.001: treatments group versus vehicle group (day 35). **B-D**. On TILs isolated from tumor extracts, the percentage of CD8$^+$KI67$^+$IFNγ$^+$ cells (panel **B**), CD56$^+$Ki67$^+$IFNγ$^+$ cells (panel **C**), Vγ9$^+$Ki67$^+$IFNγ$^+$ cells (panel **D**) was measured by flow cytometry (n=10/group). *p<0.05, **p<0.01, ***p<0.001: treatments group versus Vehicle group.

3.9 Female and male NSCLC have a different metabolic profile and sensitivity to fatty acids

In the last part of the Thesis, we expanded the analysis of the metabolic profiling of male and female NSCLC cell lines to investigate if there were other differences in the main energetic pathways, as potential vulnerabilities and/or druggable targets as immune-adjuvants. I report below my preliminary data on 2D and 3D cultures. As shown in **Figure 24A**, the oxygen consumption rate (OCR) was different but the mean value was higher in female cell lines (NCI-H2228, NCI-H18975,

NCI-H1385) than in male lines (Calu-3, NCI-H441, NCI-H1650), in line with the higher basal (**Figure 24B**) and maximal (**Figure 24C**) OCR, spare capacity (**Figure 24D**) and ATP production (**Figure 24E**). By contrast, the analysis of extracellular acidification rate (ECAR) (**Figure 24F**), an indicator of aerobic glycolysis did not show significant differences between the genders, in terms of basal (**Figure 24G**) and maximal (**Figure 24H**) glycolysis, and glycolytic reserve (**Figure 24I**).

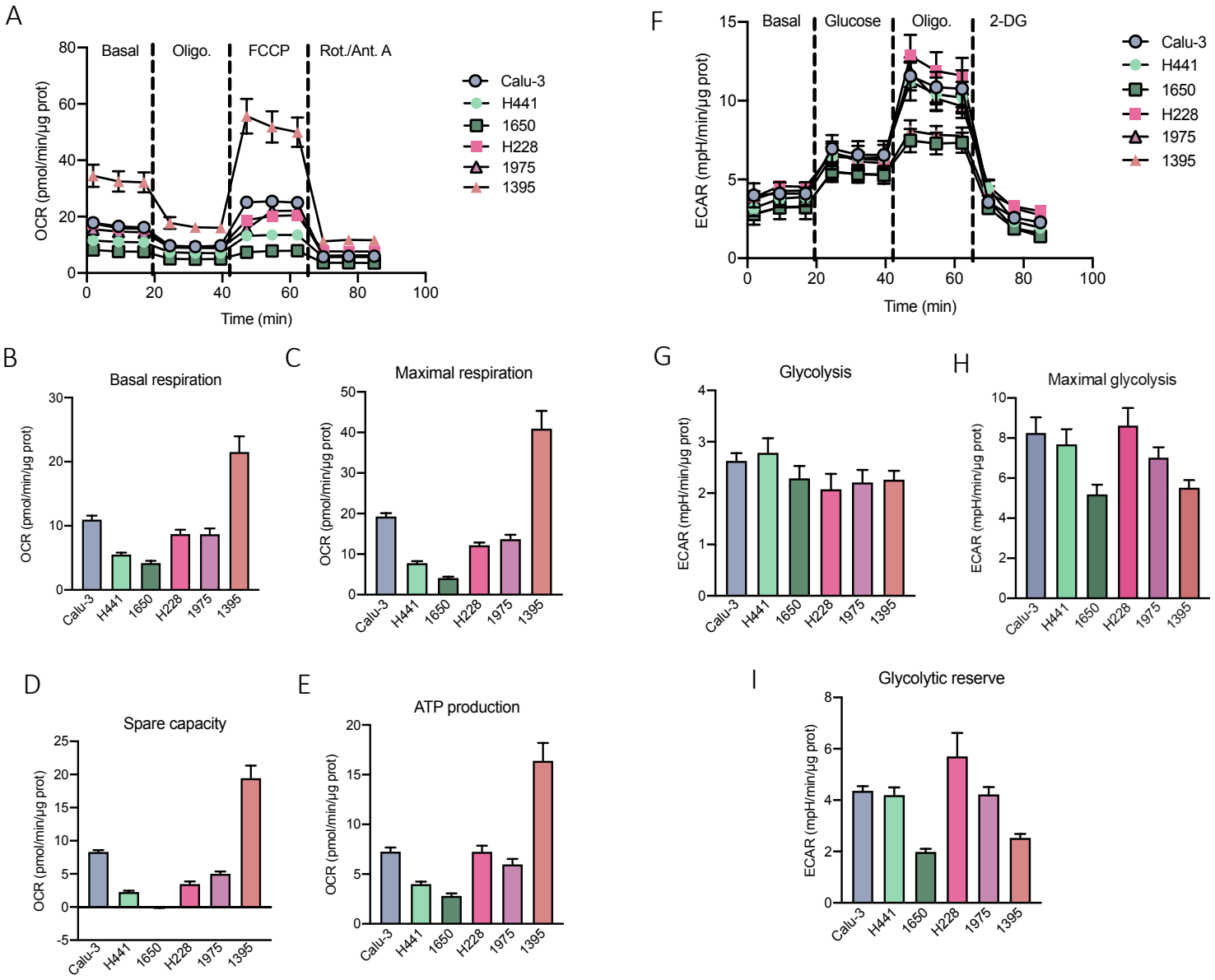

Figure 24. Female and male NSCLC have a different metabolic profile.

Extracellular acidification rate (ECAR) and steady-state oxygen consumption rate (OCR) measured in female cell lines (NCI-H2228, NCI-H18975, NCI-H1385) and in male lines (Calu-3, NCI-H441, NCI-H1650) using the Seahorse XF96 Analyzer. Box plots represent cumulative data of maximal glycolysis - ECAR values after oligomycin injection - (panel A,B,C) and maximal respiration (panels F,G,H) calculated as: OCR after FCCP – OCR after antimycin+rotenone addition.

Bioenergetics parameters for both female and male cell lines are shown. E. ATP-linked OCR was measured by subtracting the last rate measurement, before oligomycin injection (1μM) to the minimum rate measurement after the addition of oligomycin. I. Glycolytic capacity was measured by subtracting the maximum rate measurement after oligomycin injection (1μM) to the last rate measurement before the injection of glucose (10 mM).

Overall, these data suggest an energetic metabolic difference between female and male cell lines, mainly related to OXPHOS, a process that occurs in mitochondria as specific steps of sterols and steroid hormones biosynthetic pathways [64].

These results were obtained in 2D cultures. We next set up the method to generate spheroids and evaluate if specific differences in lipid homeostasis, potentially responsible for a different response to ICIs, were measurable.

3.10 Set up of a 3D platform to analyze the effects of estrogens and lipid/targeting agents as potential anti-tumor and immune-adjuvant agents

Among the female cell lines (NCI-H2228, NCI-H18975, NCI-H1385) and the male lines (Calu-3, NCI-H441, NCI-H1650), only four of them (Calu-3, NCI-H1650, NCI-1385, NCI-!975) formed spheroids in ULA plates, The most active cell line in forming spheroids (doubling time of spheroids number: 7 days) were the male Calu-3 and the female NCI-H1975 cells (**Figure 25**).

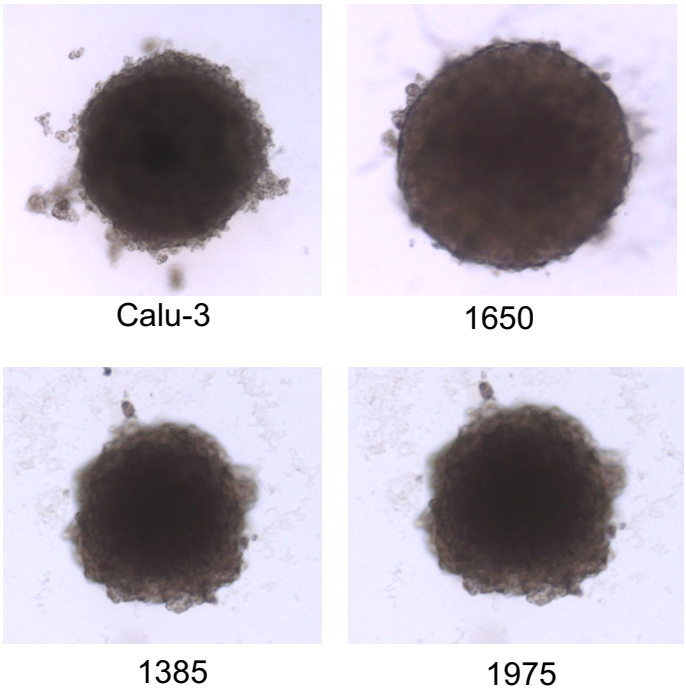

Figure 25. Spheroids formation of male and female cell lines

Using BODIPY 493/503 as a marker for neutral lipids (i.e. triglycerides) intor intracellular lipid droplets (**Figure 26A**), we were able to follow the different patterns of incorporation and uptake of the ω3 FA EPA and DHA, and of the ω6 AA. As shown in **Figure 26B**, the spatial distribution differed between male and female cell lines: while in Calu-3 cells, the uptake of FAs and the formation of lipid droplets were homogeneously distributed within the spheroid, in NCI-H1975 cells the FAs remained in the peripheral part, except for EPA. However, the digital quantification of PUFA uptake revealed that the average uptake of ω3 FA EPA and DHA was equal between female and male cell lines, while AA was more incorporated in male cell lines (**Figure 26C**).

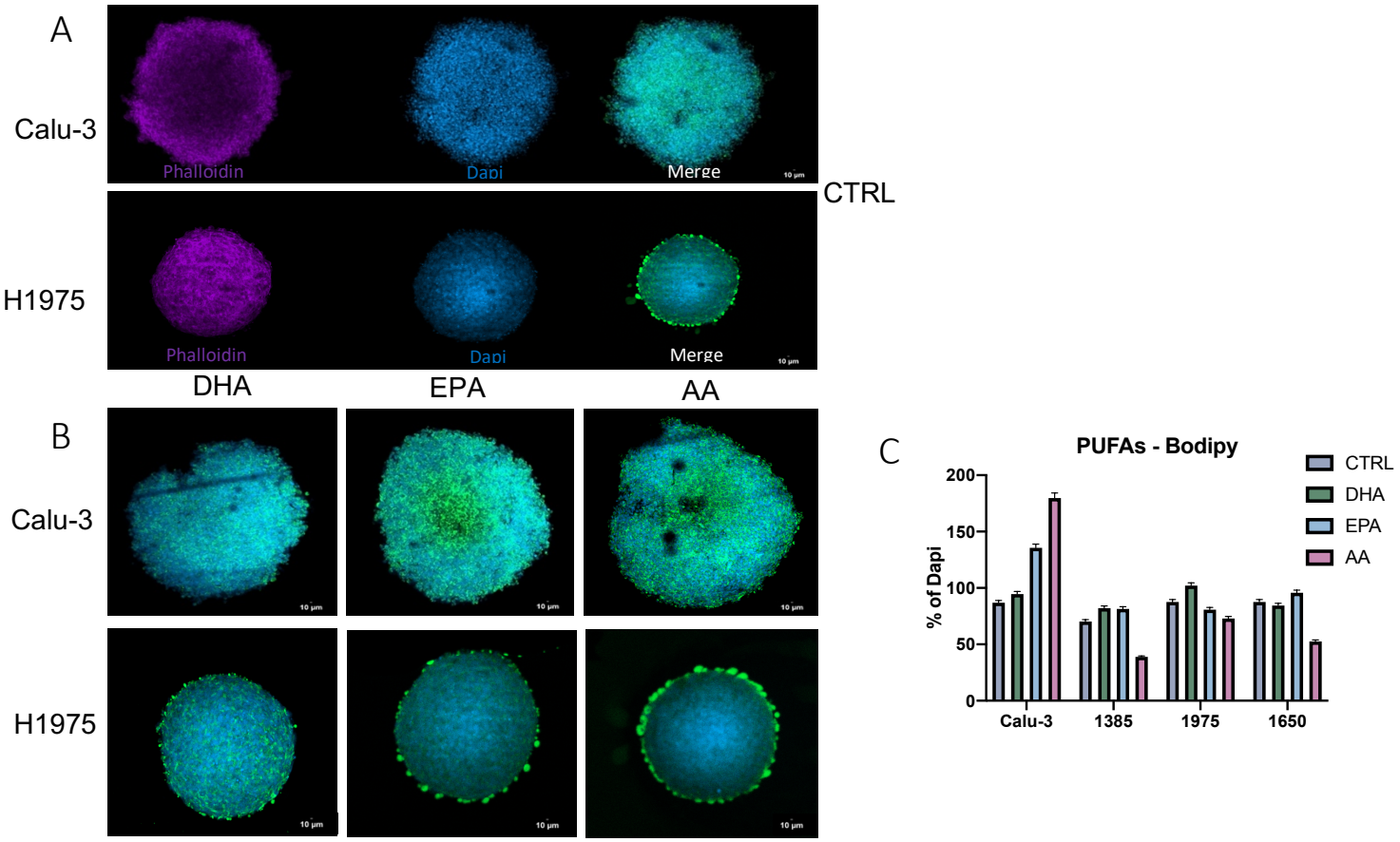

Figure 26. PUFAs accumulate into lipid droplets within 3D spheroid cultures of NSCLC cells

Representative pictures (A) (Calu-3 and H1975 cells) and quantification (C). (B) Effects of the indicated FAs (DHA, EPA, AA) on the growth of 3D tumor spheroids generated from NSCLC cells (A). FAs were added upon exposure for 72 h to 50 mM.

Male and female spheroids also have a different pattern of proliferation: the male Calu-3 cells have the highest proliferation rate in the peripheral region, while the proliferation of the female NCI-H1975 was homogeneously distributed, according to the KI67 staining (**Figure 27A**). The same pattern was maintained also in spheroids incubated with EPA, DHA and AA (**Figure 27B**), although all of them induced decreased proliferation. The ω3 EPA and DHA were the most potent inhibitors of proliferation in female cell lines, while the ω6 AA was the strongest anti-proliferative agent for male cell lines (**Figure 27C**).

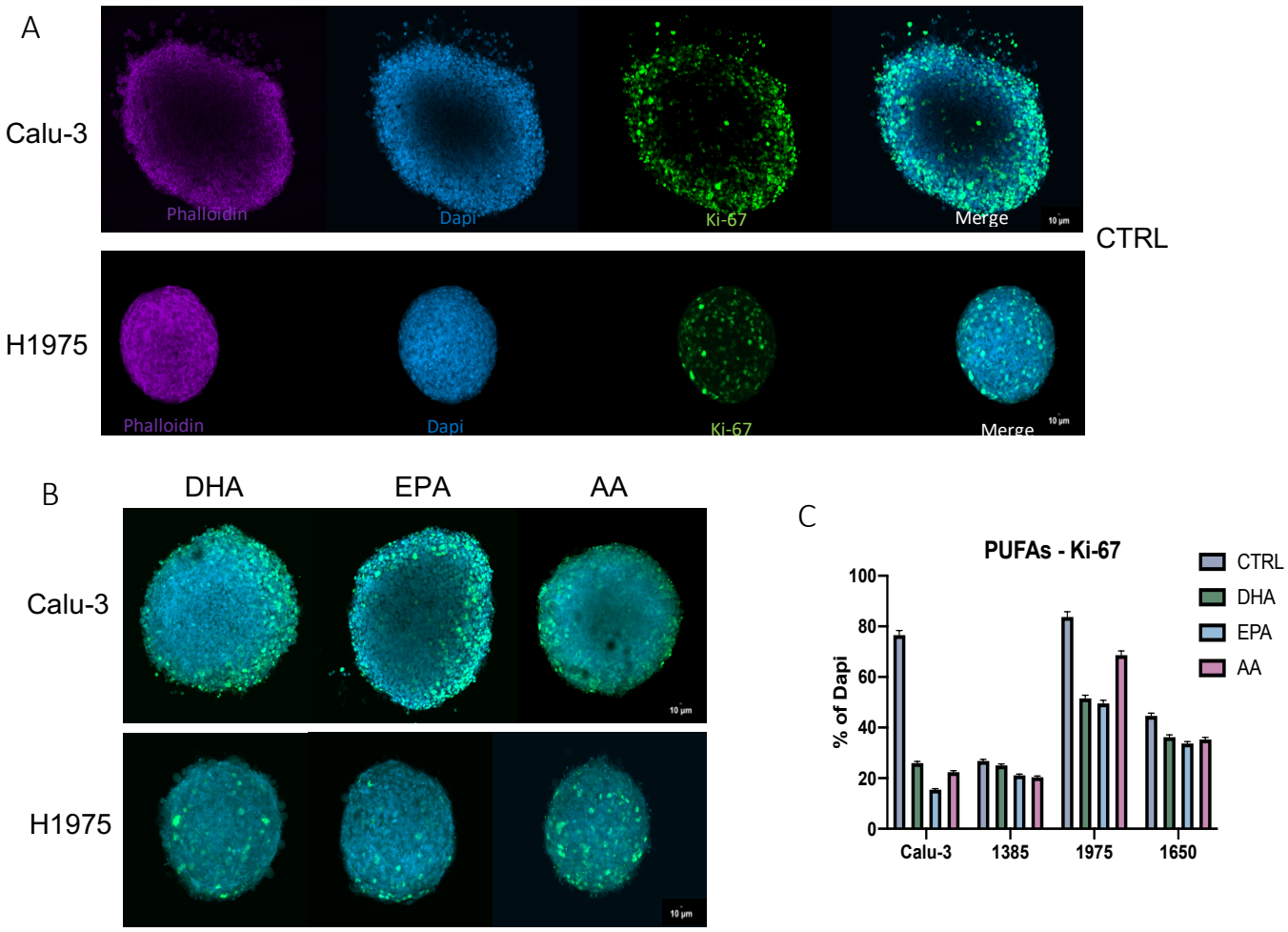

Figure 27. Ki-67 staining indicates cell proliferation status within 3D spheroid cultures of NSCLC cells

Representative pictures (A) (Calu-3 and H1975 cells) and quantification (C). (B) Effects of the indicated FAs (DHA, EPA, AA) on the growth of 3D tumor spheroids generated from NSCLC cells (A). FAs were added upon exposure for 72 h to 50 mM.

These preliminary experiments show that female and male-derived spheroids take up FAs with different patterns, and are differentially affected in their proliferation by the type of FA: female-derived spheroids are more sensitive to ω3 PUFAs, while male-derived spheroids are more sensitive to ω6 FA. We then would like to verify if the key findings observed in 2D cultures and animals were confirmed in the smart model of spheroids. The next experiments will evaluate if this prototypical in vitro 3D spheroid gender-tailored platform could be used to investigate the levels of PD-L1 and ERα,

the production of 17-β-estradiol, the signaling linkingPD-L1 to ERα, and to repurpose estrogen and lipid metabolic modifiers, as letrozole or ω3 FA, as novel immune-adjuvant agents in oncology. If successful, this represents a good compromise between the use of standard 2D cultures and the use of Hu-CD34+ animal models.

4. Discussion

How gender modulates the clinical benefit of anti-PD-1/anti-PD-L1 therapy remains largely unknown. In this Thesis, I identified gender- and hormonal-related factors predictive of response to pembrolizumab, the only ICI approved as first-line monotherapy in NSCLC patients and potentially druggable circuitries to improve ICI efficacy in this tumor.

With this goal in mind, we performed a transcriptional analysis interrogating the tumor immune microenvironment in a subset of NSCLC patients treated with ICIs as second/third line therapy, identifying specific elements associated with objective response and long-term outcomes. As awaited, cell populations (e.g. dendritic cells, CD8 T cells) and pathways (e.g. cytokine and chemokine, cytotoxicity) of immune activation and inflammation were associated with better response to ICI as well as OS at 18 months. Interestingly, among gene transcripts associated with responders and OS, two were upregulated in both categories: *IL12RB2* and *ESR1*. IL12RB2 up-regulation was not unexpected, because the properties of IL12, as player of the immune-environment, are well known in terms of enhanced antigens presentation, promotion of Th1 differentiation, expression of chemokines attracting NK, Th1 and CD8+ T cells [65]. The association of *ESR1* gene transcript with response to ICI and survival outcome could represent the missing ring between the differential gender-related response to ICIs and LC. If a potential prognostic role of *ESR1* mRNA expression, particularly in the advanced stage, has been proven [66], it is still not clear how gender may affect the response to ICIs in LC, since meta-analyses with opposite results exist [67] [68]. Here we report the association of *ESR1* with increased OS after OS, reinforcing a potential role of ER as prognostic marker itself and, perhaps, as predictor of ICI efficacy [69].

The screening of 30 NSCLC cell lines, including all possible combinations of gender, primary or metastatic localizations, smoking habits, confirming the higher expression of ERα in cell lines derived from females and primary tumors (considered a surrogate of "early stage" tumors), a finding already emerged in the analysis of patient-derived tumors, and the absence of gender- and localization-

dependent differences in PD-L1 expression. 17-β-estradiol levels followed the same trend than ERα levels, being generally higher in female-derived cells and in *ERα high* cells of both genders. The analysis of the cell line pool pointed out different scenarios existing in NSCLC cells, ranging from *17-β-estradiol/ERα high* tumors to *17-β-estradiol/ERα low* ones in both genders, but female-derived and primary tumor-derived NSCLC cell lines mostly belong to the first category, male-derived and metastatic-derived cell lines are mainly included in the second one.

To our surprise, the amount of surface PD-L1 followed a similar distribution to 17-β-estradiol/ERα levels, in particular in female cell lines. Mechanistically, we found that the complex 17-β-estradiol/ERα is a transcriptional inducer of PD-L1. Our data pointed out that gender is important but it is not the only factor determining the efficacy of anti-PD-1/PD-L1 efficacy. Higher the expression of PD-L1 is, higher is the response rate to pembrolizumab in NSCLC [70]. On the basis of this observation, female-derived NSCLC tumors, characterized by a higher percentage of *17-β-estradiol/ERα/PD-L1 high* tumors, should benefit more from Pembrolizumab treatment, in accord with some clinical studies reporting a higher benefit of ICI in women [71] [72][73]. On the other hand, a small percentage of NSCLC cells derived from males also have a *17-β-estradiol/ERα/PD-L1 high* phenotype, and a small percentage of female-derived cells are *17-β-estradiol/ERα/PD-L1 low*, a phenotype shared with the majority of male-derived NSCLC cells. This intricate biological scenario may explain why other large clinical studies sustained a higher benefit of ICIs in males [68][74][75], or no gender-dependent benefits at all [33][76]. We propose that 17-β-estradiol/ERα levels must be weighted, together with gender, as predictors of ICI benefit, because they finely regulates PD-L1 expression in NSCLC.

To be active, ERα must be translocated in the nucleus, bound to 17-β-estradiol and be phosphorylated on critical residues as Ser118 [77]. The examination of nuclear extracts in NSCLC cells indicated a detectable amount of translocated ERα, independent from gender. The transcriptional activity of ERα on *CD274/PD-L1* promoter, however, was higher in female-derived cells, in keeping with previous findings showing that female-derived NSCLC cells are more responsive to 17-β-estradiol and activate ER-transcriptional program more than male-derived NSCLC cells, in consequence of the higher

expression of ER co-activators [78]. On the other hand, ERβ, which is more detected in the nucleus of NSCLC biopsies than ERα [79] and controls the transcription of a broader spectrum of genes [73, pag. 200], has been indicated as the most prominent isoform of ER involved in NSCLC pathogenesis and progression [80]. In the case of *CD274/PD-L1* up-regulation, however, we suggest a predominant role of ERα, because ERβ expression was poorly correlated with PD-L1 expression in both genders and ERβ bounds weakly to *CD274/PD-L1* promoter. These findings are in line with the identification of *ESR1* but not *ESR2* (encoding for ERβ) as differentially linked to OS in patients treated with ICIs. 17-β-estradiol is the first element necessary for ERα activity. Lung is rich of estrogen synthesizing enzymes [81], particularly of aromatase that correlates with ER levels, is expressed in both male and female patients, in pre-menopausal and post-menopausal age [82]. These evidence support the idea that NSCLC cells have an autocrine production of estrogens, independent on ovary activity, age or gender. We indeed detected aromatase in both female and male-derived NSCLC cells, at higher levels in female cells. Aromatase expression correlated with 17-β-estradiol levels, suggesting that the enzyme is likely active in producing estrogens. Together with the absent correlation between *FSHR/LHR* expression and 17-β-estradiol amount, and the effective reduction of 17-β-estradiol levels in letrozole-treated cells, this finding supports the idea that the production of estrogens is mainly autocrine in the NSCLC cells analyzed.

Phosphorylation on Ser118 is the second condition that allows ERα to bind DNA and become transcriptionally active. The use of selective inhibitors of Akt and ERK1/2 indicated that these two kinases are involved in ERα phosphorylation of Ser118 in NSCLC cells. Both Akt and ERK1/2 are downstream effectors of EGFR [83]. Since also the EGFR inhibitor osimertinib induced a similar reduction of phospho(Ser118)ERα, we hypothesized that the EGFR/Akt and EGFR/ERK1/2 axes control the activity of ERα and consequently the levels of PD-L1. The strong correlation between phospho(Ser118)ERα and EGFR activity supported this hypothesis. Similarly, switching on the activity of EGFR in a cell line with the lowest EGFR activity, by overexpressing a constitutively active receptor, increased the phosphorylation of ERα and the amount of PD-L1 to the same level of

the cell line with the highest endogenous activity of EGFR. Multiple cross-talks between ER and EGFR signaling have been reported in NSCLC, where both EGF and 17-β-estradiol synergize in inducing cell proliferation and migration, by activating ERK1/2 [84][83] [85]. In our work, we linked EGFR signaling with the expression of PD-L1, demonstrating that higher is the EGFR activity, higher is ERα phosphorylation and PD-L1 transcriptional induction. Our data explain previously observations demonstrating that the introduction of exogenous EGFR carrying driver mutations up-regulates PD-L1 in bronchial epithelium [86]. c-Jun and STAT3 have been also implicated in the PD-L1 transcription induced by Ras/ERK1/2 [87]. We cannot exclude the involvement of these transcription factors in PD-L1 up-regulation. We pointed out for the first time that ERα was responsible for a gender-dependent differential expression of PD-L1. Although mutated EGFR is usually associated with a higher tyrosine kinase activity, the simple EGFR mutations do not correlate with PD-L1 expression in NSCLC patients [88]. Instead the phosphorylation activity of EGFR has shown a more robust correlation with PD-L1 levels [88], in line with our findings, showing a direct correlation between EGFR kinase activity and ERα activity.

In a translational perspective, the control of PD-L1 by 17-β-estradiol/ERα complex offers a tremendous opportunity to exploit anti-estrogens or aromatase inhibitors in ICI-based protocols. Both fulvestrant and letrozole have been safely tested in phase I/II trials, in combination with chemotherapy or EGFR inhibitors [80][71], but they have still not been used in association with ICIs. Here, we set up a gender-tailored platform of humanized mice to test the association of Pembrolizumab and letrozole against NSCLC immunoxenografts of the same gender of the host. The combination of these drugs was effective in reducing tumor growth, particularly in female-derived tumors characterized by a $^{17\text{-}\beta\text{-}estradiol/ER\alpha\ high}$ phenotype. By contrast, a minimal benefit was observed in male-derived patients with a $^{17\text{-}\beta\text{-}estradiol/ER\alpha\ low}$ phenotype. Tumors with a $^{17\text{-}\beta\text{-}estradiol/ER\alpha\ intermediate}$ phenotype have a moderate benefit. This experimental set identified a four biomarkers-based signature – EGFR activity, 17-β-estradiol amount, ERα levels, PD-L1 levels – that may be predictive of response to pembrolizumab and may help to select patients who will obtain the highest benefit

from pembrolizumab and letrozole combination. Being characterized by higher estrogens production and ERα levels, female-derived tumors have a higher benefit in terms of tumor reduction, OS and PFS compared to male-derived tumors.

In line with *in vitro* setting, letrozole down-regulated PD-L1 also in tumors. This decrease relieved the tumor-induced immune-suppression on the microenvironment and enhanced the efficacy of pembrolizumab. Indeed, in responsive tumors, the combination of pembrolizumab and letrozole increased the amount of active $CD8^+$ T-lymphocytes and NK cells, two populations with pronounced anti-tumor activity, whose expansion is an index of ICI efficacy [86] [61] [57]. The increase of proliferating and activated Vγ9Vδ2 T-cells was a third factor determining a durable immune control of tumor growth. Indeed, γδ T-cells are the most favorably prognostic tumor-infiltrating population in solid cancers, including lung adenocarcinomas [89]. The beneficial imprinting on immune environment was the *deus ex machina* explaining the benefits of prolonged treatments with letrozole. Indeed, while a 5-week treatment with pembrolizumab and letrozole only delayed tumor growth, the continuation of letrozole after this first cycle produced a long-term control of tumor that became a regression in animals subjected to a second cycle of the combination therapy. The decrease in PD-L1, as produced by the prolonged letrozole treatment, is a clinical sign of acquired resistance to pembrolizumab [90]. In contrast with this finding, however, we found that higher was the reduction of PD-L1 elicited by letrozole, higher was the anti-tumor efficacy of a second cycle of pembrolizumab and letrozole. This was likely due to the durable re-activation of anti-tumor TILs, an event that may sensitize the tumors to a second exposure to pembrolizumab. Estrogens play a key role in modulating the immune-environment: 17-β-estradiol strongly inhibits the cytotoxic functions of $CD8^+$ T-lymphocytes and NK cells, while aromatase inhibitors increase TILs in ER^+-breast cancers, a feature associated with improved OS [91]. Letrozole may have a dual benefit, acting on cancer cells, where it reduces PD-L1, and on immune environment, where it recruits anti-tumor TILs. To the best of our knowledge, this is the first work reporting the benefit of aromatase inhibitors on the immune-environment of NSCLC. As expected, the benefit was greater in female-derived tumors, where 17-β-

estradiol and ERα levels were higher. In males, the benefit was proportional to the intratumor amount of estrogens and ERα.

On the other hand, the rewiring of cellular metabolism is crucial for sustaining the increased growth and proliferation of tumor cells, and resistance to therapies. To investigate if blocking the endogenous production of estrogen may impact on metabolism, mainly lipid metabolites, we performed an untargeted lipidome analysis of female and male NSCLC cell lines. The lipidome profile revealed that aromatase inhibitors decrease SFAs/MFAs+PUFAs ratio, and the Chol/CE ratio. An increased amount of SFA and Chol increases the rigidity of plasma-membrane and may help specific integral membrane proteins, such as ATP binding cassette transporters, to maintain their proper conformation [92]. Also PD-L1 is an integral membrane protein and it has been reported that a rigid membrane allows it to maintain the optimal conformation to bind PD-1 [93]. By blocking the conversion of testosterone into 17-β-estradiol, letrozole increases the accumulation of upstream sterol metabolites and Chol that is usually accumulated as CE to buffer an extensive membrane rigidity [94]. A higher accumulation of CE is usually associated with an increased pool of MFAs and PUFAs that are usually integral part of CE, being esterified by the Acetyl-CoA Acetyltransferase 1 (ACAT1). Interestingly DHA is an excellent substrate of ACAT1 and can be either incorporated into CE droplets or released and be incorporated in membrane PLs [95]. This homeostatic compensation may explain why letrozole-treated cells have low MFAs+PUFAs and Chol/CE ratio. As a consequence, the rigidity of the membrane is decreased and the binding of PD-L1 with PD-1 is reduced, likely because of an altered conformation of PD-L1.

As proof of concept that letrozole could act with this second mechanism, i.e. increasing membrane fluidity, we directly modified the membrane fluidity with DHA, which is well incorporated in the plasma membrane of cancer cells [62], altering conformation, localization and functions of integral proteins involved in immune-recognition as calreticulin [63]. Intriguingly, DHA recapitulated in vitro and in vivo the effect of letrozole, suggesting that modifying the membrane fluidity – bypassing the transcriptional regulation of PD-L1 – could be an effective immune-adjuvant strategy for ICI

treatment in NSCLC. Notably, DHA exerted equal effects on both genders, thus appearing a more potent immune-sensitizer than letrozole.

In conclusion, we suggest that the differential efficacy of ICI in NSCLC between gender could be due to two factors: the PD-L1 levels controlled by the 17-β-estradiol/ERα complex, which appears more gender-related, and the membrane fluidity that is gender-independent. Indeed, 17-β-estradiol production and ERα activity, controlled by EGFR downstream signaling, up-regulate PD-L1 and determine the response to anti-PD-1/PD-L1 agents in NSCLC. In this circuitry, gender is an important co-primary factor: indeed, since high levels of 17-β-estradiol and ERα are common in female-derived tumors, females may benefit more than males from ICIs, but a high intratumor level of 17-β-estradiol and ERα determines the same response to pembrolizumab also in males. Based on these results, we propose that: i) aromatase inhibitors may be useful enhancers of pembrolizumab, thanks to their reduction of PD-L1 and consequent relief of tumor-induced immune-suppression, with different benefits depending on gender and 17-β-estradiol/ERα status; ii) the routinely assessment of 17-β-estradiol/ERα in NSCLC samples may represent a new stratification process to predict the response to ICIs and to identify patients who may benefit from the inclusion of aromatase inhibitors in ICI-based protocols. Since a second mechanism by which acts letrozole is the increased fluidification of the plasma-membrane, that hampers the conformation of PD-L1 and its binding with PD-1, a second immune-adjuvant approach could be represented by membrane fluidifiers, as DHA, which is equally effective in both genders (**Figure 28**). We believe that Aromatase inhibitors and ω3 fatty acids are noteworthy of further investigation in clinical settings .

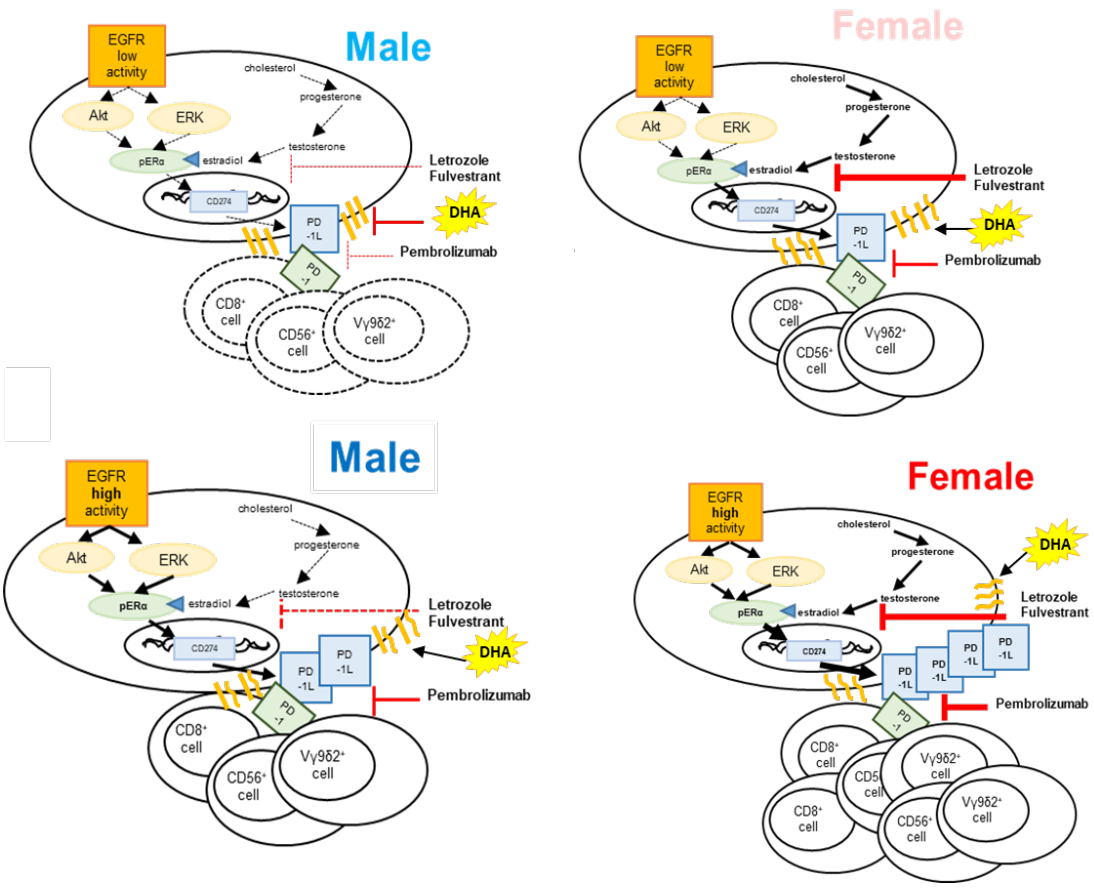

Figure 28.

Molecular and metabolic circuitries regulating anti-PD-L1 efficacy in NSCLC

ERα, which is activated by the binding of 17-β-estradiol and by the phosphorylation on Ser118 via EGFR/Akt and ERK1/2 axes, up-regulates PD-L1 and predicts a better response to Pembrolizumab. Lowering the synthesis of 17-β-estradiol with letrozole or the activity of ERα with fulvestrant, however, sensitizes NSCLC tumors to Pembrolizumab, reducing the PD-L1 levels and the PD-L1-dependent immune-suppression. We suggest the existence of four possible scenarios, dependent on gender and ERα/estrogen status, with a differential sensitivity to Pembrolizumab and aromatase inhibitors: 1) male patients with low 17-β-estradiol synthesis, low EGFR signaling, low ERα amount/activity and low PD-L1 amount; 2) male patients with high EGFR signaling, low 17-β-estradiol synthesis, high ERα amount/activity and intermediate PD-L1 amount; 3) female patients

with low EGFR signaling, high 17-β-estradiol synthesis, low ERα amount/activity and intermediate PD-L1 amount; 4) female patients with high EGFR signaling, high 17-β-estradiol synthesis, high ERα amount/activity and high PD-L1 amount. The efficacy of Pembrolizumab and the additional benefit of aromatase inhibitors increase progressively form scenario 1 to scenario 4. Increasing membrane fluidity, e.g. using the ω3 fatty acid docosahexaenoic acid (DHA) produces the same benefits of aromatase inhibitors in terms of relief of the tumor-induced immune-suppression, independently from gender.

.

5. Future perspectives

Since metabolic rewiring is crucial to induce resistance to chemotherapy and immunotherapy [96], we started to investigate if other classical energy-producing pathways were different between male and female NSCLC, and if these differences could imply a different sensibility to ICIs and/or could represent new druggable targets. The preliminary results indicated that OXPHOS-related pathways and ATP production is higher in female cell lines. This phenotype could theoretically favor resistance to ICIs by at least two mechanisms. First, an active production of ATP favors the production of membrane building blocks that can maintain a proper conformation of PD-L1 [97]. Second, most of biosynthetic steps of sterol hormones occur in mitochondria and requires ATP [64]. Indeed, in most solid tumors an active mitochondrial metabolism is associated with immune-resistance or immune-anergy [98]. These preliminary results open the way to the possibility to test Mitocans and other mitochondrial-metabolism targeting agents as possible adjuvants of anti-PD-L1 treatment.

Second, we are aware that 2D co-cultures have severe limitations to study the immune-response of solid tumors, because for instance they lack the hypoxic environment that strongly limit the efficacy of ICIs [99]. Humanized mice are at the moment the golden standard for these type of studies, but they also suffer of limitations: the experiments are expensive, time-consuming, may have variable engraftment of the human immune system and do not reproduce all the features of the human immune-system (as cytokines and chemokines). To overcome these limitations, we planned to set up immune-spheroids or immune-tumoroid cultures that could be used for functional assays in vitro. As preliminary steps, we set up the conditions to generate in vitro 3D gender-tailored platform to investigate the metabolic circuitries causing the gender-related differential response to ICIs, and to repurpose metabolic modifiers as novel immune-adjuvant agents. We are aware of the limited number of cell lines analyzed and of the absence of the immune component in this experimental set, but we were able to observe a differential sensitivity to FAs that could pave the way to our future experiments; i) the addition of TILs to the spheroids; ii) the validation of the key metabolic events

and molecular circuitries found out in 2D cultures; iii) the validation of estrogen- and/or lipid-targeting drugs as immune-adjuvant in this system. Our final goal is to build a platform, well characterized for the metabolic and lipidomic profile, the hormonal phenotype, the response to anti-PD-1/anti-PD-L1 sufficient to perform medium-high throughput screening of novel or repurposed agents, as first predictive tests to identify agents improving the efficacy of ICIs and overcoming the gender inequality in NSCLC immunotherapy.

6. References

[1] R. L. Siegel, K. D. Miller, H. E. Fuchs, e A. Jemal, «Cancer Statistics, 2021», *CA. Cancer J. Clin.*, vol. 71, n. 1, pagg. 7–33, gen. 2021, doi: 10.3322/caac.21654.

[2] L. Guida, «NEOPLASIE DEL POLMONE», pag. 462, 2020.

[3] A. J. Alberg, M. V. Brock, e J. M. Samet, «Epidemiology of Lung Cancer: Looking to the Future», *J. Clin. Oncol.*, vol. 23, n. 14, pagg. 3175–3185, mag. 2005, doi: 10.1200/JCO.2005.10.462.

[4] O. Raaschou-Nielsen *et al.*, «Air pollution and lung cancer incidence in 17 European cohorts: prospective analyses from the European Study of Cohorts for Air Pollution Effects (ESCAPE)», *Lancet Oncol.*, vol. 14, n. 9, pagg. 813–822, ago. 2013, doi: 10.1016/S1470-2045(13)70279-1.

[5] J. Yokota, K. Shiraishi, e T. Kohno, «Genetic Basis for Susceptibility to Lung Cancer: Recent Progress and Future Directions», pag. 22.

[6] D. J. Raz, J. Y. Kim, e D. M. Jablons, «Diagnosis and treatment of bronchioloalveolar carcinoma»:, *Curr. Opin. Pulm. Med.*, vol. 13, n. 4, pagg. 290–296, lug. 2007, doi: 10.1097/MCP.0b013e32816ebc62.

[7] P. B. Bach *et al.*, «Benefits and Harms of CT Screening for Lung Cancer: A Systematic Review», *JAMA*, vol. 307, n. 22, pag. 2418, giu. 2012, doi: 10.1001/jama.2012.5521.

[8] R. Wender *et al.*, «American Cancer Society lung cancer screening guidelines: American Cancer Society Lung Cancer Screening Guidelines», *CA. Cancer J. Clin.*, vol. 63, n. 2, pagg. 106–117, mar. 2013, doi: 10.3322/caac.21172.

[9] D. Planchard *et al.*, «Metastatic non-small cell lung cancer: ESMO Clinical Practice Guidelines for diagnosis, treatment and follow-up», *Ann. Oncol.*, vol. 29, pagg. iv192–iv237, ott. 2018, doi: 10.1093/annonc/mdy275.

[10] H. J. de Koning *et al.*, «Reduced Lung-Cancer Mortality with Volume CT Screening in a Randomized Trial», *N. Engl. J. Med.*, vol. 382, n. 6, pagg. 503–513, feb. 2020, doi: 10.1056/NEJMoa1911793.

[11] W. Travis *et al.*, «International association for the study of lung cancer/american thoracic society/european respiratory society international multidisciplinary classification of lung adenocarcinoma.», pag. 199, 2011.

[12] W. D. Travis *et al.*, «An Official American Thoracic Society/European Respiratory Society Statement: Update of the International Multidisciplinary Classification of the Idiopathic Interstitial Pneumonias», *Am. J. Respir. Crit. Care Med.*, vol. 188, n. 6, pagg. 733–748, set. 2013, doi: 10.1164/rccm.201308-1483ST.

[13] Y. Yatabe *et al.*, «Best Practices Recommendations for Diagnostic Immunohistochemistry in Lung Cancer», *J. Thorac. Oncol.*, vol. 14, n. 3, pagg. 377–407, mar. 2019, doi: 10.1016/j.jtho.2018.12.005.

[14] E. H. F. M. van der Heijden *et al.*, «Guideline for the Acquisition and Preparation of Conventional and Endobronchial Ultrasound-Guided Transbronchial Needle Aspiration Specimens for the Diagnosis and Molecular Testing of Patients with Known or Suspected Lung Cancer», *Respiration*, vol. 88, n. 6, pagg. 500–517, 2014, doi: 10.1159/000368857.

[15] K. L. Reckamp *et al.*, «A Highly Sensitive and Quantitative Test Platform for Detection of NSCLC EGFR Mutations in Urine and Plasma», *J. Thorac. Oncol.*, vol. 11, n. 10, pagg. 1690–1700, ott. 2016, doi: 10.1016/j.jtho.2016.05.035.

[16] T. Mitsudomi *et al.*, «Mutations of the Epidermal Growth Factor Receptor Gene Predict Prolonged Survival After Gefitinib Treatment in Patients With Non–Small-Cell Lung Cancer With Postoperative Recurrence», *J. Clin. Oncol.*, vol. 23, n. 11, pagg. 2513–2520, apr. 2005, doi: 10.1200/JCO.2005.00.992.

[17] T. S. Mok *et al.*, «Gefitinib or Carboplatin–Paclitaxel in Pulmonary Adenocarcinoma», *N. Engl. J. Med.*, vol. 361, n. 10, pagg. 947–957, set. 2009, doi: 10.1056/NEJMoa0810699.
[18] D. M. Jackman *et al.*, «Exon 19 Deletion Mutations of Epidermal Growth Factor Receptor Are Associated with Prolonged Survival in Non–Small Cell Lung Cancer Patients Treated with Gefitinib or Erlotinib», *Clin. Cancer Res.*, vol. 12, n. 13, pagg. 3908–3914, lug. 2006, doi: 10.1158/1078-0432.CCR-06-0462.
[19] L. Qiu *et al.*, «Synthesis, crystal structure and antitumor effect of a novel copper(II) complex bearing zoledronic acid derivative», *Eur. J. Med. Chem.*, vol. 89, pagg. 42–50, gen. 2015, doi: 10.1016/j.ejmech.2014.10.028.
[20] E. Gobbini *et al.*, «Implementing ctDNA Analysis in the Clinic: Challenges and Opportunities in Non-Small Cell Lung Cancer», *Cancers*, vol. 12, n. 11, pag. 3112, ott. 2020, doi: 10.3390/cancers12113112.
[21] R. Chiarle, C. Voena, C. Ambrogio, R. Piva, e G. Inghirami, «The anaplastic lymphoma kinase in the pathogenesis of cancer», *Nat. Rev. Cancer*, vol. 8, n. 1, pagg. 11–23, gen. 2008, doi: 10.1038/nrc2291.
[22] B. J. Solomon *et al.*, «Lorlatinib in patients with ALK-positive non-small-cell lung cancer: results from a global phase 2 study», *Lancet Oncol.*, vol. 19, n. 12, pagg. 1654–1667, dic. 2018, doi: 10.1016/S1470-2045(18)30649-1.
[23] D. R. Camidge *et al.*, «Brigatinib versus Crizotinib in *ALK* -Positive Non–Small-Cell Lung Cancer», *N. Engl. J. Med.*, vol. 379, n. 21, pagg. 2027–2039, nov. 2018, doi: 10.1056/NEJMoa1810171.
[24] D. Kazandjian, «Multiple myeloma epidemiology and survival: A unique malignancy», *Semin. Oncol.*, vol. 43, n. 6, pagg. 676–681, dic. 2016, doi: 10.1053/j.seminoncol.2016.11.004.
[25] M. Del Re, E. Vasile, A. Falcone, R. Danesi, e I. Petrini, «Molecular analysis of cell-free circulating DNA for the diagnosis of somatic mutations associated with resistance to tyrosine kinase inhibitors in non-small-cell lung cancer», *Expert Rev. Mol. Diagn.*, vol. 14, n. 4, pagg. 453–468, mag. 2014, doi: 10.1586/14737159.2014.908120.
[26] M. L. G. Janssen-Heijnen, F. N. van Erning, D. K. De Ruysscher, J. W. W. Coebergh, e H. J. M. Groen, «Variation in causes of death in patients with non-small cell lung cancer according to stage and time since diagnosis», *Ann. Oncol.*, vol. 26, n. 5, pagg. 902–907, mag. 2015, doi: 10.1093/annonc/mdv061.
[27] T.-F. Lou *et al.*, «Cancer-Specific Production of N-Acetylaspartate via NAT8L Overexpression in Non–Small Cell Lung Cancer and Its Potential as a Circulating Biomarker», *Cancer Prev. Res. (Phila. Pa.)*, vol. 9, n. 1, pagg. 43–52, gen. 2016, doi: 10.1158/1940-6207.CAPR-14-0287.
[28] E. E. Vietsch *et al.*, «Reprint of: Circulating cell-free DNA mutation patterns in early and late stage colon and pancreatic cancer», *Cancer Genet.*, vol. 228–229, pagg. 131–142, dic. 2018, doi: 10.1016/j.cancergen.2018.11.001.
[29] J. P. Burnham e M. H. Kollef, «Treatment of severe skin and soft tissue infections: a review», *Curr. Opin. Infect. Dis.*, vol. 31, n. 2, pagg. 113–119, apr. 2018, doi: 10.1097/QCO.0000000000000431.
[30] M. J. Grant, R. S. Herbst, e S. B. Goldberg, «Selecting the optimal immunotherapy regimen in driver-negative metastatic NSCLC», *Nat. Rev. Clin. Oncol.*, vol. 18, n. 10, pagg. 625–644, ott. 2021, doi: 10.1038/s41571-021-00520-1.
[31] S. L. Klein e R. Morgan, «The impact of sex and gender on immunotherapy outcomes», *Biol. Sex Differ.*, vol. 11, n. 1, pag. 24, dic. 2020, doi: 10.1186/s13293-020-00301-y.
[32] S. Novello *et al.*, «Metastatic non-small-cell lung cancer: ESMO Clinical Practice Guidelines for diagnosis, treatment and follow-up», *Ann. Oncol.*, vol. 27, pagg. v1–v27, set. 2016, doi: 10.1093/annonc/mdw326.
[33] M. Reck *et al.*, «Pembrolizumab versus Chemotherapy for PD-L1–Positive Non–Small-Cell Lung Cancer», *N. Engl. J. Med.*, vol. 375, n. 19, pagg. 1823–1833, nov. 2016, doi:

10.1056/NEJMoa1606774.
[34] M. Reck *et al.*, «Pembrolizumab versus Chemotherapy for PD-L1–Positive Non–Small-Cell Lung Cancer», *N. Engl. J. Med.*, vol. 375, n. 19, pagg. 1823–1833, nov. 2016, doi: 10.1056/NEJMoa1606774.
[35] M. B. Cook, K. A. McGlynn, S. S. Devesa, N. D. Freedman, e W. F. Anderson, «Sex Disparities in Cancer Mortality and Survival», *Cancer Epidemiol. Biomarkers Prev.*, vol. 20, n. 8, pagg. 1629–1637, ago. 2011, doi: 10.1158/1055-9965.EPI-11-0246.
[36] J. Wang, X. Li, e H. Chen, «Organoid models in lung regeneration and cancer», *Cancer Lett.*, vol. 475, pagg. 129–135, apr. 2020, doi: 10.1016/j.canlet.2020.01.030.
[37] V. Rodriguez-Lara, J.-M. Hernandez-Martinez, e O. Arrieta, «Influence of estrogen in non-small cell lung cancer and its clinical implications», *J. Thorac. Dis.*, vol. 10, n. 1, pagg. 482–497, gen. 2018, doi: 10.21037/jtd.2017.12.61.
[38] C. Patrone *et al.*, «Regulation of Postnatal Lung Development and Homeostasis by Estrogen Receptor ␢», *MOL CELL BIOL*, vol. 23, pag. 11, 2003.
[39] T. F. Burns e L. P. Stabile, «Targeting the estrogen pathway for the treatment and prevention of lung cancer», *Lung Cancer Manag.*, vol. 3, n. 1, pagg. 43–52, feb. 2014, doi: 10.2217/lmt.13.67.
[40] L. Hsu *et al.*, «Estrogen adversely affects the prognosis of patients with lung adenocarcinoma», *Cancer Sci.*, vol. 106, n. 1, pagg. 51–59, gen. 2015, doi: 10.1111/cas.12558.
[41] L. Yang *et al.*, «Posttranscriptional Control of PD-L1 Expression by 17β-Estradiol via PI3K/Akt Signaling Pathway in ERα-Positive Cancer Cell Lines», *Int. J. Gynecol. Cancer*, vol. 27, n. 2, pagg. 196–205, feb. 2017, doi: 10.1097/IGC.0000000000000875.
[42] M. A. Velez, T. F. Burns, e L. P. Stabile, «The estrogen pathway as a modulator of response to immunotherapy», *Immunotherapy*, vol. 11, n. 13, pagg. 1161–1176, set. 2019, doi: 10.2217/imt-2019-0024.
[43] V. Mah *et al.*, «Aromatase Expression Predicts Survival in Women with Early-Stage Non–Small Cell Lung Cancer», *Cancer Res.*, vol. 67, n. 21, pagg. 10484–10490, nov. 2007, doi: 10.1158/0008-5472.CAN-07-2607.
[44] V. Mah *et al.*, «Expression levels of estrogen receptor beta in conjunction with aromatase predict survival in non-small cell lung cancer», *Lung Cancer*, vol. 74, n. 2, pagg. 318–325, nov. 2011, doi: 10.1016/j.lungcan.2011.03.009.
[45] L. P. Stabile *et al.*, «Combined Analysis of Estrogen Receptor β-1 and Progesterone Receptor Expression Identifies Lung Cancer Patients with Poor Outcome», *Clin. Cancer Res.*, vol. 17, n. 1, pagg. 154–164, gen. 2011, doi: 10.1158/1078-0432.CCR-10-0992.
[46] A. J. van der Wekken *et al.*, «Overall survival in EGFR mutated non-small-cell lung cancer patients treated with afatinib after EGFR TKI and resistant mechanisms upon disease progression», *PLOS ONE*, vol. 12, n. 8, pag. e0182885, ago. 2017, doi: 10.1371/journal.pone.0182885.
[47] E. B. Garon *et al.*, «Antiestrogen Fulvestrant Enhances the Antiproliferative Effects of Epidermal Growth Factor Receptor Inhibitors in Human Non–Small-Cell Lung Cancer», *J. Thorac. Oncol.*, vol. 8, n. 3, pagg. 270–278, mar. 2013, doi: 10.1097/JTO.0b013e31827d525c.
[48] D. M. Collins *et al.*, «Tyrosine kinase inhibitors potentiate the cytotoxicity of MDR-substrate anticancer agents independent of growth factor receptor status in lung cancer cell lines», *Invest. New Drugs*, vol. 28, n. 4, pagg. 433–444, ago. 2010, doi: 10.1007/s10637-009-9266-0.
[49] H. Ishibashi *et al.*, «Progesterone Receptor in Non–Small Cell Lung Cancer—A Potent Prognostic Factor and Possible Target for Endocrine Therapy», *Cancer Res.*, vol. 65, n. 14, pagg. 6450–6458, lug. 2005, doi: 10.1158/0008-5472.CAN-04-3087.
[50] M. Cheng e S. Hu, «Lung-resident *γδ* T cells and their roles in lung diseases», *Immunology*, vol. 151, n. 4, pagg. 375–384, ago. 2017, doi: 10.1111/imm.12764.
[51] J. Mazieres *et al.*, «Vemurafenib in non-small-cell lung cancer patients with BRAFV600 and BRAFnonV600 mutations», *Ann. Oncol.*, vol. 31, n. 2, pagg. 289–294, feb. 2020, doi: 10.1016/j.annonc.2019.10.022.

[52] E. B. Garon *et al.*, «Five-Year Overall Survival for Patients With Advanced Non–Small-Cell Lung Cancer Treated With Pembrolizumab: Results From the Phase I KEYNOTE-001 Study», *J. Clin. Oncol.*, vol. 37, n. 28, pagg. 2518–2527, ott. 2019, doi: 10.1200/JCO.19.00934.
[53] A. Grassadonia *et al.*, «Effect of Gender on the Outcome of Patients Receiving Immune Checkpoint Inhibitors for Advanced Cancer: A Systematic Review and Meta-Analysis of Phase III Randomized Clinical Trials», *J. Clin. Med.*, vol. 7, n. 12, pag. 542, dic. 2018, doi: 10.3390/jcm7120542.
[54] I. Campia *et al.*, «Digoxin and ouabain induce the efflux of cholesterol via liver X receptor signalling and the synthesis of ATP in cardiomyocytes», *Biochem. J.*, vol. 447, n. 2, pagg. 301–311, ott. 2012, doi: 10.1042/BJ20120200.
[55] B. A. Inman, T. A. Longo, S. Ramalingam, e M. R. Harrison, «Atezolizumab: A PD-L1–Blocking Antibody for Bladder Cancer», *Clin. Cancer Res.*, vol. 23, n. 8, pagg. 1886–1890, apr. 2017, doi: 10.1158/1078-0432.CCR-16-1417.
[56] G. E. Weitsman *et al.*, «Estrogen Receptor-α Phosphorylated at Ser ^{118} Is Present at the Promoters of Estrogen-Regulated Genes and Is Not Altered Due to HER-2 Overexpression», *Cancer Res.*, vol. 66, n. 20, pagg. 10162–10170, ott. 2006, doi: 10.1158/0008-5472.CAN-05-4111.
[57] J. Choi, B. Psarommatis, Y. R. Gao, Y. Zheng, D. J. Handelsman, e U. Simanainen, «The role of androgens in experimental rodent mammary carcinogenesis», *Breast Cancer Res.*, vol. 16, n. 6, pag. 483, dic. 2014, doi: 10.1186/s13058-014-0483-x.
[58] L. P. Stabile, J. S. Lyker, C. T. Gubish, W. Zhang, J. R. Grandis, e J. M. Siegfried, «Combined Targeting of the Estrogen Receptor and the Epidermal Growth Factor Receptor in Non–Small Cell Lung Cancer Shows Enhanced Antiproliferative Effects», *Cancer Res.*, vol. 65, n. 4, pagg. 1459–1470, feb. 2005, doi: 10.1158/0008-5472.CAN-04-1872.
[59] M. Moerkens, Y. Zhang, L. Wester, B. van de Water, e J. H. Meerman, «Epidermal growth factor receptor signalling in human breast cancer cells operates parallel to estrogen receptor α signalling and results in tamoxifen insensitive proliferation», *BMC Cancer*, vol. 14, n. 1, pag. 283, dic. 2014, doi: 10.1186/1471-2407-14-283.
[60] P. K. Premsrirut *et al.*, «A Rapid and Scalable System for Studying Gene Function in Mice Using Conditional RNA Interference», *Cell*, vol. 145, n. 1, pagg. 145–158, apr. 2011, doi: 10.1016/j.cell.2011.03.012.
[61] V. Nardone *et al.*, «Radiomics predicts survival of patients with advanced non-small cell lung cancer undergoing PD-1 blockade using Nivolumab», *Oncol. Lett.*, dic. 2019, doi: 10.3892/ol.2019.11220.
[62] T. Harayama e T. Shimizu, «Roles of polyunsaturated fatty acids, from mediators to membranes», *J. Lipid Res.*, vol. 61, n. 8, pagg. 1150–1160, ago. 2020, doi: 10.1194/jlr.R120000800.
[63] G. Gelsomino *et al.*, «Omega 3 fatty acids chemosensitize multidrug resistant colon cancer cells by down-regulating cholesterol synthesis and altering detergent resistant membranes composition», *Mol. Cancer*, vol. 12, n. 1, pag. 137, dic. 2013, doi: 10.1186/1476-4598-12-137.
[64] G. Bassi, S. K. Sidhu, e S. Mishra, «The Expanding Role of Mitochondria, Autophagy and Lipophagy in Steroidogenesis», *Cells*, vol. 10, n. 8, pag. 1851, lug. 2021, doi: 10.3390/cells10081851.
[65] P. Berraondo, I. Etxeberria, M. Ponz-Sarvise, e I. Melero, «Revisiting Interleukin-12 as a Cancer Immunotherapy Agent», *Clin. Cancer Res.*, vol. 24, n. 12, pagg. 2716–2718, giu. 2018, doi: 10.1158/1078-0432.CCR-18-0381.
[66] W. Li, L. A. Tse, e F. Wang, «Prognostic value of estrogen receptors mRNA expression in non-small cell lung cancer: A systematic review and meta-analysis», *Steroids*, vol. 104, pagg. 129–136, dic. 2015, doi: 10.1016/j.steroids.2015.09.005.
[67] A. Botticelli *et al.*, «A nomogram to predict survival in non-small cell lung cancer patients treated with nivolumab», *J. Transl. Med.*, vol. 17, n. 1, pag. 99, dic. 2019, doi: 10.1186/s12967-019-1847-x.

[68] F. Conforti *et al.*, «Cancer immunotherapy efficacy and patients' sex: a systematic review and meta-analysis», *Lancet Oncol.*, vol. 19, n. 6, pagg. 737–746, giu. 2018, doi: 10.1016/S1470-2045(18)30261-4.
[69] «Expression of Estrogen Receptor-α and Survival in Advanced-stage Non-small Cell Lung Cancer», *Anticancer Res.*, vol. 38, n. 4, mar. 2018, doi: 10.21873/anticanres.12470.
[70] M. Santarpia *et al.*, «Non-Small-Cell Lung Cancer Signaling Pathways, Metabolism, and PD-1/PD-L1 Antibodies», *Cancers*, vol. 12, n. 6, pag. 1475, giu. 2020, doi: 10.3390/cancers12061475.
[71] L. Gandhi *et al.*, «Pembrolizumab plus Chemotherapy in Metastatic Non–Small-Cell Lung Cancer», *N. Engl. J. Med.*, vol. 378, n. 22, pagg. 2078–2092, mag. 2018, doi: 10.1056/NEJMoa1801005.
[72] M. A. Socinski *et al.*, «Current and Emergent Therapy Options for Advanced Squamous Cell Lung Cancer», *J. Thorac. Oncol.*, vol. 13, n. 2, pagg. 165–183, feb. 2018, doi: 10.1016/j.jtho.2017.11.111.
[73] K. M. Kerr *et al.*, «Prevalence and clinical association of gene mutations through multiplex mutation testing in patients with NSCLC: results from the ETOP Lungscape Project», *Ann. Oncol.*, vol. 29, n. 1, pagg. 200–208, gen. 2018, doi: 10.1093/annonc/mdx629.
[74] C. J. D. Wallis *et al.*, «Association of Patient Sex With Efficacy of Immune Checkpoint Inhibitors and Overall Survival in Advanced Cancers: A Systematic Review and Meta-analysis», *JAMA Oncol.*, vol. 5, n. 4, pag. 529, apr. 2019, doi: 10.1001/jamaoncol.2018.5904.
[75] J. Wang, X. Li, e H. Chen, «Organoid models in lung regeneration and cancer», *Cancer Lett.*, vol. 475, pagg. 129–135, apr. 2020, doi: 10.1016/j.canlet.2020.01.030.
[76] A. Rittmeyer *et al.*, «Atezolizumab versus docetaxel in patients with previously treated non-small-cell lung cancer (OAK): a phase 3, open-label, multicentre randomised controlled trial», *The Lancet*, vol. 389, n. 10066, pagg. 255–265, gen. 2017, doi: 10.1016/S0140-6736(16)32517-X.
[77] G. E. Weitsman *et al.*, «Estrogen Receptor-α Phosphorylated at Ser ^{118} Is Present at the Promoters of Estrogen-Regulated Genes and Is Not Altered Due to HER-2 Overexpression», *Cancer Res.*, vol. 66, n. 20, pagg. 10162–10170, ott. 2006, doi: 10.1158/0008-5472.CAN-05-4111.
[78] S. M. Dougherty *et al.*, «Gender difference in the activity but not expression of estrogen receptors α and β in human lung adenocarcinoma cells», *Endocr. Relat. Cancer*, vol. 13, n. 1, pagg. 113–134, mar. 2006, doi: 10.1677/erc.1.01118.
[79] H. Kawai *et al.*, «Estrogen Receptor α and β are Prognostic Factors in Non–Small Cell Lung Cancer», *Clin. Cancer Res.*, vol. 11, n. 14, pagg. 5084–5089, lug. 2005, doi: 10.1158/1078-0432.CCR-05-0200.
[80] N. Kazmi *et al.*, «The role of estrogen, progesterone and aromatase in human non-small-cell lung cancer», *Lung Cancer Manag.*, vol. 1, n. 4, pagg. 259–272, dic. 2012, doi: 10.2217/lmt.12.44.
[81] G. F. J. Konings *et al.*, «Increased levels of enzymes involved in local estradiol synthesis in chronic obstructive pulmonary disease», *Mol. Cell. Endocrinol.*, vol. 443, pagg. 23–31, mar. 2017, doi: 10.1016/j.mce.2016.12.001.
[82] V. Mah *et al.*, «Aromatase Expression Predicts Survival in Women with Early-Stage Non–Small Cell Lung Cancer», *Cancer Res.*, vol. 67, n. 21, pagg. 10484–10490, nov. 2007, doi: 10.1158/0008-5472.CAN-07-2607.
[83] J. Choi, B. Psarommatis, Y. R. Gao, Y. Zheng, D. J. Handelsman, e U. Simanainen, «The role of androgens in experimental rodent mammary carcinogenesis», *Breast Cancer Res.*, vol. 16, n. 6, pag. 483, dic. 2014, doi: 10.1186/s13058-014-0483-x.
[84] L. P. Stabile, J. S. Lyker, C. T. Gubish, W. Zhang, J. R. Grandis, e J. M. Siegfried, «Combined Targeting of the Estrogen Receptor and the Epidermal Growth Factor Receptor in Non–Small Cell Lung Cancer Shows Enhanced Antiproliferative Effects», *Cancer Res.*, vol. 65, n. 4, pagg. 1459–1470, feb. 2005, doi: 10.1158/0008-5472.CAN-04-1872.
[85] L. Hsu *et al.*, «Estrogen adversely affects the prognosis of patients with lung adenocarcinoma», *Cancer Sci.*, vol. 106, n. 1, pagg. 51–59, gen. 2015, doi: 10.1111/cas.12558.

[86] E. A. Akbay *et al.*, «Activation of the PD-1 Pathway Contributes to Immune Escape in EGFR-Driven Lung Tumors», *Cancer Discov.*, vol. 3, n. 12, pagg. 1355–1363, dic. 2013, doi: 10.1158/2159-8290.CD-13-0310.
[87] H. Sumimoto, A. Takano, K. Teramoto, e Y. Daigo, «RAS–Mitogen-Activated Protein Kinase Signal Is Required for Enhanced PD-L1 Expression in Human Lung Cancers», *PLOS ONE*, vol. 11, n. 11, pag. e0166626, nov. 2016, doi: 10.1371/journal.pone.0166626.
[88] Y. He *et al.*, «LAG-3 Protein Expression in Non–Small Cell Lung Cancer and Its Relationship with PD-1/PD-L1 and Tumor-Infiltrating Lymphocytes», *J. Thorac. Oncol.*, vol. 12, n. 5, pagg. 814–823, mag. 2017, doi: 10.1016/j.jtho.2017.01.019.
[89] A. J. Gentles *et al.*, «The prognostic landscape of genes and infiltrating immune cells across human cancers», *Nat. Med.*, vol. 21, n. 8, pagg. 938–945, ago. 2015, doi: 10.1038/nm.3909.
[90] K. Nakagawa *et al.*, «Ramucirumab plus erlotinib in patients with untreated, EGFR-mutated, advanced non-small-cell lung cancer (RELAY): a randomised, double-blind, placebo-controlled, phase 3 trial», *Lancet Oncol.*, vol. 20, n. 12, pagg. 1655–1669, dic. 2019, doi: 10.1016/S1470-2045(19)30634-5.
[91] H. Hosokawa e E. V. Rothenberg, «Cytokines, Transcription Factors, and the Initiation of T-Cell Development», *Cold Spring Harb. Perspect. Biol.*, vol. 10, n. 5, pag. a028621, mag. 2018, doi: 10.1101/cshperspect.a028621.
[92] J. Kopecka, P. Trouillas, A. Č. Gašparović, E. Gazzano, Y. G. Assaraf, e C. Riganti, «Phospholipids and cholesterol: Inducers of cancer multidrug resistance and therapeutic targets», *Drug Resist. Updat.*, vol. 49, pag. 100670, mar. 2020, doi: 10.1016/j.drup.2019.100670.
[93] S. Li *et al.*, «Choline phosphate lipid insertion and rigidification of cell membranes for targeted cancer chemo-immunotherapy», *Chem. Commun.*, vol. 57, n. 11, pagg. 1372–1375, 2021, doi: 10.1039/D0CC08011J.
[94] E. H. K. Mok e T. K. W. Lee, «The Pivotal Role of the Dysregulation of Cholesterol Homeostasis in Cancer: Implications for Therapeutic Targets», *Cancers*, vol. 12, n. 6, pag. 1410, mag. 2020, doi: 10.3390/cancers12061410.
[95] C. J. Antalis, T. Arnold, B. Lee, K. K. Buhman, e R. A. Siddiqui, «Docosahexaenoic acid is a substrate for ACAT1 and inhibits cholesteryl ester formation from oleic acid in MCF-10A cells», *Prostaglandins Leukot. Essent. Fatty Acids*, vol. 80, n. 2–3, pagg. 165–171, feb. 2009, doi: 10.1016/j.plefa.2009.01.001.
[96] A. C. Gonçalves *et al.*, «Impact of cancer metabolism on therapy resistance – Clinical implications», *Drug Resist. Updat.*, vol. 59, pag. 100797, dic. 2021, doi: 10.1016/j.drup.2021.100797.
[97] T. Alexa-Stratulat, M. Pešić, A. Č. Gašparović, I. P. Trougakos, e C. Riganti, «What sustains the multidrug resistance phenotype beyond ABC efflux transporters? Looking beyond the tip of the iceberg», *Drug Resist. Updat.*, vol. 46, pag. 100643, set. 2019, doi: 10.1016/j.drup.2019.100643.
[98] J. Kopecka *et al.*, «Mitochondrial metabolism: Inducer or therapeutic target in tumor immune-resistance?», *Semin. Cell Dev. Biol.*, vol. 98, pagg. 80–89, feb. 2020, doi: 10.1016/j.semcdb.2019.05.008.
[99] J. Kopecka *et al.*, «Hypoxia as a driver of resistance to immunotherapy», *Drug Resist. Updat.*, vol. 59, pag. 100787, dic. 2021, doi: 10.1016/j.drup.2021.100787.